FLOOD RISK ASSESSMENT IN HAITI

USING

REMOTE SENSING AND GEOGRAPHIC INFORMATION SYSTEMS

By

Fredline ILORME

A REPORT

Submitted in partial fulfillment of the requirements

For the degree of

Master of Science in Civil Engineering

MICHIGAN TECHNOLOGICAL UNIVERSITY

2007

This report, "Flood Risk Assessment Using Remote Sensing and Geographic Information Systems," is hereby approved in partial fulfillment of the requirements for the Degree of MASTER OF SCIENCE IN CIVIL ENGINEERING.

DEPARTMENT of Civil and Environmental Engineering

Signatures:

Report Advisor _____

Dr. David W. Watkins, Jr.

Department Chair _____

Dr. Neil J. Hutzler

Date _____

ABSTRACT

Haiti is a densely populated country that frequently lies in the path of major hurricanes, and thus constitutes a critical region for effective flood risk management policies to be developed. Recent catastrophic floods in Gonaives (Artibonite), Fonds Verrettes (West), and Mapou (South-East) have increased awareness of Haiti's heightened risk of flooding, Unfortunately, lack of flood risk assessment for the island constitutes a major barrier to proper policy design and risk management, and significantly contributes to the slow economic development of the region.

This report describes the use of remote sensing (RS) and geographic information systems (GIS) to quantify flood risk in "data-poor" regions, with a case study of the city of Gonaives, Haiti. Available daily rainfall data in the region were applied to develop a rainfall-runoff model. A one-dimensional flood hydraulics model was used with 30m-resolution digital elevation data to model the floodplain. This model gave inaccurate floodplain delineations mainly because of the multiple channels created during high flows in an alluvial plain. Hazard assessment was augmented with ASTER satellite images of the region before and after flooding. Finally, a vulnerability map was developed for Gonaives and used in conjunction with the hazard map to determine a flood risk map for the area.

Results from the analyses show that coastal Gonaives is less at risk to flooding impacts than upstream areas. It also appears that the natural path of the Quinte River goes straight into the city as shown by the 30m and 90m DEMs. Evacuation, if necessary, should be carried out early to shelters that would be located on the hill next to Savane Desolee. However, if little lead time is available, routing evacuees toward Morne Bienac is probably the best choice.

This study illustrates how combining hydrologic models, geographic information systems and remotely sensed data in an integrated manner can help quantify flood risk, as well as identify priorities for investments in infrastructure and warning systems for regions with limited information. It advocates the cross-validation of methods to identify the uncertainties, whenever possible. It also discusses areas for further research.

ACKNOWLEDGEMENTS

This research was made possible thanks to a Fulbright scholarship and the support of the Civil and Environmental Engineering Department of Michigan Technological University.

My thanks go to my advisor, Dr. David W. WATKINS, Jr. for his guidance and valuable insights on the research during those two years, to the school of Forestry particularly Dr. Ann L. MACLEAN for letting me use the computing resources of this department, to Dr. Veronica W. GRIFFIS for constant availability and advice, to Dr. Betül SAF for overlooking my work and providing encouragements, to Ms. Anna S. COLVIN and Mr. Wieland KUNZEL, ESC, Ingenieurs-Conseils for helping me get very useful data for my research, to Ing. Kelly JOSPITRE for facilitating my trip to Gonaives and to Ms. Helen MUGA for suggestions and ideas.

My thanks also go to numerous students and professors here at Tech, who each has taught me valuable lessons that go beyond my studies. Just having had the chance to exchange somewhat with you all made me a different person. I also want to thank my fellow Fulbright scholars and my best friend Yeliana, who are a second family for me at Tech. Finally, I wish to thank my former professors in Haiti for constant support and encouragement as well as my parents, brothers, family and friends for their unconditional love. This list would not be complete if I didn't thank Lawrence AYONG, my Florida sunshine, for his constant presence across the miles and the greatest gift of all: his love.

This work is dedicated to the people of Gonaives, to all who touched my life one way or another who made me who I am today, and to all who opened their homes and their hearts to me. This work is indubitably as much theirs as mine.

TABLE OF CONTENTS

LIST OF TABLES

LIST OF FIGURES

LIST OF ABBREVIATIONS

AMS	Annual Maximum Series
ASI	Italian Space Agency
ASTER	Advanced Spaceborne Thermal Emission and Reflection Radiometer
AVHRR	Advanced Very High Resolution Radiometer
CDERA	Caribbean Disaster Emergency Response Agency
CDMP	Climate Data Modernization Program
CEPALC	Economic Commission for Latin America and the Caribbean
CIMH	Caribbean Institute for Meteorology and Hydrology
CN	Curve Number
CNSA	National Coordination of Food Security
DEM	Digital Elevation Model
DLR	German Space Agency
DN	Digital Number
ECVH	Survey on living conditions in Haiti
FEWS NET	Famine Early Warning Systems Network
GEV	Generalized Extreme Value distribution
GIS	Geographic Information Systems
GUM	Gumbel distribution
HEC-GeoHMS	The Geospatial Hydrologic Modeling Extension
HEC-GeoRAS	The Geospatial River Analysis System Extension
HEC-HMS	Hydrologic Engineering Center - Hydrologic Modeling System
HEC-RAS	Hydrologic Engineering Center- River Analysis System
IHSI	Haitian Institute of Statistics and Computer Science
LGL	Lalonde, Girouard, Letendre & Associes
LIDAR	Light Detection and Ranging
LN2	Lognormal 2-parameter distribution
LP3	Log Pearson type III distribution
MLE	Maximum Likelihood Estimator
MLM	Maximum Likelihood Method
MOM	Method of Moments
MPCE	Ministry of Planning and External Cooperation
NASA	National Aeronautics and Space Administration
NDVI	Normalized Difference Vegetation Index
NIMA	National imagery and mapping agency
NOAA	National Oceanic and Atmospheric Administration
NRCS	National Resource Conservation Service
NWS	National Weather Service
OAS	Organization of American States
P3	Pearson Type III distribution
PCA	Principal Component Analysis
PCT	Principal Component Transformation
PDS	Partial Duration Series
POT	Peaks Over Threshold

PPC	Probability Plot Correlation
PWM	Probability Weighted Moments
RS	Remote Sensing
SCS	Soil Conservation Service
SRTM	Shuttle Radar Topography Mission
SUH	Synthetic Unit Hydrograph
SWIR	Short-Wave Infrared
T_c	Time of Concentration
TIN	Triangulated Irregular Network
TIR	Thermal Infrared
TSO	The Stationery Office
USACE	US Army Corps of Engineers
USAID	US Agency of International Development
USDE	US Department of Education
USGS	US Geological Survey
UTM	Universal Transverse Mercator
UTSIG	Unit of Remote Sensing and Geographic Information Systems
VNIR	Very Near Infrared

CHAPTER 1- INTRODUCTION AND STUDY OBJECTIVES

1.1 Study Objectives

The island of Hispaniola in the Caribbean is one of the four islands of the "greater Antilleans". The island is shared by two countries, the Dominican Republic to the east, and Haiti to the west. As are all the countries in the Caribbean region, Haiti is prone to natural disasters. Due to its geographical location and topographical characteristics (approximately 60% of the country is mountainous), flooding from hurricanes and storms is quite frequent.

Between 1968 and 2001, Haiti was affected by 30 hurricanes and 90 floods due to heavy precipitation (CNSA 2002). The effects of those natural events are aggravated by human activities, such as deforestation, and social conditions, such as rapid urbanization. These events have had an important impact on the productive sectors of the economy such as agriculture and tourism, and have severely affected the communities and the poor, in particular (WorldBank 2002). Catastrophic floods can then be viewed as barriers to sustainable development (Kundzewicz and Kaczmarek 2000), especially because the less developed a country is, the more prone it is to loss of life and economic damages (Linnerooth-Bayer et al. 2005, Dilley 2006, D'Ercole 2003). More so, D'ercole (2003) identifies Haiti as a country where there is a strong link between the level of development and the impact of natural hazards. Effective flood risk management plans consisting of forecasting and warning systems, and plans for evacuation and relief and post-flood recovery can substantially reduce losses (Kundzewicz and Kaczmarek 2000). Dilley

(2006) recognizes that one of the key challenges in promoting a shift from disaster management to risk management is to make the risk factors that cause disasters more visible.

Previous efforts to assess disaster risk in Haiti have not been extensive. CDERA (2003) notes three efforts made in hazard mapping in Haiti: an island wide seismic map done by OAS/USDE/CDMP, an island wide atlas of probable storms effects prepared by OAS/USDE/CDMP/CIMH, and a national multihazard map produced by OXFAM. Some vulnerability assessment projects have been undertaken (CNSA 2002, WorldBank 2006). However, with the exception of UTSIG (2004), FewsNet (2005) and USAID (2007), no mapping efforts were made. The scale at which information is gathered is important to decision makers. Broad scale studies often result in generalization of the spatial dimensions of risk and vulnerability, with minimization of their complexity and variability (Stephen and Downing 2001). To date, no study has quantified flood risk at a useful scale in Haiti. Recent floods in the city of Gonaives and other parts of the country (Mapou, Fond Verrettes) have increased community, government and international awareness of the need for more research.

The present study focuses on the area of Gonaives, which has been greatly affected by the 2004 precipitation event, with the goal of quantifying the flood risk to the population of the city and surrounding areas. Such studies will help in reducing human lives and goods. Similar work has been carried out in many places of the world. However, data are scarce in Haiti as in many developing countries, and the study focuses on the

uncertainties accompanying the analysis and on possible refinements. Although scarcity of data is always an issue in scientific research, in countries such as Haiti, the problem deepens. Much of the spatial data freely or readily available for countries of the developing world comes from remote sensing (RS). Field data and ground truth are used as complements to satellite images. However, in many cases, field investigations may not be possible, either because of lack of financial and material resources, geographical location or political reasons. One then has no other choice than to make the best use possible out of the remotely sensed data. Even though geographical information systems (GIS) and RS have been around for some time, increased computational capabilities and more detailed and readily available data explains the growing interest of these fields, especially in developing countries (Hudson and Colditz 2003; Hudson et al. 2006; Mosquera-Machado and Ahmad 2007). It is then important to assess the performance of coarse GIS and RS data with no ground truth and to develop ways to alleviate arising uncertainties. This study proposes to use a combination of RS, GIS analysis, and hydrologic and hydraulic modeling for flood risk mapping of low land areas in "data-poor" regions. It is shown that this set of tools can help to alleviate uncertainties to some extent. However, with the notable exception of Overton (2005) who combined hydraulic modeling, GIS and RS with the support of field data, RS has not been widely used to ascertain the accuracy of floodplain delineation done using GIS and hydraulic models (HM). In developing countries where resources are scarce and the political or economical situation may not permit lengthy field research, GIS, RS and HM may be a useful combination for the preparation of preliminary flood risk maps necessary for effective flood risk management.

The goal of this study is to investigate the performance of GIS and RS tools in conjunction with hydraulic models in the absence of ground truth. Software tools such as HEC-HMS (Scharffenberg et al. 2006), HEC-RAS (Brunner et al. 2001), ArcGIS 9, HEC, GeoRAS (USACE 2005), and ERDAS IMAGINE 9.1 are used. The current study specifically addresses the following challenges in flood hazard quantification: 1) uncertainties in rainfall frequency analysis; 2) uncertainties in watershed modeling; 3) uncertainties in Manning's roughness; and 4) their effects on the resulting floodplain delineation. This study also provides some guidelines for flood risk mapping in developing countries.

Chapter 2 reviews previous watershed studies using GIS and remote sensing; Chapter 3 provides background information about the study area; Chapter 4 presents the rainfall frequency analysis; Chapter 5 discusses the rainfall-runoff modeling; and Chapter 6 delineates the floodplain. Chapter 7 assesses flood risk and the vulnerability of the population of Gonaives city and surrounding areas; and Chapter 8 summarizes conclusions and recommendations.

CHAPTER 2- LITERATURE REVIEW

2.1 Introduction

Flooding has always been a cause of concern for humanity. Severe floods occurring in areas occupied by humans can create natural disasters involving significant loss of human life and property, as well as serious disruption to the ongoing activities of large urban and rural communities (Smith and Ward 1998). Flood risk management focuses on flood prevention, preparedness, mitigation and recovery. Flood risk maps are key tools in flood risk management. They are drawn as a combination of a flood hazard map and a population vulnerability map. Most flood hazard maps show floodplains with their associated risk level (e.g., the 100-yr flood). A floodplain is the normally dry land area adjoining rivers, streams, lakes, bays or oceans that is inundated during flood events. Although there is no real basis for the choice of the 100-yr flood, and flood hazard assessment in the U.S. focuses on the 100-yr flood, a more rational approach would consider impacts of both less and more severe floods.

TSO (2006) recognizes six types of floods : 1) from rivers, 2) from the sea, 3) from land, 4) from groundwater, 5) from sewers, and 6) from reservoirs, canals or other artificial sources.

Although most floods are more or less natural phenomena, flood risk is largely of human origin, i.e., if there are no human settlements in an area, there is no flood risk (Smith and Ward 1998). With varying levels of flood hazard and human vulnerability, the

population is exposed to varying levels of risk. Flood risk maps typically quantify risk and identify at-risk areas using a hierarchical index (i.e., from lowest to highest or highest to lowest risk).

Traditional floodplain mapping involves data collection including topographic maps, flow data if a gauging station is nearby, rainfall data if flow data are not available, and surveyed cross sections and channel roughness estimates at a number of points along the stream (Chow et al. 1988). Recent developments in GIS and remote sensing are offering alternative procedures for topographic data. For instance, USGS has used LIDAR capabilities to produce a high resolution digital elevation model (DEM) of 1.5m grid for inundation mapping in Honduras (Kresch et al. 2002; Mastin et al. 2002).

2.2 Watershed Modeling

GIS now routinely provides a set of spatial tools to water resources practitioners. Most floodplain delineation work involves the use of GIS with a digital elevation model (DEM) coupled with hydraulic software. Willems (2002) made use of a 4m DEM with Mike-11, the Danish hydraulic software, to produce floodplain maps in Belgium. Bradbrook et al. (2005) used a 5m DEM and a two-dimensional floodplain hydraulics model for England and Wales. Wonkovich (2007) investigated the use of high resolution DEMs for floodplain mapping using HEC-RAS developed by the US Army Corps of Engineers (USACE). Mosquera-Machado and Ahmad (2007) coupled rainfall data, stream flow data, surveyed cross sections, and a 20m DEM produced from topographic maps to obtain a floodplain map using GIS and HEC-RAS for the Atrato River near

Quibdo in Colombia. Gall et al. (2007) used USGS's stream flow model (SFM) and FEMA's natural hazard loss estimation software HAZUS with 30m DEM to delineate floodplains.

The use of DEMs with hydraulic software is well established. However, 30m DEM and other low resolution DEMs are often reported not to perform well for floodplain management, and better resolutions are advised (Gall et al. 2007). Effects of DEM resolution on estimates of main channel length, slope, area and time of concentration are also reported (Hill and Neary 2005; Moglen and Hartman 2001; Singh 2004).

Even though the most popular hydraulic models perform only one-dimensional analyses (HEC-RAS, Mike 11 and others), some two-dimensional models have been developed. However, their weakness is that they are very time-consuming and require more data. Bates and De Roo (2000) proposed a model that merged the simplicity of a one-dimensional model and the accuracy of a two-dimensional model.

Noman et al. (2001) reviewed available tools and procedures for floodplain delineation from DEMs as well as their limitations. They found two major issues: 1) inadequate selection criteria for water level points for interpolation, and 2) poor consideration of floodplain connectivity. Noman et al. (2003) proposed an improved process for floodplain modeling. Whiteaker et al. (2006) coupled HEC-HMS, HEC-RAS, and ArcGIS to produce a floodplain map of Rosillo Creek in Texas. The coupling of HEC-HMS, HEC-RAS and ArcGIS is now widely done in the United States.

2.3 Floodplain Delineation

Remote sensing uses measurements of the electromagnetic spectrum to characterize the landscape, infer its properties, and in some cases, actually measure hydrologic state variables (Melesse and Graham 2004). The use of remotely sensed data is growing. Islam and Sado (2002) used three NOAA AVHRR images to delineate the floodplain for three hydro-meteorological events in Bangladesh; a DEM was superimposed onto a flood occurrence map to extract flood depths. Hudson and Colditz (2003) used Landsat images to delineate floodplains in Mexico. Wang (2002) offers examples of success stories using satellite images. One reason for the popularity of RS may be that more and more of the data is becoming freely available. Websites such as the global land cover facility of the University of Maryland (http://glcf.umiacs.umd.edu/index.shtml) now offer a wide range of free data. A list of geospatial data available for Haiti has been compiled by Quinones et al. (2006).

Although the use of remotely sensed data for floodplain delineation requires past occurrence of at least one significant flood event recorded by a satellite, this is an alternative procedure to hydrologic and hydraulic modeling as it is less time consuming and less costly (Wang 2002).

2.4 Flood Risk Assessment Methods

Risk is commonly referred to as the product of hazard (the physical agent and its impact) and vulnerability (the susceptibility to damage or injury) (Alexander 1997). Accordingly, flood risk assessment involves two steps: hazard assessment and vulnerability assessment. Hazard assessment deals with the characteristics of the event itself in terms of magnitude and frequency. Vulnerability assessment takes into account the effects of the event on the population, considering social, economical, and environmental aspects and impacts on transportation infrastructure.

Flood hazard and vulnerability assessments are made in a variety of ways. Islam and Sado (2002) used flood depth and frequency of occurrence of floods to produce a flood hazard map for Bangladesh. Rao et al. (2005) developed a vulnerability index for the east coast of India using population density, land use/land cover, distance from the coast, ground slope and location with respect to cyclone tracks. D'Ercole (1996) used a variety of factors to quantify vulnerability to volcano activity: population density, risk perception, knowledge of means of protection, distance to volcano, socio-economical level, professional activity, urban/rural/suburban, sex, age, time of residence and others.

CHAPTER 3- BACKGROUND INFORMATION

3.1 Climate, Topography and Hydrological Network

The island of Hispaniola comprises two countries: the Republic of Haiti and the Dominican Republic. The island lies within the hurricane belt and is subject to a variety of natural disasters. Between 1968 and 2001, Haiti has recorded about 30 hurricanes and 90 inundations due to heavy precipitation. Mora (1995) and USAID (2007) each shows a map of most known historical storms passing through the island. Even though the images differ somewhat in terms of the frequency of hurricanes in the northern and southern part of Haiti, they both show that the entire country is subject to the effects of hurricanes. O'Connor et al. (2003) located large flood events in the US and postulated why these areas were subject to such events. Their conclusions show that Puerto Rico and Hawaii islands recorded relatively high flows because "they are mountainous areas in the midst of the tradewind belt, where moisture-laden tropical storms and hurricanes are intercepted and forced upward by the island masses, triggering orographic and convective uplift and enhanced precipitation" (O'Connor et al., 2003 p. 8). This statement also applies directly to Haiti.

In Haiti, there are 30 hydrographic basins and zones which drain from the mountains to the coastal waters (USACE 1999). These were ranked in terms of vulnerability by (USAID 2007). The 30 major basins were ranked according to their topography, climate, ecological importance, productive infrastructure, and settlement location and density. Results were presented by type of vulnerability and in the second group which

focuses on human life losses and infrastructure; the Gonaives watershed appears second in terms of high vulnerability.

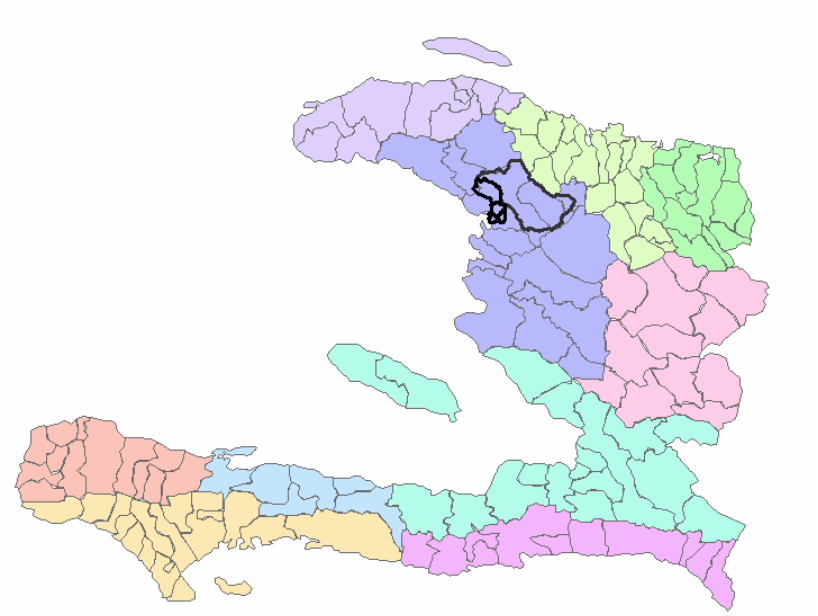

Figure 1: Ten departments of Haiti and Gonaives basin in the Artibonite department , source IHSI (2003)

The Gonaives watershed, outlined in Figure 1, is located within the Artibonite department of Haiti. It comprises two counties (administrative units) entirely and occupies approximately a total of 600 km^2. It is formed by four major tributaries: Bayonnais, Ennery, Branle and Deux-Bassins which are, respectively, 21%, 40% and 22% and 11% of the total watershed area (see Figure 2). After the tributaries have merged, the river bears the name of Quinte River until it ends in the sea. It is a narrow river (approximately 5-8 meters wide at the bottom and 20m wide at the top width) next to the bridge (Pont Gaudin), which is located on the National Road #1 (Route Nationale #1). The Quinte River is intermittent along most of its length, carrying water only during the rainy season and the first part of the dry season (Taylor and Lemoine 1949). The Quinte

River does not usually run through the city of Gonaives (perhaps due to diversion) but goes instead about 1km south of the city.

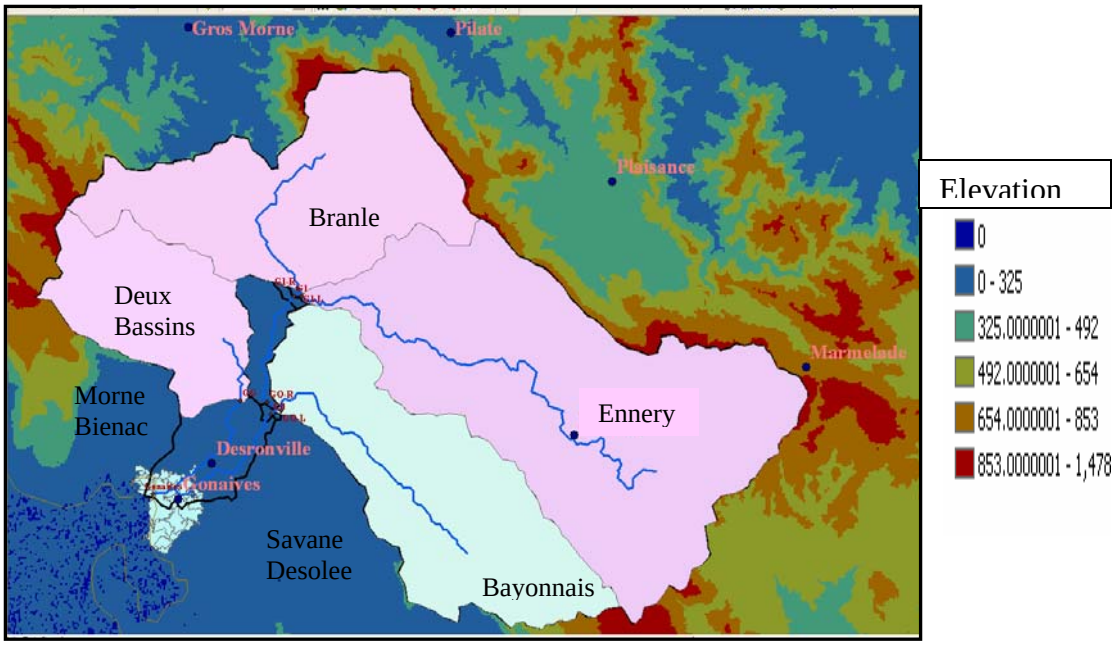

Figure 2: The Gonaives watershed and hydrological network

The topography of the upper watershed (Branle, Ennery, Bayonnais, Deux-Bassins) is dominated by mountainous formations, and small valleys. This contrasts with the lower watershed, which is an alluvial plain near Gonaives. The highest average slope (6%) is found in the Ennery subbasin. The main river of the Gonaives watershed is the Quinte River which is formed by the confluence of the Branle and Ennery rivers. Further south in the central part of the plain, the Quinte River is joined by the DeuxBassins and Bayonnais rivers. The main thalweg of the Quinte River is 49.1 km long and starts at an elevation of 874m, with an average slope of 1.69%.

3.2 Socio-Economical Information

The city of Gonaives covers 10 km^2 and has 104,825 inhabitants (IHSI, 2003). It is the third most populated city in Haiti, after Port-au-Prince and Cap-Haitian . The main source of income of the population in the Gonaives county is agriculture (rice, plantains, onions, carrots, pepper, and tomatoes are found in the lower part of the watershed; corn, sweet potatoes, manioc, and beans are found in the upper part). The second largest source of income is stock breeding (cows, pigs) (Prophete 2006).

The population (urban and rural) is increasing in Haiti; however there is a sharp increase in the urban population compared to the rural. Rural population percentage has decreased from 87.8% in 1950 to 59.8 % in 2003, while the urban population has tripled (UTSIG 2004).

UTSIG (2004) reports that 55% of the population are living under the extreme poverty line (< 1 US$ a day), and 71% (<2 US$ a day) are under the poverty line. Approximately 20%, 56% and 58% of the households in metropolitan, urban and rural areas are extremely poor (WorldBank 2006). With a mean annual growth rate of 2.2% from 1982 to 2003 (UTSIG 2004), and a youth percentage of 50% (WorldBank 2006), it is likely that the population will continue to grow and therefore increase the pressure on the environment (land, forest, fresh water).

In 2004, the Ministry of Planning and External Cooperation (MPCE), through its unit of remote sensing and geographic information systems (UTSIG), produced a relative

poverty (access to basic services) map of Haiti. According to this map, the county of Gonaives has moderately low access to education, extremely low access to health and sanitation, extremely low access to water and overall, the county is ranked low in terms of access to basic social services.

3.3 Precipitation

The rainy and dry seasons are quite distinctive through the monthly rainfall data as shown in Table 1. Seven rainfall stations (Gonaives, Desronville, Ennery, Gros Morne, Marmelade, Pilate and Plaisance) were chosen for this analysis. Gonaives and Desronville receive the least precipitation throughout the year (500-600mm), while Gros Morne, Ennery, Marmelade, Pilate and Plaisance, located in the upper part of the watershed, receive significantly more (1100-1900mm).

Table 1: Average Monthly precipitation (mm) (Source: LGL, 1977)

Stations	Gonaives	Ennery	Gros Morne	Desronville	Marmelade	Plaisance	Pilate
Jan	9.8	20.2	24.6	42.0	74.1	76.6	63.8
Feb	8.9	22.2	36.1	20.5	69.9	69.0	74.0
March	13.2	28.3	35.3	25.1	67.6	67.0	72.8
April	13.0	78.1	89.9	27.2	129.4	127.4	136.7
Mai	56.5	196.8	225.2	67.7	252.4	246.4	245.7
June	92.3	191.6	200.0	102.3	202.6	207.4	188.2
July	81.6	105.3	120.1	81.4	132.2	164.7	140.0
Aug	74.9	129.0	142.9	86.9	173.0	185.2	170.5
Sept	61.6	167.9	171.5	77.7	193.3	223.0	202.3
Oct	53.1	141.3	139.6	42.4	208.7	214.5	199.0
Nov	14.6	82.7	109.2	40.2	174.0	215.8	187.5
Dec	3.8	24.0	50.3	13.4	104.6	124.5	101.9
Total	483.3	1187.4	1344.7	626.80	1781.8	1921.5	1782.4

The rainy season starts in May and ends in October. Most of the flood events occur during the rainy season, particularly in August and September. Those are the months when the soil is already wet from previous rainfall events, the groundwater table is high, and the sea temperature is also high, triggering storms and hurricane events which move primarily in the east-west direction. During such events, it is likely that entire watersheds are going to be wetted to an extent where infiltration becomes low. Excess precipitation then runs off down bare steep slopes, increasing water depth in river channels and possibly causing them to go out of their banks and into alluvial plains where the cities lie. In the case of the Gonaives watershed, the population living in the low land areas may not be aware of a storm intensity in the higher elevations of the watershed since the orographic effects cause Gonaives to receive much less rainfall than Ennery or places such as Gros Morne, Pilate, Plaisance and Marmelade that may receive heavy rainfall due to windward effects. This could also explain why during the 2004 event, Gonaives only recorded 40mm while Ennery recorded 261mm of precipitation.

3.4 Impact of floods

Haiti was identified by D'ercole (2003) as being one country of Latin America where the number of disasters and the impacts of disasters are relatively high. In September 2004, the city of Gonaives experienced severe flooding that caused 265 million gourdes (approximately 26.5 million US$) of direct damages, with 80% of the city population affected (CEPALC, 2005). The flood disaster had much impact on the population:

agricultural production, stock farming, irrigation infrastructure, electricity, water infrastructure, housing and environment (see Table 2). The social sector (housing, health, education) and the production sector (agriculture, industry, commerce, stock breeding) registered, respectively, 47% and 20% of the damages (see Figure 3). USACE (1999) describes as follows the effects of Hurricane Georges in 1998. The same could be said for Gonaives.

> "The loss of these crops and livestock will resort in short term food shortages. These losses represent a staggering blow to a country where agriculture provides one third of the Gross National Product (GNP). Flooding contaminated the water supply and the lack of uncontaminated water is expected to produce deadly waterborne diseases such as cholera and dengue fever." (USACE, 1999, p.3)

Table 2: Direct Loss from Hurricane Jeanne (Millions of Gourdes) source: CEPALC, 2005

Environment	Emergency	Production	Social	Infrastructure	Total
127.4	1771.1	1891.1	4531.6	1220.7	9541.9

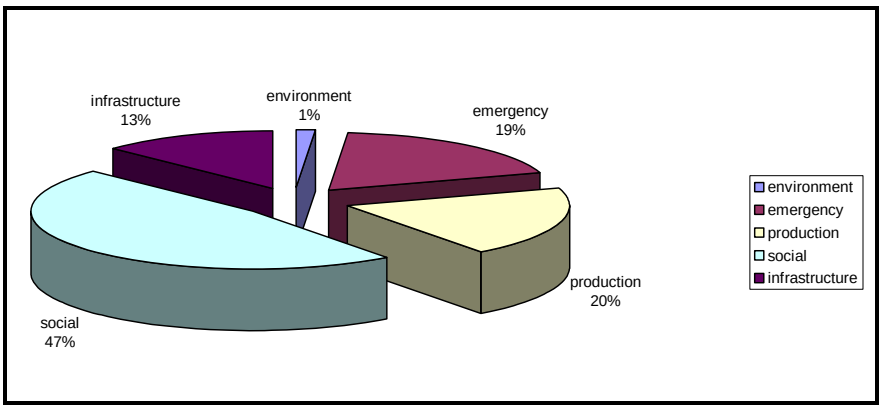

Figure 3: Sectors impacted by hurricane Jeanne, September 2004.

The subsequent chapters will assess the flood risk in the Gonaives area. The graph below summarizes the procedure that will be used.

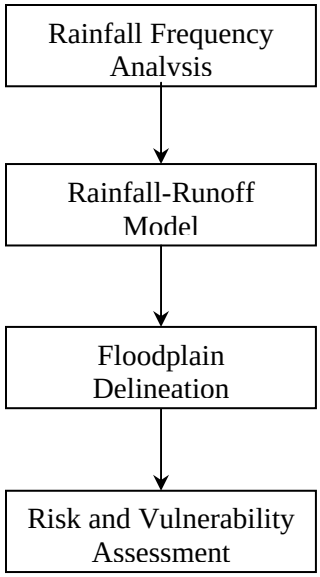

Figure 4: Study procedure for flood risk and vulnerability assessment.

CHAPTER 4- RAINFALL FREQUENCY ANALYSIS

4.1 Introduction

The term "frequency analysis" refers to techniques whose objective is to analyze the occurrence of hydrologic variables within a statistical framework (Ponce, 1989). Frequency analysis techniques are applied here to seven rainfall stations in Haiti located in the vicinity of the Gonaives watershed. Average monthly precipitation at those stations (Desronville, Ennery, Gonaives, Gros Morne, Marmelade, Pilate and Plaisance) is shown Table 3. The shortest record period is 21 years, and the longest is 46 years.

Table 3: Summary of daily rainfall data at 7 sites

NAME	Number of years	Period of record	Absolute daily max (mm)
Desronville	21	1964-1967; 1969-1971; 1976-1989	74.6
Ennery	46	1923; 1925; 1931; 1939-1962; 1964-1967;1977-1988; 2002-2004	261
Gonaives	46	1949-1951; 1953-1956; 190-1998	99.5
Gros Morne	36	1923; 1925; 1931-1932; 1939-1968; 1978-1979	160
Marmelade	29	1923; 1925; 1931; 1939-1940; 1942-1958; 1960-1961; 1964-1968	136
Pilate	26	1923; 1925; 1948-1951; 1954-1970; 1984-1986	188
Plaisance	40	1923; 1925; 1931-1932; 1940-1951; 1965-1966; 1975-1996	295.9

The data was analyzed for gross errors and trends in precipitation. The years of relatively low annual precipitation correspond to years of incomplete records; those years were discarded unless the maximum precipitation was representative of other years or occurred during the rainy season.

The goal of frequency analysis is to identify a suitable probability distribution for each station in order to estimate extreme quantiles. Although the estimation of flood (precipitation) risk would seem to be a straightforward analysis, the lack of a physical basis for determining the form of the underlying flood (precipitation) frequency distribution and the necessity of evaluating flood (precipitation) risk for return periods that exceed the length of the observed record makes it more complex (Lettenmaier et al. 1987).

There are two general approaches available for modeling floods, rainfall and many other hydrologic series: annual maximum series (AMS), where one considers the largest event in each year; and partial duration series (PDS), or the peaks over threshold (POT) approach, which includes all peaks above a truncation or threshold level (Maidment 1993). According to Linsley et al. (1992), the two series give nearly the same recurrence intervals for larger events. However, Linsley et al. (1992) advise not using PDS for the frequency of rare events. Further, the PDS framework has the added disadvantage that an appropriate threshold or truncation level must be which ensures the peaks are independent. Therefore, this study uses the AMS method.

In the following analysis, four commonly used distributions are considered as models of the rainfall data: two-parameter lognormal (LN2), Gumbel (GUM), Generalized Extreme Value (GEV) and Log-Pearson type III (LP3). The normal (N) or Gaussian distribution is the most commonly used distribution in statistics. However, the two-parameter lognormal (LN2) distribution, which is based on the normal distribution, is generally

preferred as a model for hydrologic variables. As the annual flood (precipitation) is the largest flood (precipitation) during a year, one might expect its distribution to belong to the set of extreme value distributions. These are the distributions obtained in the limit, as *n* becomes large, by taking the largest of *n* independent random variables. The extreme value type 1 distribution is often called the Gumbel distribution. The GEV distribution is a more versatile three-parameter extreme value distribution, which converges to the Gumbel distribution when the third parameter (shape) is zero. Another family of distributions used in hydrology is based on the Pearson type 3 (P3) distribution. The log-Pearson type 3 (LP3) distribution describes a random variable whose logarithms have a Pearson type 3 distribution. The LP3 distribution is a flexible three-parameter distribution capable of taking many different shapes and has been widely used in many countries for modeling original (untransformed) annual flood series.

For the estimation of LN2 parameters, the Maximum Likelihood Method (MLM) is preferred to the method of moments (MOM). Stedinger (1980) shows that MLM is a competitive method for parameter estimation of the LN2 distribution for samples of 25 or more. However, MLEs do not perform that well for Gumbel or GEV distributions, and alternatives such as L-moments are preferred (Hosking 1990; Landwehr et al. 1979). Therefore the L-moment method was used to estimate the parameters for Gumbel and GEV. A log space MOM procedure is used for LP3. Griffis and Stedinger (2007b) demonstrate that the log space MOM procedure is competitive with methods such as MLEs. They observe that log space MOM estimators significantly outperform MLEs for small samples (i.e n=25) with log space skews within ±0.5. However, as the sample size

increases, the efficiency of the MLEs greatly improves. In samples of n=100 and for skews within ±0.5, there is less than a 10% difference in the efficiency of the MLEs and the log space MOM estimators. Similar results were obtained by Nozdryn-Plotnicki and Watt (1979). Overall, the simple log space MOM without regional skew information performs quite well compared to MLEs. Griffis and Stedinger (2007b) also demonstrate that the efficiency of the log space MOM procedure for LP3 parameter estimation is significantly improved when an informative regional skew is employed; this method is commonly employed in flood frequency analysis (IACWD, 1982; Griffis and Stedinger 2007a). Unfortunately, regional information is not available for this study; however, the simple MOM procedure without regional information is more consistent with the methods used for the other distributions.

The following table summarizes the parameter estimation methods chosen. For more information about the density function of the distributions and methods of parameter estimation, please, refer to Chapter 18 of the *Handbook of Hydrology* by Maidment (1993).

Table 4: Parameter Estimation Method for each distribution

Distribution	Parameter estimation	Reference(s)
LN2	MLM	Stedinger 1980
GUM	L-moments	Landwehr et al. 1970 Hosking, 1990
GEV	L-moments	Landwehr et al. 1979
LP3	MOM	Griffis and Stedinger (2007b) Nozdryn-Plotnicki and Watt (1979)

4.2 Goodness of Fit Test

To assess the goodness of fit of each distribution the probability plot correlation (PPC) test (Filliben 1975; Vogel 1986; Vogel and McMartin 1991) will be used. A 5% significance level is considered acceptable for the use of the PPC test.

PPC Test

The PPC test introduced by Filliben (1975) was originally a test for normality even though the author pointed out that it could be developed for other distributions. Vogel (1986) extended the test to suit the Gumbel distribution. Chowdhury et al. (1991) considered the PPC test for the GEV distribution, and Vogel and McMartin (1991) for the P3 distribution. Essentially, the PPC test is a measure of linearity of a quantile-quantile plot; the data is concluded to have come from the specified distribution if the correlation coefficient (ρ) exceeds a critical correlation (ρ_c) value corresponding to a specified significance level (Vogel and McMartin 1991). A 5% significance level is usually considered acceptable and is used by most federal agencies. It is means that on average, 95% of the same sized samples drawn from the distribution had a correlation coefficient higher than $\rho_{c.}$ In practice, the ρ_c value is read from tables in the available literature.

In order to get the best quantile estimates for construction of a probability plot, one must be careful in his/her choice of plotting positions (Harter 1984). For LN2 and LP3 distributions, Blom plotting positions $\left(\frac{i-3/8}{n+1/4}\right)$ are recommended, while Cunnane

plotting positions $\left(\frac{i-0.40}{n+0.2}\right)$ are recommended for GEV, and Gringorten plotting positions $\left(\frac{i-0.44}{n+0.12}\right)$ are recommended for the Gumbel distribution. In estimating plotting positions for the empirical distribution, the Weibull formula $\left(\frac{i}{n+1}\right)$ will be used (Maidment 1993).

4.3 Choosing a Parent Distribution

Table 5 summarizes the results of the PPC tests for each station with shading indicating that the distribution is acceptable. Figure 5-Figure 11 provide a graphical comparison of the distributions for each station. The results indicate that the LN2 and Gumbel distributions do not provide a good fit to the data for Desronville, Ennery or Plaisance, but they are suitable for all of the other rainfall stations. Critical values for the PPC test with the GEV distribution are not available for Desronville or Ennery. However, the lower (upper) bound of the critical correlation coefficient for Desronvilles (Ennery) has been identified. While the critical correlation coefficient for Desronville is unknown except that it is greater than 0.953, the sample correlation coefficient obtained at the station is so large that is most likely a significant result. According to the critical correlation coefficient, both GEV and LP3 distributions provide a good fit to all the stations.

Table 5: Correlation Coefficient and critical value at 0.05 significance level

Stations	GEV		LN2		Gumbel		LP3	
	ρc	ρ	ρc	ρ	ρc	ρ	ρc	ρ
Desronville	>0.953	0.992	0.95	0.92	0.939	0.909	0.940	0.987
Ennery	<0.91	0.991	0.974	0.924	0.939	0.906	0.960	0.985
Gonaives	0.958	0.985	0.974	0.990	0.962	0.985	0.970	0.991
Gros Morne	0.958	0.987	0.960	0.98	0.957	0.985	0.955	0.988
Marmelade	0.961	0.991	0.962	0.991	0.961	0.991	0.940	0.992
Pilate	0.945	0.991	0.9571	0.992	0.9458	0.990	0.960	0.992
Plaisance	0.915	0.985	0.9715	0.965	0.9594	0.939	0.970	0.981

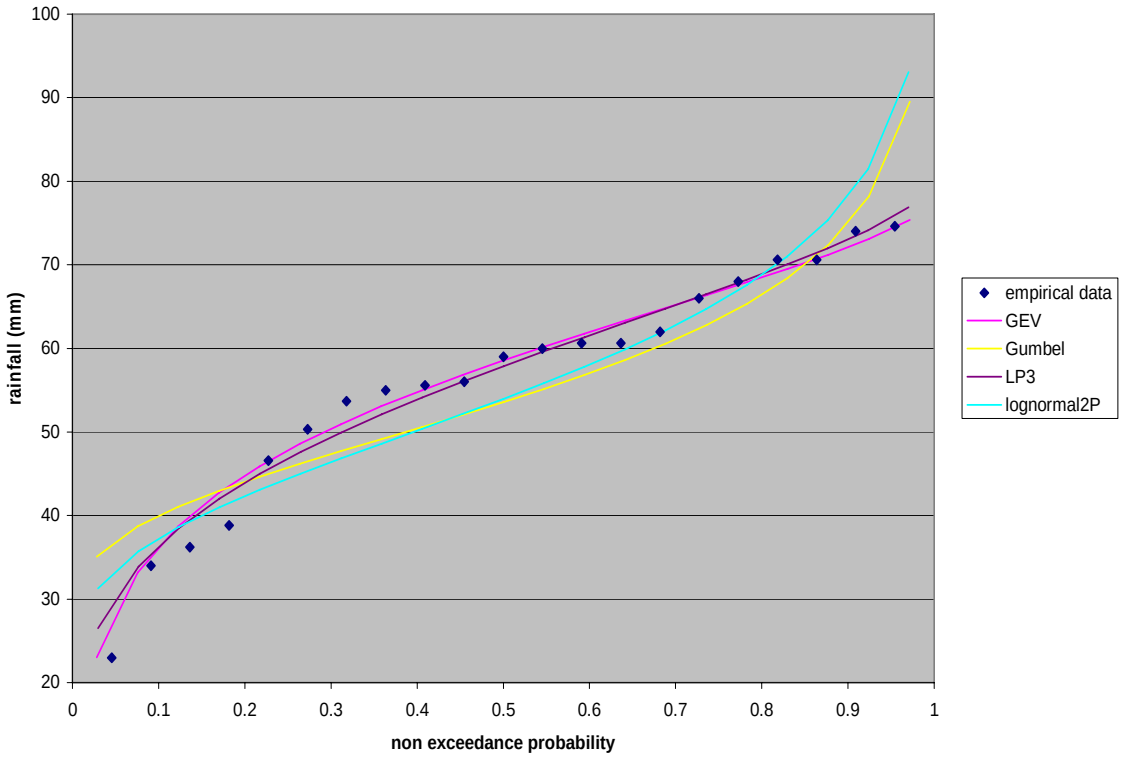

Figure 5: Distribution comparison for Desronville station

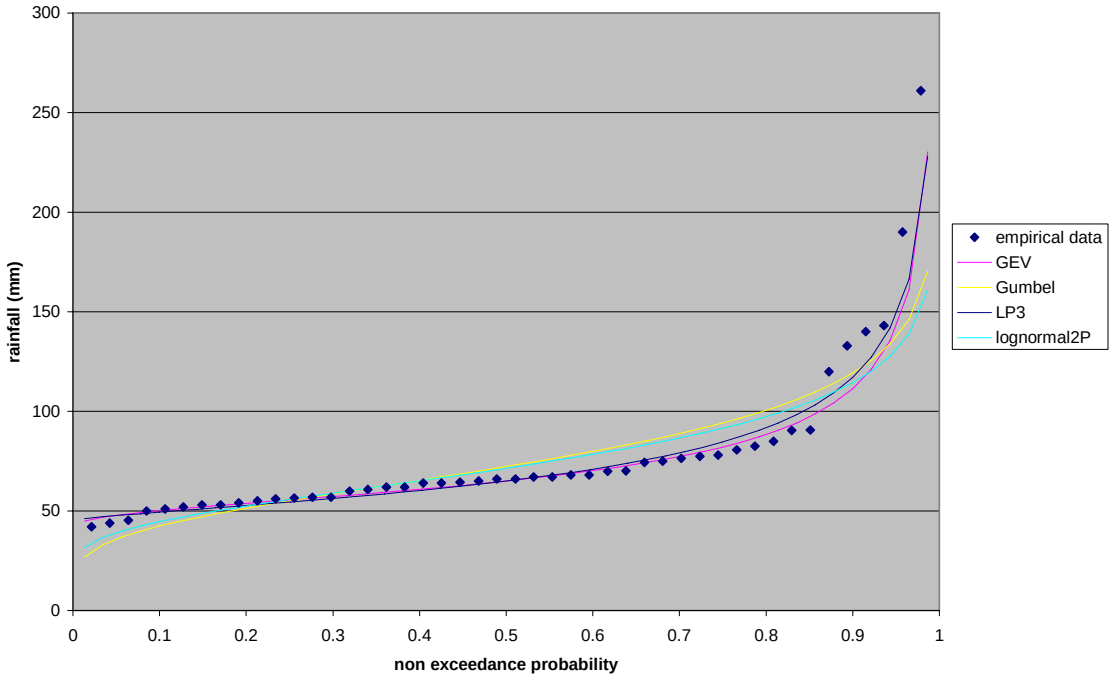

Figure 6: Distribution comparison for Ennery Station

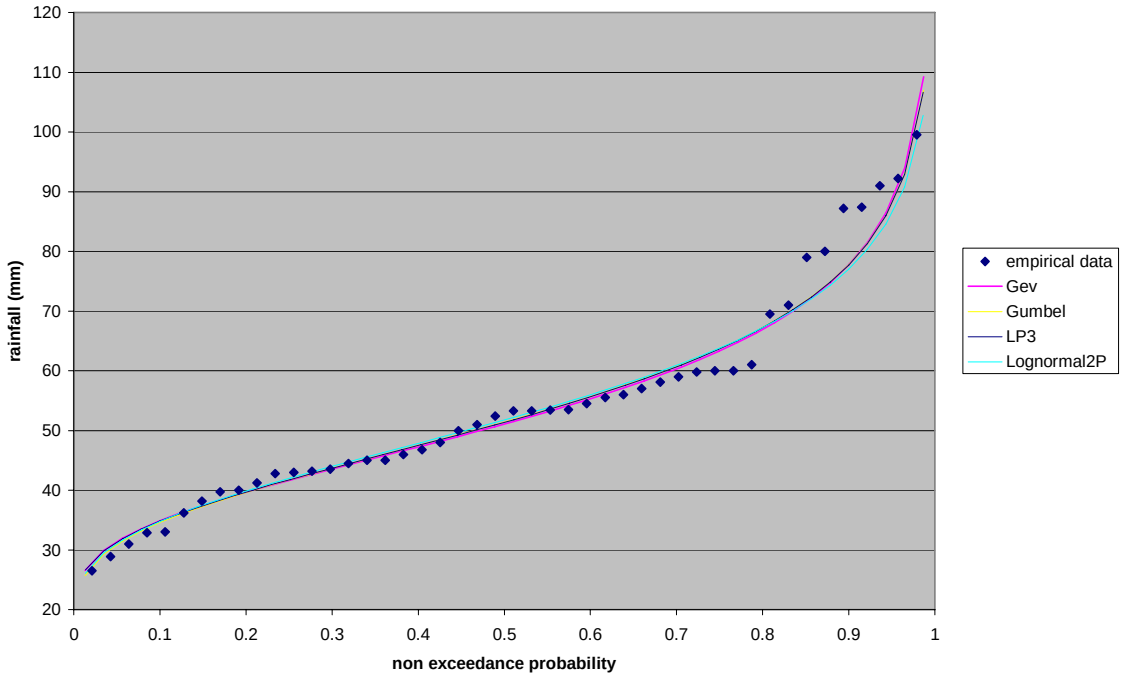

Figure 7: Distribution comparison for Gonaives station

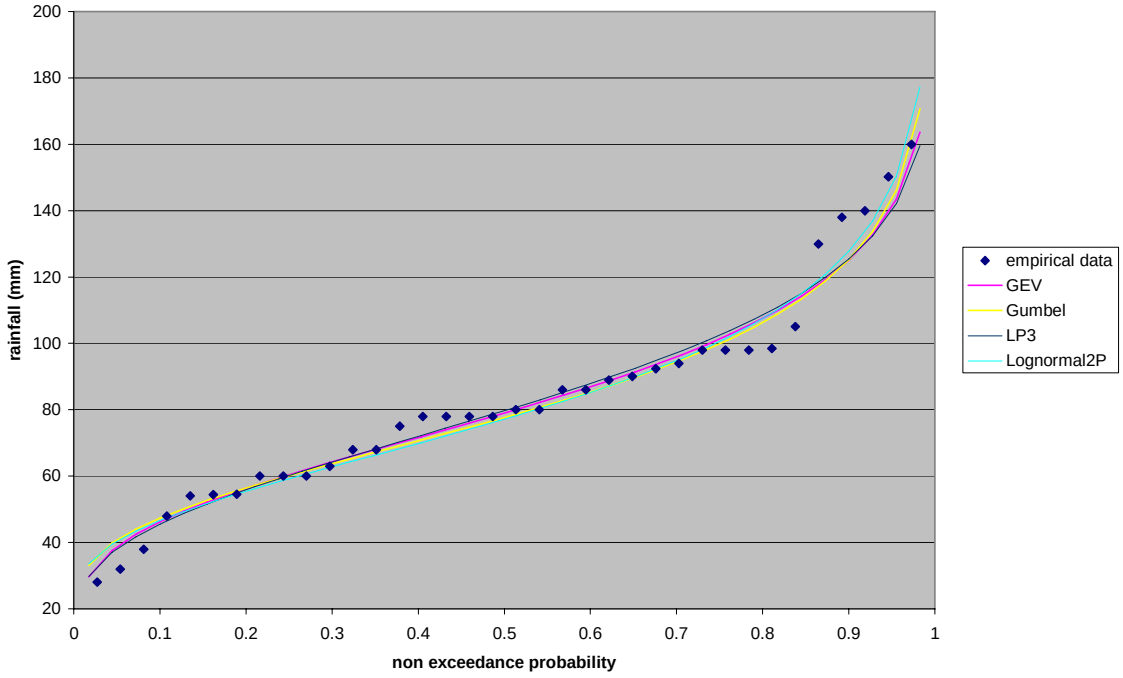

Figure 8: Distribution comparison for Gros-Morne station

.

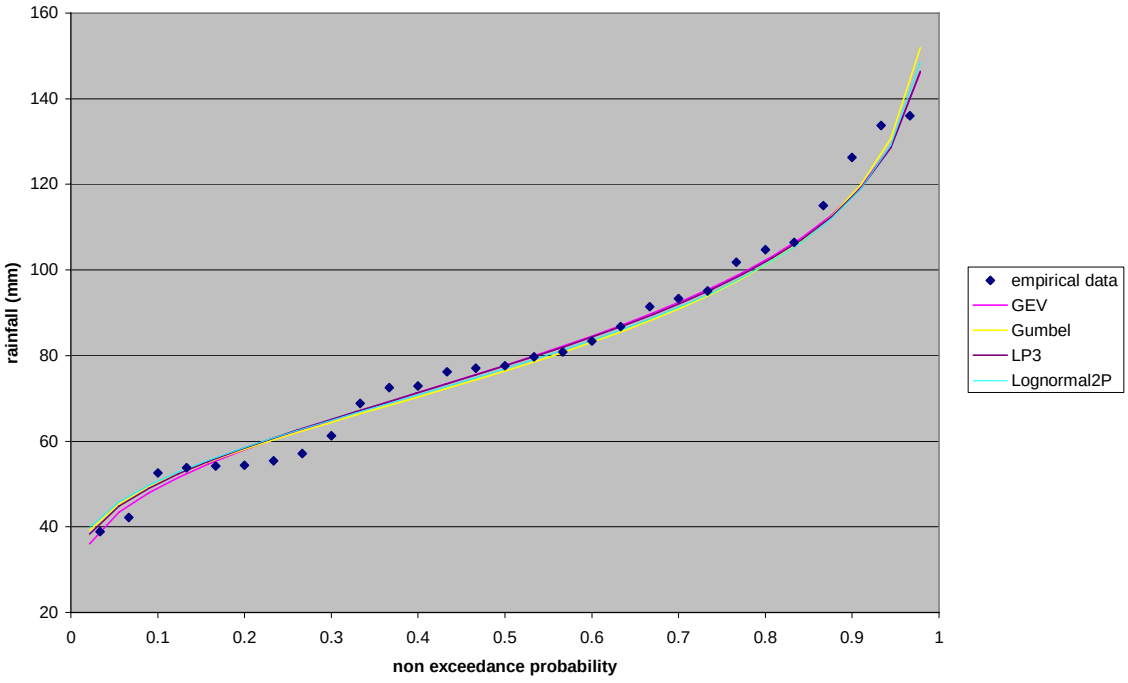

Figure 9: Distribution comparison for Marmelade station

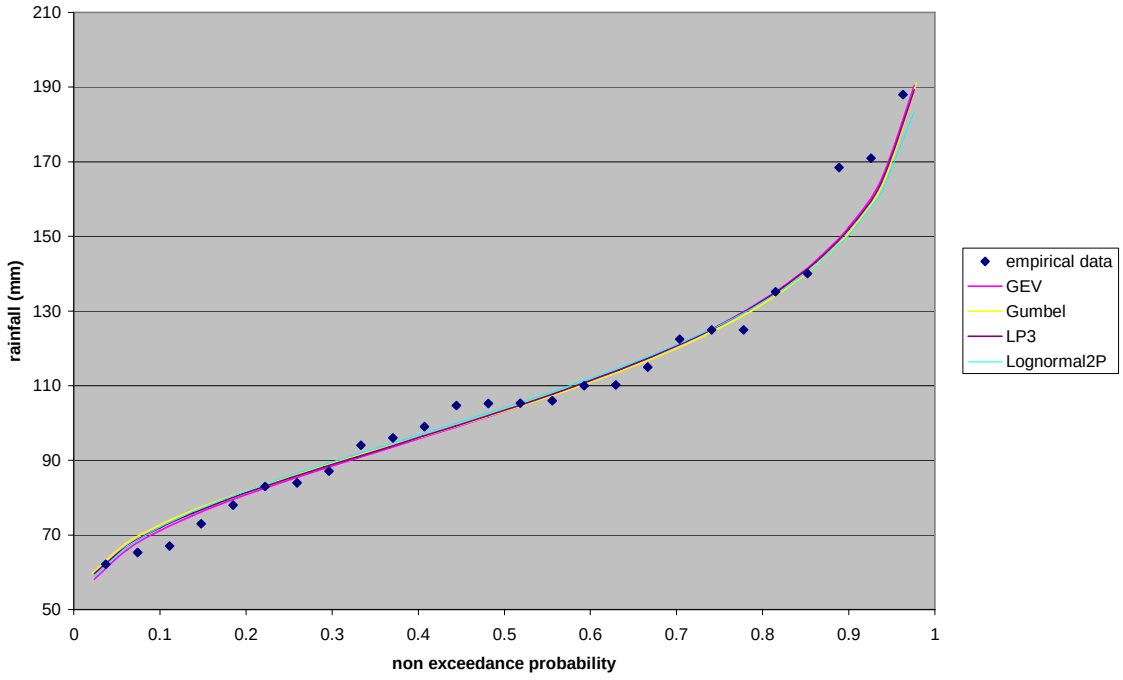

Figure 10: Distribution comparison for Pilate Station

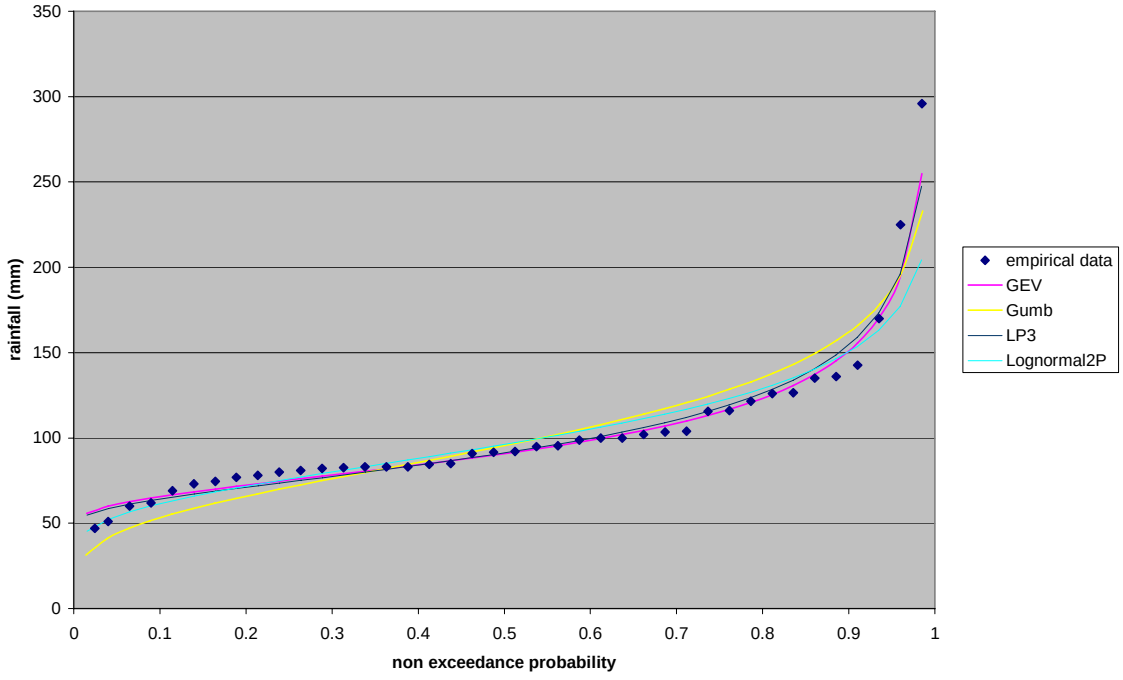

Figure 11: Distribution comparison for Plaisance station

Of interest is a common distribution to apply to all of the stations. The results above suggest that either GEV or LP3 are reasonable. In order to choose between the two distributions, the value of the correlation coefficient could be compared for the GEV and LP3 distributions for each station, as a larger coefficient of correlation indicates a better fit to the data. However, the correlation coefficients for LP3 reported in Table 5 were calculated in log space since the test in Vogel and McMartin (1991) applies to the logarithms of the data which are assumed to follow a P3 distribution. Instead of comparing the values of the correlation coefficient themselves, it would be more appropriate to compare their associated significance levels (Vogel and Kroll, 1989). However, Chowdhury et al. (1991) and Vogel and McMartin (1991) do not provide enough information to do so. From their tables or figures only critical values of the correlation coefficient can be found for fixed significance levels (usually 0.01, 0.05 or 0.10). Therefore, we will consider an alternative method that assumes the same growth rates for the two distributions and compares the percent the difference between the observed and critical coefficient of correlation, since the higher this percentage, the higher the significance level. It also gives us a distribution-free basis for comparing the two distributions. However, Ennery and Desronvilles were not included in the calculations since the critical coefficient of correlation is unknown for those two stations. The results in Table 6 show clearly that GEV outperforms LP3 on a regional basis. (Note that the regional averages reported in the table omit the results for Desronville and Ennery as the critical correlation coefficients for the GEV distribution are not known at these stations.) As at-site quantiles can be more uncertain, a regionalization procedure using GEV as the parent distribution is appropriate.

Table 6: Choice of a regional distribution

Stations	sample size	GEV			LP3		
		ρc	ρ	$(\rho - \rho_c)/\rho_c$	ρ_c	ρ	$(\rho - \rho_c)/\rho_c$
Gonaives	46	0.958	0.985	0.0282	0.97	0.991	0.0216
Gros Morne	36	0.958	0.987	0.0303	0.955	0.988	0.0346
Marmelade	29	0.961	0.991	0.0312	0.94	0.992	0.0553
Pilate	26	0.945	0.991	0.0487	0.96	0.992	0.0333
Plaisance	40	0.915	0.985	0.0765	0.97	0.981	0.0113
Regional average				0.0430			0.0312

Table 7 presents the at site characteristics of the GEV distribution obtained using the L-moments parameter estimation method for all the rainfall stations

Table 7: GEV at-site parameters for all the stations

	k	α	ξ
Desronville	0.63	15.55	53.46
Ennery	-0.43	13.59	59.64
Gonaives	-0.03	13.59	46.07
Gros Morne	0.07	26.88	69.30
Marmelade	0.08	23.37	69.31
Pilate	0.01	26.54	93.4
Plaisance	-0.27	22.20	82.22

The GEV cumulative density function and quantile estimates are given by:

$$F(x) = \exp -\left[1 - k\frac{(x-\xi)}{\alpha}\right]^{1/k}, \text{ k}\neq 0$$

$$x_p = \xi + \frac{\alpha}{k}\left[1 - (-\ln(p))^k\right], \text{ k}\neq 0$$

4.4 Regionalization

Frequency analysis is a problem in hydrology because sufficient information is seldom available at a site to adequately determine the frequency of rare events. Results from Rosbjerg and Madsen (1995) show the "index method" to be a competitive regionalization method. Stedinger and Lu (1995) arrived at the same conclusion. The "index flood" procedure is a simple regionalization technique that uses data sets from several sites in an effort to construct more reliable quantile estimates than possible from data at a single site. With the GEV index flood procedure, the location and shape parameters of a single dimensionless average GEV distribution are obtained by pooling information from many sites in a region (Chowdhury et al. 1991). The concept underlying this method is that the distribution of floods (precipitation) at different sites in a region is the same except for a scale or index-flood parameter (Maidment 1993). Although the procedure has obviously been constructed to estimate regional flood quantiles, the same approach can be applied to rainfall frequency analysis.

Using the procedure outlined in Maidment (1993), and formulas and values available in De Michele and Rosso (2001), regional quantiles and associated 95% confidence intervals are calculated. The procedure used is outlined as follows:

1- At each site j, compute the three L-moment estimators $\hat{\lambda}_1(j)$, $\hat{\lambda}_2(j)$, $\hat{\lambda}_3(j)$ using the unbiased probability weighted moment estimators (PWM) b_r.

2- To obtain a normalized frequency distribution for the region, compute the regional average of the normalized L moments of order r = 2 and 3:

$$\lambda_r^R = \frac{\sum_{j=1}^{J} w_k[\lambda_r(j)/\lambda_1(j)]}{\sum_{j=1}^{J} w_j}$$ for r = 2,3; J being the number of sites.

For r = 1, $\lambda_1^R = 1$, with $w_j = \frac{n_j n_R}{n_j + n_R}$ where n_j is the sample size for site j and

$n_R \approx \frac{\sum n_j}{J}$.

3- Using the normalized L-moments $\hat{\lambda}_1^R(j)$, $\hat{\lambda}_2^R(j)$, $\hat{\lambda}_3^R(j)$, determine the parameters and quantiles x_p^R of the normalized regional GEV distribution.

4- The estimator of the 100p percentile of the flood distribution at any site j is

$\hat{x}_p(j) = \hat{\lambda}_1^j \hat{x}_p^R$,

where $\hat{\lambda}_1^j$ is the at site sample mean for site k $\lambda_1^j = \frac{1}{n_k}\sum_{1}^{n_k} x_t(j)$.

5- The variances of the regional estimates are calculated using De Michele and Rosso (2001):

$\text{var}(x_p^R) = \frac{\alpha}{n}\exp\{y_T \exp[-1.823k - 0.165]\}$ For k ≤ 0

with $y_T = -\ln\{-\ln[(T-1)/T]\}$

$\text{var}(\hat{x}_p) = E^2(\lambda_1^j) * \text{var}(x_p^R) + E^2(x_p^R) * \text{var}(\lambda_1^j) + \text{var}(x_p^R) * \text{var}(\lambda_1^j)$.

6- Efficiency of the procedure is estimated by

$$\eta = \frac{\text{var(regional)}}{\text{var(singlesite)}}$$

$$\eta = \frac{n_j}{N} + \frac{[\xi + \frac{\alpha}{k}(1 - e^{-ky_T})]^2 \Xi_k}{k^2 H_{k,T}} + \frac{\alpha^2 \Xi_k}{Nk^2}, \text{ k < 0;}$$

with N being the normalized sample size

and $\Xi_k = \Gamma(1+2k) - \Gamma^2(1+k)$

$H_{k,T} = \exp[y_T \exp(-1.823k - 0.165)]$.

The following figures present the results, along with 5% and 95% confidence intervals.

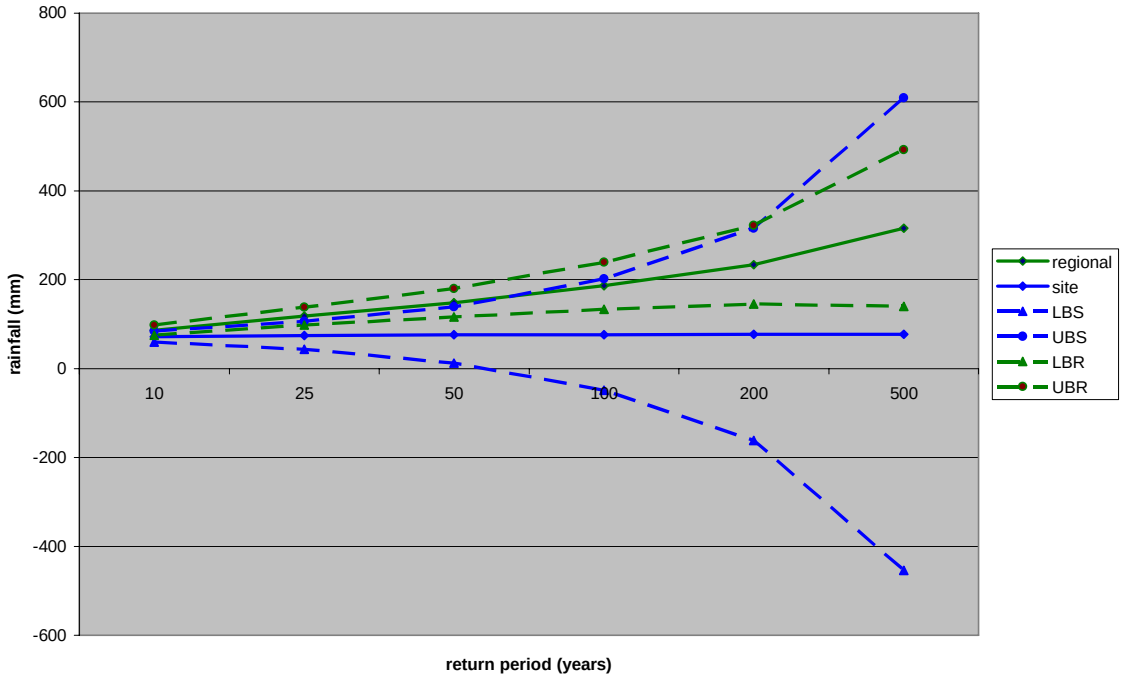

Figure 12: Desronvilles: At site and Regional quantiles along with 5% and 95% confidence intervals.

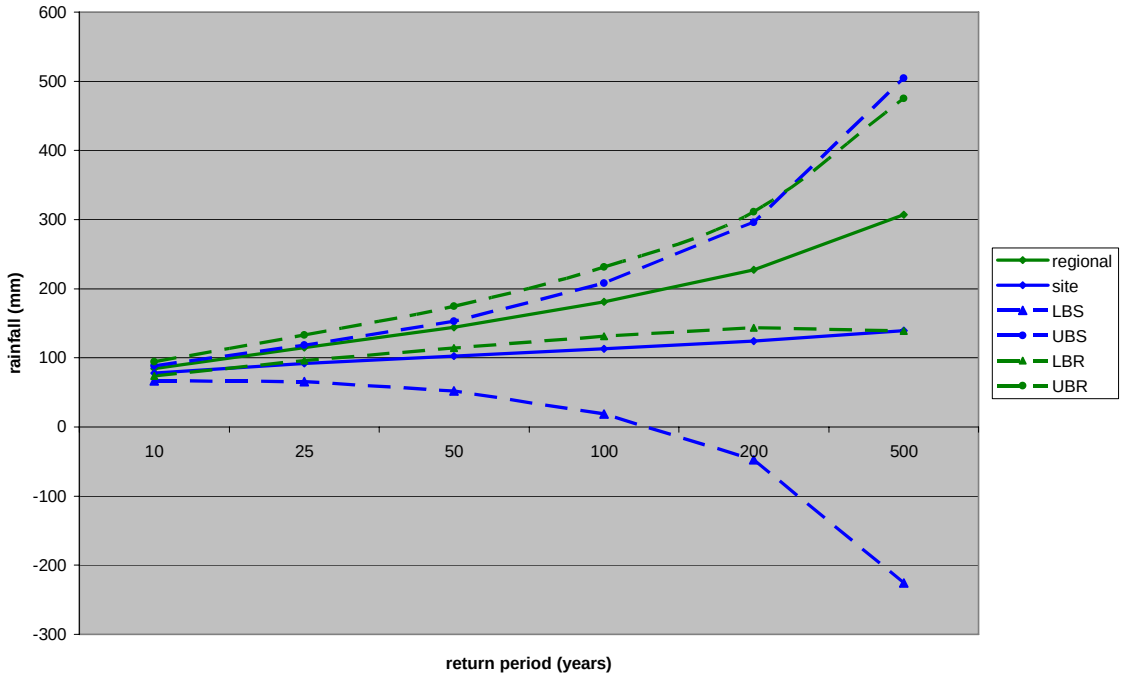

Figure 13: Gonaives: At site and regional quantiles, along with 5% and 95% confidence intervals.

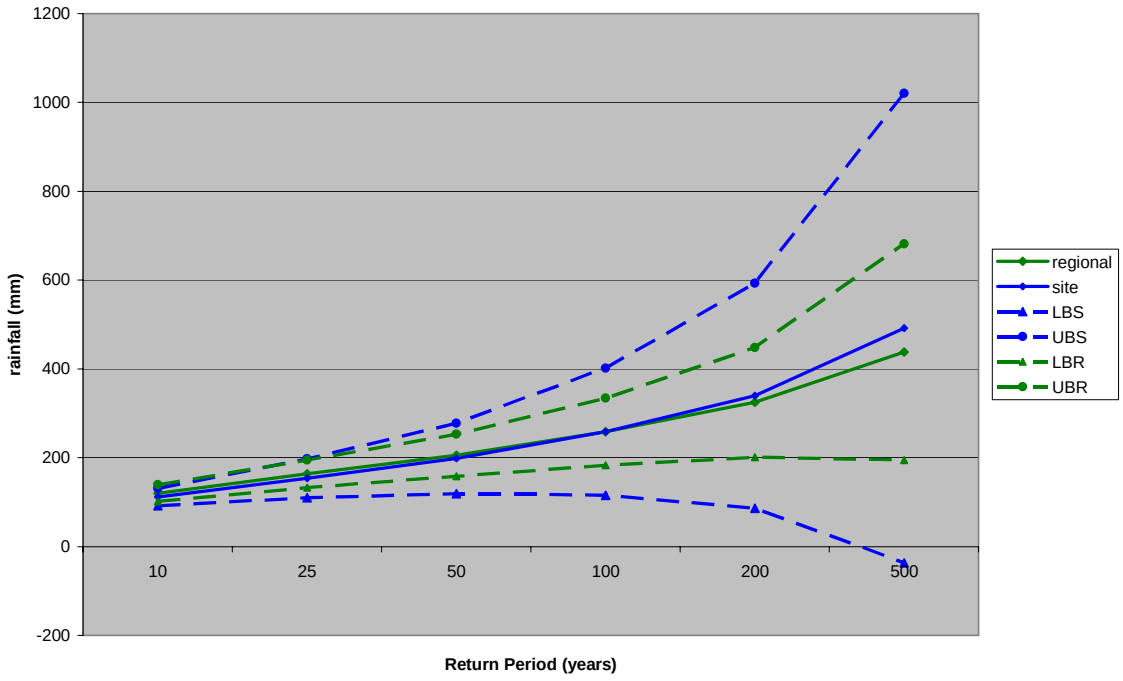

Figure 14: Ennery: At site and regional quantiles, along with 5% and 95% confidence intervals.

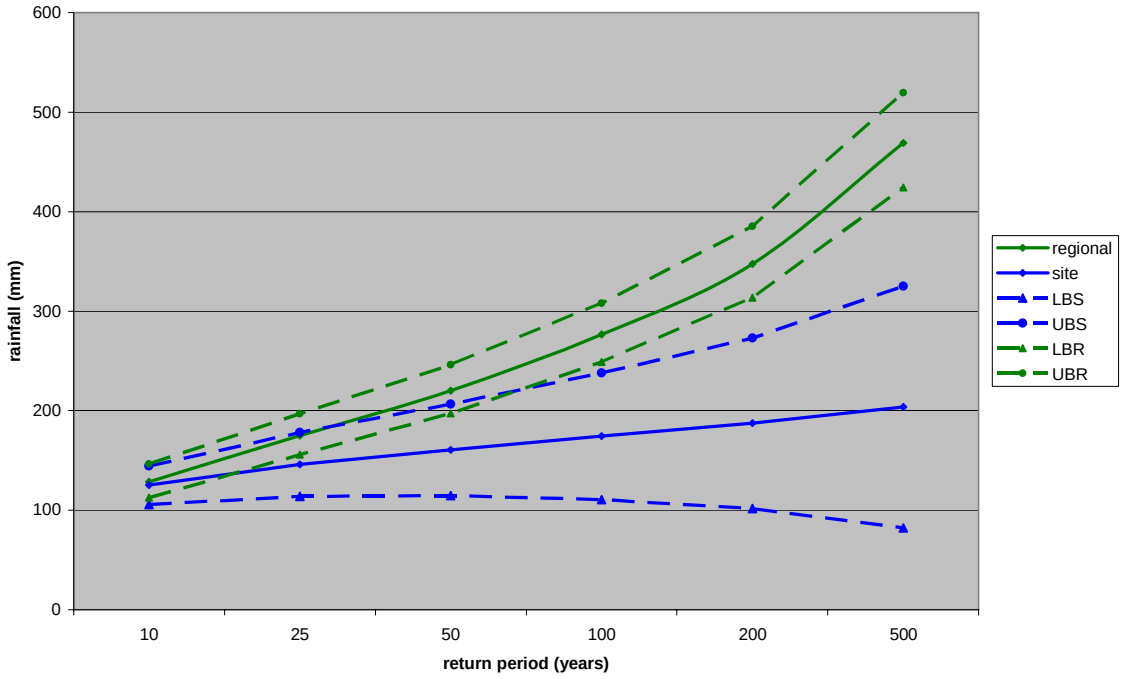

Figure 15: Gros Morne: At site and regional quantiles, along with 5% and 95% confidence intervals.

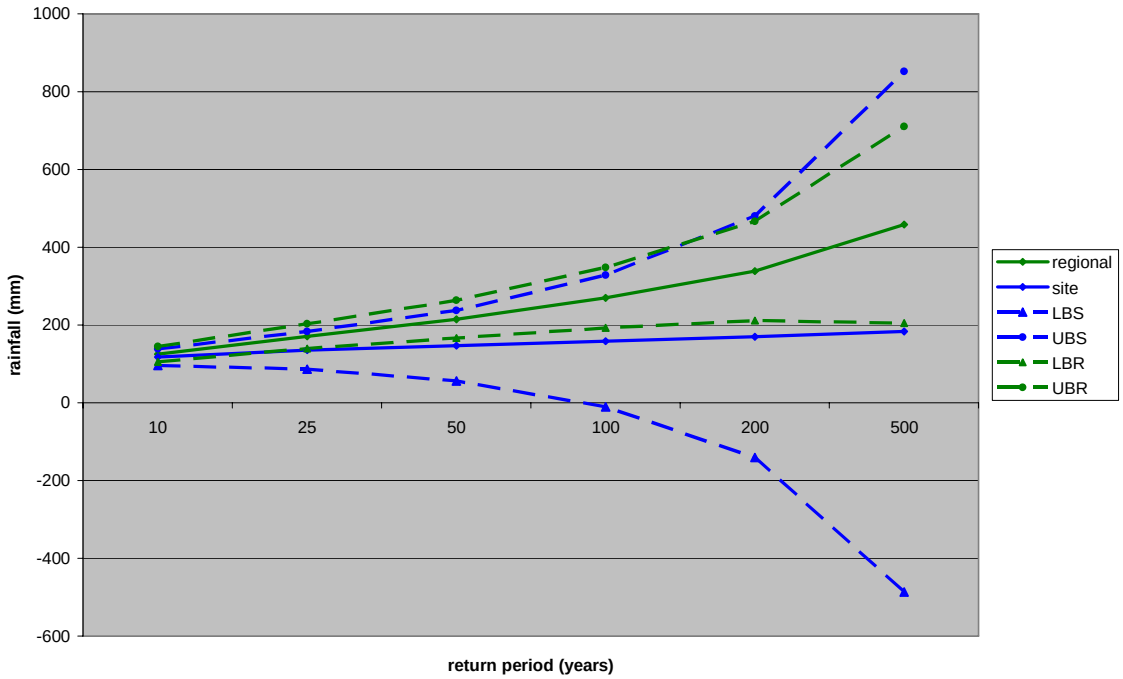

Figure 16: Marmelade: At site and regional quantiles, along with 5% and 95% confidence intervals.

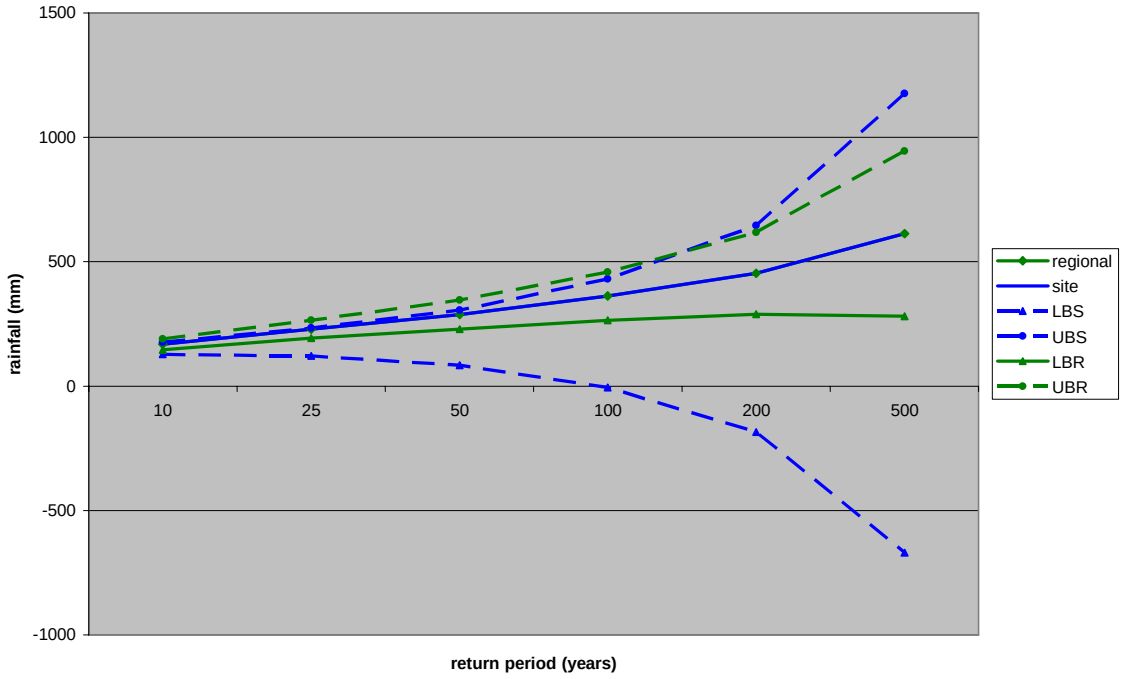

Figure 17: Pilate: At site and Regional quantiles, along with 5% and 95% confidence intervals.

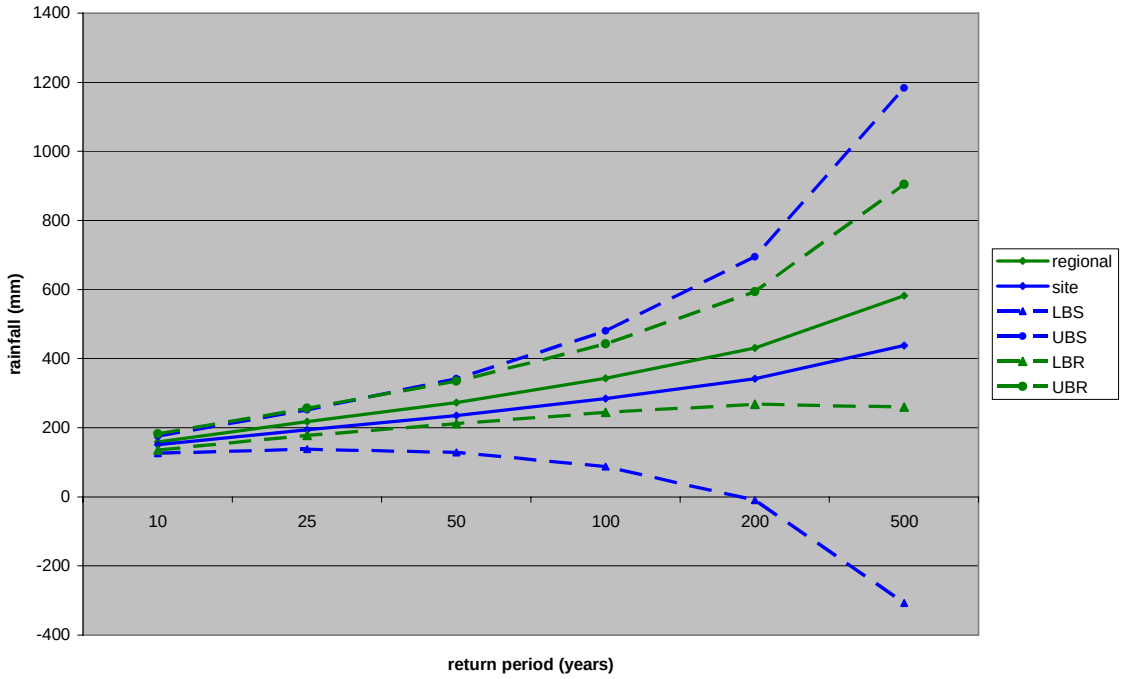

Figure 18: Plaisance: At site and regional quantiles, along with 5% and 95% confidence intervals.

A look at the lower bound of the confidence intervals could be quite startling for some locations. The lower bound value decreases for longer return periods. Although this result can be surprising, other studies, such as Coles et al. (2003) and Reis and Stedinger (2005); show similar results. This is attributed to the fact that the variance was obtained using the first-order asymptotic approximation (Reis and Stedinger 2005).

Figure 19 shows the correlations between at-site and regional quantile estimates seem to decrease with the distance [distance =ABS (at_site - regional)] between the at-site k value and the regional k value (-0.33), with the highest correlation in Plaisance and the lowest in Desronvilles.

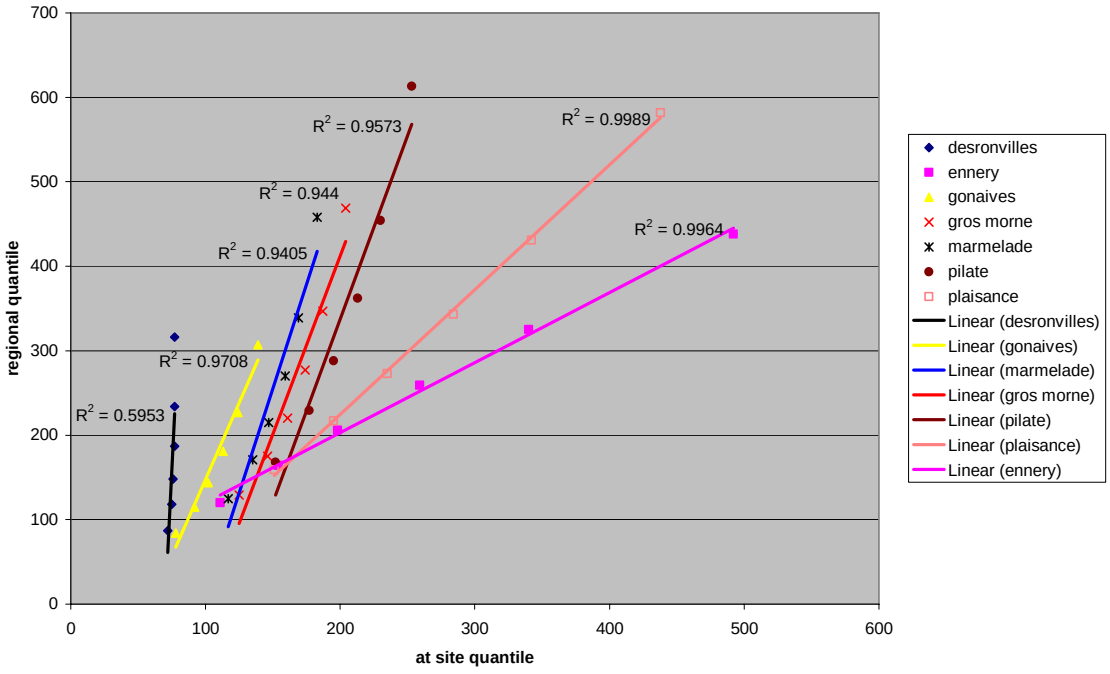

Figure 19: Correlation between at site and regional quantile estimates

These results generally corroborate the underlying assumption of the index flood that, except for a scale factor, the distribution is the same over the region. The assumption of a scale factor, which in this study is chosen to be the mean, does not seem to be contradictory to at site estimations. Only the estimation of the regional k value (shape of the distribution) seems to be determinant. This would mean that if indeed the estimated regional k value is accurate then the quantile estimates should also be reliable. The overall accuracy of the quantile estimates is likely to be improved using the regional k value instead of the individual at-site k values which were estimated using relatively short records.

In the previous calculations for regional analysis, the region under study has been considered as a whole. To test the underlying assumption that the region is homogeneous, the Lu and Stedinger (1992a) regional homogeneity test is used. This test uses the 10-year normalized quantile properties. Dalrymple (1960) noticed that the variance of the 10-year quantile is relatively small and therefore more reliable. According to Lu and Stedinger (1992a), in a homogeneous region, the differences in estimated (normalized) 90^{th} percentile estimates between sites are due only to sampling error.

The regional homogeneity test procedure is outlined below:

1- Calculate the sampling variance

$\sigma^2_{0.90}(j) = \frac{C_f V}{n_j}$, where V is n_j times the asymptotic variance for the regional distribution and C_f is the corresponding correction factor for sample size n_j.

2- Calculate the weighted average normalized 10-year estimate

$$\hat{y}_p(R) = \sum_{j=1}^{K} n_j \hat{y}_p(j) / \sum_{j=1}^{K} n_j \ .$$

3- Calculate the chi-square regional homogeneity statistic

$$\chi^2_{(R)}(y_{0.90}) = \sum_{j=1}^{K} \{[\hat{y}_{0.90}(j) - \hat{y}_{0.90}(R)] / \hat{\sigma}_{0.90}(j)\}^2 \ .$$

The results of this test show that the assumption of a homogeneous region is reasonable. The chi-square statistic is equal to 4.5. Compared to the critical value 12.57 for 6 degrees of freedom, the chi-square statistic shows that the hypothesis of a homogeneous region cannot be rejected at a significance level of 5%.

4.5 Design Storm

A design storm is a precipitation pattern defined for use in the design of a hydrologic system. Usually, the design storm serves as the input, and the resulting rates of flow through the system are calculated using rainfall-runoff and flow routing procedures (Chow et al. 1988). Considerations in defining a design storm include the return period, the total storm depth, the storm duration, the storm temporal distribution, the storm spatial characteristics, the time response of the watershed, and the antecedent state of the watershed (Loukas and Quick 1995). Design storms can be based upon historical

precipitation data at a site or can be constructed using the general characteristics of precipitation in the surrounding region (Chow et al. 1988).

Use of single-site estimates as input to a rainfall-runoff model is not recommended because failure to consider spatial variability in rainfall patterns could result in serious errors in prediction models (Schuursmans and Bierkens, 2006). However, frequency analysis of precipitation over an area has not been as well developed as analysis of point precipitation. In the absence of information on the true probability distribution of areal precipitation, point precipitation estimates are usually interpolated to develop an average precipitation depth over an area (Chow et al. 1988). Shah et al. (1996) report that several studies have shown that the spatial distribution and accuracy of the rainfall input strongly influence the volume of storm runoff, time-to-peak and the peak runoff. Although spatial variability of rainfall can be expected to increase with an increase in the watershed size, Arnaud et al. (2002) and Chang et al. (2007) found that the difference in using uniform or non-uniform rainfall is generally moderate when estimating extreme flood events. Schuursmans and Bierkens (2006) suggest that the use of spatially averaged precipitation is sufficient to understand the general behavior of the hydrological system.

However, for average rainfall to be representative of the region, a minimum number of rainfall gauges must be provided. Curtis and Burnash (1996) found that the average rainfall was a good representation of the rainfall on a watershed if the rain gauge network is adequately dense in the vicinity of the storm. The US National Weather Service (NWS) suggests a minimum of $N=A^{0.33}$ (A in square miles) for a local flood warning

network. In the case of the present study, 6 rain gauges would be needed. Using the rule of Benton reported by Horton (1923), the minimum rainfall gauges to have inside a basin is N=1 + A/5 (A in square miles), which would be 4 rain gauges. Seven rainfall stations (two in the lower part of the watershed, one at mid elevation and the others either at the highest elevation or on the other side of the basin) should be enough to provide a good idea of the spatial precipitation pattern over the region.

Table 8: Precipitation for different return periods

Stations	**T-10**	**T=25**	**T=50**	**T=100**	**T=200**	**T=500**
Desronville	87	118	145	187	234	316
Ennery	120	164	206	259	325	438
Gonaives	84	115	144	181	227	307
Gros Morne	129	175	220	277	347	469
Marmelade	125	170	215	270	339	458
Pilate	168	229	288	362	454	613
Plaisance	159	217	273	343	431	582

Herschfield (1965) used three procedures to estimate average rainfall over a region - Thiessen, isohyetal and arithmetic mean- and did not find much difference between them. (Mather 1975) found similar results for monthly average rainfall. Average rainfall is calculated over the Gonaives watershed using two methods: arithmetic average and Thiessen polygons. As shown in Table 9, the two methods give similar results when applied to quantile estimates, though it is recognized that larger differences may occur for actual storm events.

Table 9: Daily average rainfall from arithmetic average and Thiessen methods

Method	T-10	T=25	T=50	T=100	T=200	T=500
Arithmetic	125	170	213	268	337	455
Thiessen	120	163	204	258	323	436

Linsley et al. (1992) point out that it is incorrect to average the individual N-year values at a number of rainfall stations to determine the N-year average value over an area. They continue by saying that unless the events occur simultaneously, the average value has a return period greater than that of the individual values. Use of the areal reduction factor can alleviate this problem. Accordingly, in this study, with a watershed of 600 km^2, an areal reduction factor of 0.93 will be applied to the arithmetic average rainfall.

Table 10: Lower and Upper Bound of Design storm events

Method	T-10	T=25	T=50	T=100	T=200	T=500
Design storm	116	158	198	250	313	423
Lower bound	100	132	158	186	209	218
Upper bound	132	184	239	314	418	628

Regarding the temporal distribution of the storm, it has been found that in general, time-varying rainfall produces greater peak discharge than does constant rainfall (Singh and Woolhiser 2002). The NRCS (SCS) type II distribution (central loaded storm) will be used in this study. El-Jabi and Sarraf (1991) found while evaluating the effect of maximum rainfall position (e.g., early, centered, late), that hydrograph timing was altered, but not the hydrograph peak. Finally regarding the storm duration, Levy and McCuen (1999) found that for watersheds up to 52.6 mi^2, the rainfall duration causing the annual maximum discharge is often slightly longer than 24h. Results from Levy and

McCuen (1999) also show that the storm duration increases slightly with watershed area. For the purpose of this study, a 24-h storm duration will be used.

4.6 Discussion

One limitation of the rainfall frequency analysis is that historical data are used to predict future observations in terms of magnitude and frequency. In doing this, it is assumed that the data are stationary, which would not hold true in case of climate change. The earliest rainfall record used in this analysis is 1923 and the latest is from 2004, and it is likely that the data have been affected by climate change or long term climate variability. Another problem that arises is the limited amount of data compared to the recurrence interval of interest. As stated earlier, our shortest length of record is 21 and the largest is 46 years. However, our recurrence interval of interest ranges from 10-500 years. De Michele and Rosso (2001) report that return period of 2*n* can be reasonably modeled with n years of data. Use of regional analysis can partially alleviate this problem.

Another limitation is that the true distribution from which the observations are drawn will probably never be known and most likely is too complex to be modeled. Thus, the goal is to find the distribution that would lead to reasonably accurate and robust estimates of design quantiles and hydrologic risk. The GEV distribution provides a good fit to rainfall data in Haiti and has the advantages of being relatively insensitive to violations of distributional assumptions and having low variability and bias when using the regional L-moments method (Lettenmaier et al. 1987)

CHAPTER 5- RAINFALL RUNOFF MODEL

Singh and Woolhiser (2002) report that hydrology has been defined by Penman (1961) as the science that attempts to answer the question, “What happens to the rain”? Although the question may appear to be simple enough, this task is subject to a great deal of uncertainty. The branch of hydrology dealing with this type of question is called watershed hydrology. Very often, models are developed to describe the interactions of the water and the land. Frequently, model complexity is dictated by the availability of data (Singh and Woolhiser 2002). However, Kokkonen and Jakeman (2001) found that simpler methods are usually more accurate for stream flow prediction.

Many basins in the world have no stream gauges, especially in developing countries. The hydrologist, then, has no other choice than to use accepted empirical methods or, at best, regional information from nearby gauged sites. One method of estimating flood runoff frequencies in the case of no flow record is to use a rainfall-runoff model which computes the stream flows that result from precipitation runoff. The watershed is the system being modeled, precipitation is the input, flows are the output and the goal is to estimate a flood of selected exceedance (or non-exceedance) probability from rainfall inputs (Wurbs and James 2002). The problem in using this method is that each step of the design introduces some uncertainties which are not clearly identified, obscuring the relation between the probabilities of the design rainfall event and the flood event estimated from it.

5.1 Watershed Characteristics

The Gonaives watershed, delineated using GIS and a DEM, is shown in Figure 20. Catchment characteristics can have a substantial impact on watershed response and are an important part of rainfall-runoff models. Watersheds vary greatly in size, shape, topography, land use, geology, soils, vegetation, stream configuration, and other characteristics (Wurbs and James 2002). The procedure used to estimate watershed parameters from DEM data is discussed below.

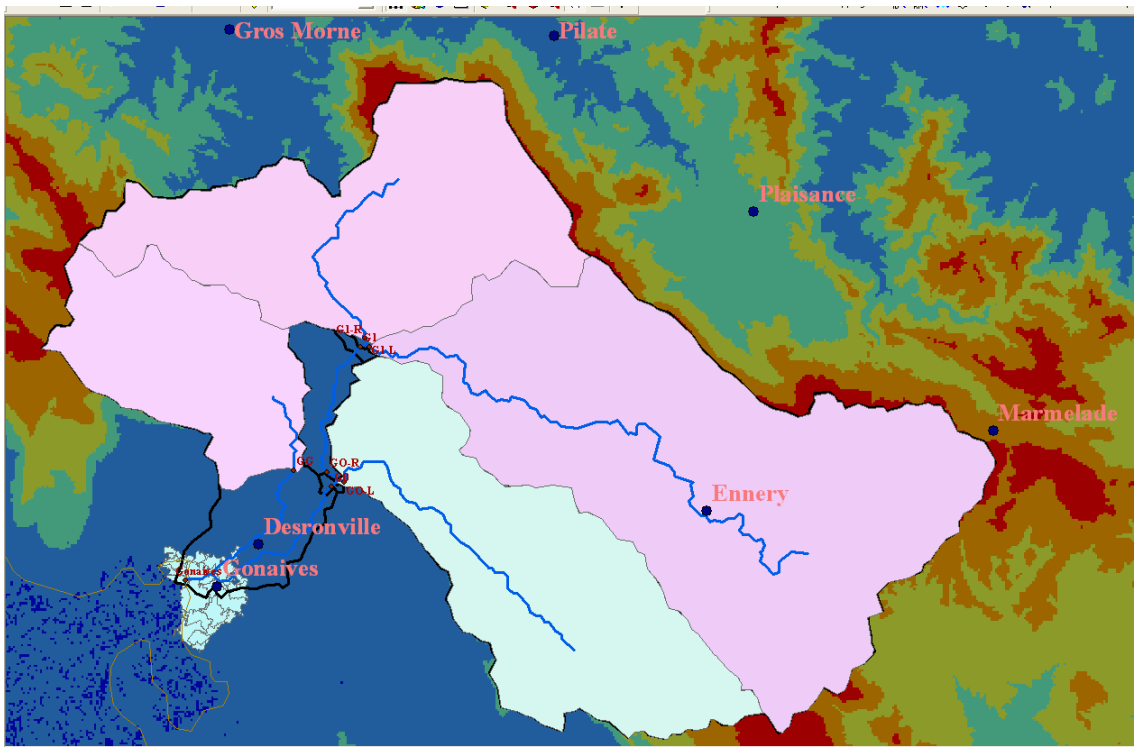

Figure 20: Gonaives watershed rainfall stations and city limit

Drainage Basin

To delineate the watershed, and sub-basin boundaries, we first need to choose the outlets. These are points of interest, usually a bridge, confluence of streams or a gauging station.

For the Gonaives watershed, seven outlets have been chosen for convenience, and their respective watershed boundaries will be drawn using GIS. From the delineation of the watersheds, physical characteristics such as drainage area, perimeter, shape, slope, and main channel length will be calculated. Most of these parameters are intuitive except for the shape parameter. We define watershed shape as

$$\mathrm{K} = \frac{0.282P}{A^{0.5}}$$

where A is the drainage area and P the drainage perimeter. A shape factor close to 1 describes a catchment having a fast and peaked runoff response, while a much larger ratio describes a catchment with delayed runoff response (Ponce 1989).

The use of GIS is growing in watershed analysis. GIS tools are valuable and are welcomed by the hydrologic engineer because they provide reproducible results and eliminate much of the drudgery previously associated with setting up such analyses (Moglen and Hartman 2001). GIS is a tool that can process, display, and integrate different data sources including maps, digital elevation models (DEMs), GPS (global positioning system) data, images and tables (Chang 2006). More specifically related to the watershed management field,

> "GIS can be used to automate the delineation of the watershed into a number of sub-areas, and for the determination of the topological connectivity of these sub-areas. Once this is accomplished, the GIS can also be used to determine a variety of watersheds or sub-areas based on characteristics such as drainage area, flow length, slope, average curve number (CN), and time of concentration. Ultimately

these characteristics are used to develop models to estimate the magnitude and timing of a flood peak." (Moglen and Hartman 2001, p 490)

However, there is a recurring question: How does the quality and resolution of the data impact measurements of watershed characteristics? Studies made by Moglen and Hartman (2001) show the drainage area is not impacted by DEM resolution up to the coarsest DEM considered, which was 90m. This is an important finding since discharge estimates are heavily impacted by drainage area (Maidment and Hoogerwerf, 2002). However, they noticed a linear bias in flow length, presumably because finer resolution captures better the meanders of the river. They also found that the range in elevation became smaller with coarser resolution, and that the 90m DEM slope was smaller compared to 12ft DEM slope. However, in this regard, the 30m DEM compared favorably with the 12ft DEM. This problem is of smaller importance since slope and flow path errors have relatively low impact on discharges estimates (Maidment and Hoogerwerf, 2002). A 90m DEM should then lead to reasonable values of watershed characteristics and subsequently discharge estimates.

For this study, 90m DEM and 1km DEM data were available for the entire catchment. The 90m DEM showed a smaller drainage area than the 1km DEM. Stream rendering occurred at 1km resolution. Using the 1km DEM to delineate the watershed boundary, the watershed size was found to be 746 km2. This boundary was used on both the 90m and 1km DEM to compute the elevation range. Using the 90m DEM, the watershed size

was found to be 591 km2. Using this boundary on both the 90m and 1km DEM resulted in a different elevation range. The results are summarized in Table 11 and illustrated in Figures 20 and 21.

Table 11: Elevation range (m) comparison between 90m and 1km DEMs

	90m DEM	1km DEM
90m boundary	0-1478	0-1300
1km boundary	0-1134	1-1387

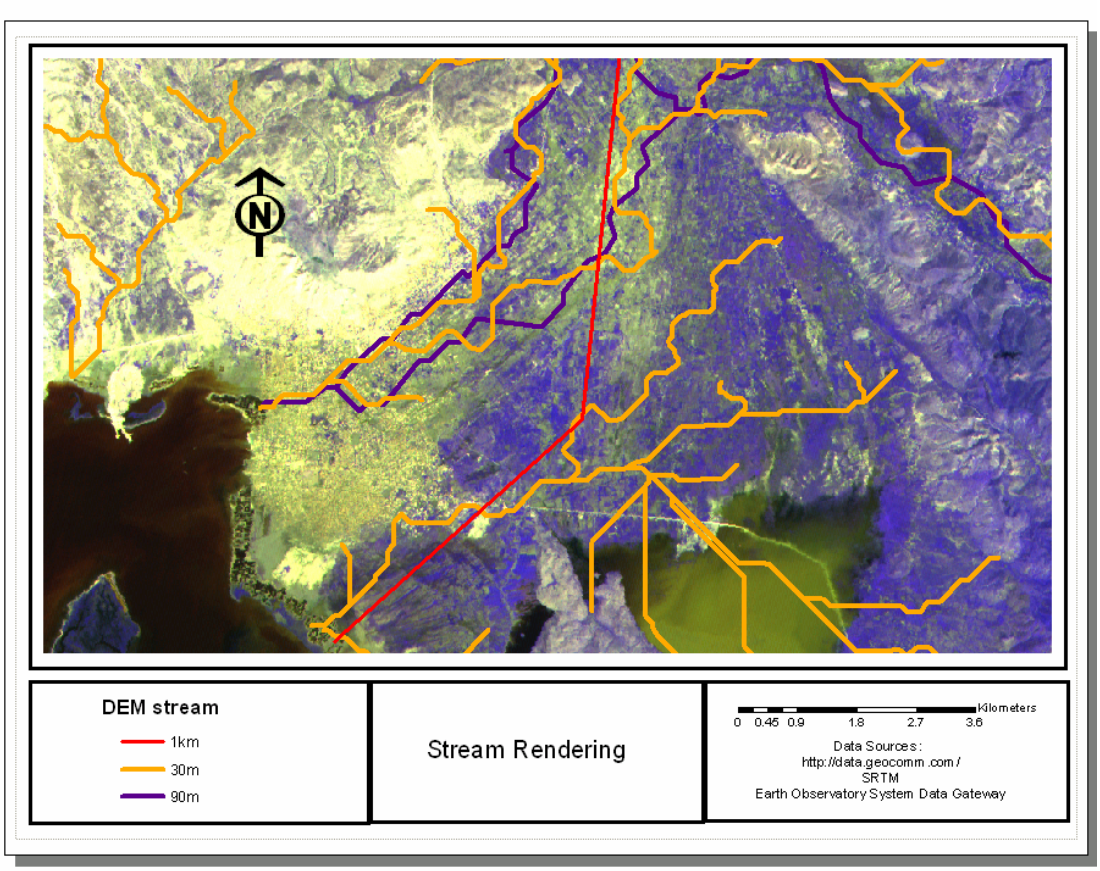

Figure 21: Flow paths using 30m, 90m and 1km DEM resolution

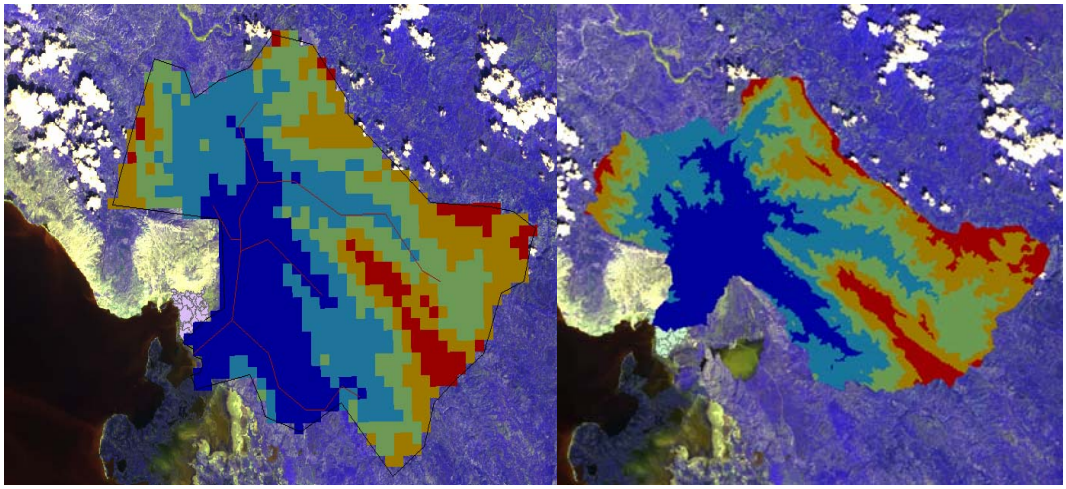

Figure 22: Watershed delineation using 1km and 90m DEMs

The previous results are in accordance with Moglen and Hartman (2001) concerning the decrease of the range in elevation with coarser DEMs. Subsequent calculations to compute basin characteristics (Table 12) were made using ArcGIS 9.0 and the 90m DEM.

Table 12: Basin Characteristics

Outlets	Area(km2)	Perimeter (km)	Main channel (km)	Highest point (m)	Lowest point(m)	Slope (%)	Shape
G0	500.4	124.2	49.1	874	46	1.69	1.57
G0-L	125.5	61.2	23.6	1464	47	6.01	1.54
G0-R	374.5	129.7	49.1	874	49	1.68	1.89
G1	362.3	118.9	41.6	874	100	1.86	1.76
G1-L	234.4	81.6	41.6	874	100	1.86	1.50
G1-R	127.6	63.4	18.2	1040	99	5.18	1.58
GG	66.9	40.2	15.4	1040	54	6.40	1.39

Curve Number Estimation

The curve number is a parameter that indicates the permeability of the soil. It is determined by a detailed evaluation of soil type, vegetative and land use patterns (Ponce

1989). For ungauged watersheds, estimates of runoff curve numbers are given in tables supplied by federal agencies. In general, as the curve number increases, so does the peak discharge. It varies from 1 to 100 being a function of the following catchment properties: (1) hydrologic soil type, (2) land use and treatment, (3) ground surface condition and (4) antecedent moisture condition (Ponce 1989). The estimation of this parameter has been done somewhat subjectively using tables provided by Ponce (1989). The entire watershed has been considered pasture, grassland, or range-continuous forage for grazing. This assumption is confirmed by available maps of the area that show that much of the area of the watershed is savannah, pasture and some agricultural areas. The soil group is B (soils with moderate infiltration rates when wetted thoroughly, primarily moderately deep to deep, moderately drained to well drained, with moderately fine to moderately coarse textures) which leads to the range in CN values shown in Table 13. These soils have a moderate rate of water transmission (Ponce 1989). The hydrologic condition is considered to be poor (less than 50% of ground cover on heavily grazed with no mulch). We will investigate the effects of variation in the curve number on the discharge and the floodplain.

Table 13: Curve number for rangeland, soil group B, with different land management practices (source: Ponce 1989)

	Poor	Fair	Good
CN	79	69	61

Poor: less than 50% ground cover and not heavily grazed, with no mulch

Fair: 50 to 75% ground cover and not heavily grazed

Good: more than 75% ground cover and lightly or only occasionally grazed.

A poor CN is considered for the present condition, as rapid deforestation is a major environmental problem which is affecting surface water resources in Haiti. "The removal of trees and vegetation allows for increased and faster runoff of rainfall. The faster runoff causes a rapid increase in the amount of water entering the stream resulting in water levels that rise faster with larger peak discharges. It also causes less rain water to infiltrate into the soil to recharge the aquifers" (USACE 1999). A CN number of 79 is thus a reasonable choice.

Time of Concentration

The time of concentration (Tc) is defined as the time required for runoff occurring at the hydraulically most remote location in the watershed to reach the outlet (Wurbs and James 2002). It is widely used in hydrological models and many formulas have been developed to estimate this parameter. Errors in Tc will propagate in the estimation of the peak discharge. Among the formulas, we find the Kirpich equation ($t_c = \frac{0.06628L^{0.77}}{S^{0.385}}$, L being the length of main channel in km and S channel slope) which was developed from SCS data for seven rural basins in Tennessee with slopes varying from 3% to 10%; and the Giandotti method ($t_c = \frac{4\sqrt{A} + 1.5L}{0.8\sqrt{\Delta H}}$) (Daniil and Michas 2006). The NRCS lag time ($t_l = \frac{L^{0.8}(2540 - 22.86CN)^{0.7}}{1410CN^{0./}Y^{0.5}}$) can also used to calculate the time of concentration assuming that $t_c = 1.67 * t_l$. A comparison of the different methods is shown in Table 14. Bondelid et al. (1982) showed that as much as 75% of the total error in an estimate of peak discharge can result from errors in the Tc estimation. It is obvious then that care

must be taken in estimation of the time of concentration. Stephenson (1984) noted that the time of concentration was nearly the same for uneven rainfall as for uniformly distributed rainfall. As the estimates given by Kirpich and Giandotti formulas were not very different, we decided to take the average as the estimated value of the estimates of the time of concentration.

Table 14: Time of concentration (hours)

Outlets	Kirpich	Giandotti	Choice (average)	Lag time(hr)
G0	6.39	7.09	6.74	4.04
G0-L	2.23	2.66	2.44	1.47
G0-R	6.41	6.57	6.49	3.89
G1	5.42	6.2	5.81	3.49
G1-L	5.42	5.55	5.49	3.29
G1-R	1.93	2.95	2.44	1.46
GG	1.57	2.22	1.90	1.14

For comparison purposes, lag time using NRCS equation was also calculated:

$$t_l = \frac{L^{0.8}(2540 - 22.86CN)^{0.7}}{1410CN^{0./}Y^{0.5}}$$

where t_l is the catchment lag in hours; L the hydraulic length in meters; Y the average slope in %; and CN the curve number. As shown in the table below, the two formulas give results that differ by as much as a factor of four. It is to be said that evaluation of the time of concentration using empirical formulas is very uncertain. Only simultaneously recorded rainfall and flow data could give a reliable estimate of the time of concentration. However, the time of concentration is a very important parameter in

flow calculations; Kirpich and NRCS results will be considered to be indicative of the lower and upper bound of the true time of concentration.

Table 15: Time of Concentration computed using the NRCS method

			CN = 79		**CN = 69**		**CN = 61**	
Outlet	Length (m)	S(%)	Lag time (hr)	t_c(hr)	Lag time (hr)	t_c(hr)	Lag time (hr)	t_c(hr)
G0	49100	1.69	14.70	24.50	19.54	32.56	24.05	40.09
G0-L	23600	6.01	4.34	7.23	5.76	9.61	7.10	11.83
G0-R	49100	1.68	14.74	24.57	19.59	32.66	24.12	40.21
G1	41600	1.86	12.27	20.45	16.31	27.18	20.08	33.47
G1-L	41600	1.86	12.27	20.45	16.31	27.18	20.08	33.47
G1-R	18200	5.18	3.80	6.33	5.04	8.41	6.21	10.35
GG	15400	6.4	2.99	4.98	3.97	6.62	4.89	8.15

5.2 The Synthetic Unit Hydrograph

One common empirical method to compute flood flows is the Synthetic Unit Hydrograph Method. A unit hydrograph is defined as the hydrograph produced by a unit depth of runoff uniformly distributed over the entire catchment and lasting a specified duration (Ponce 1989). This method makes two major assumptions: linearity and superposition.

1- Assuming linearity of watershed response, a hydrograph for a runoff depth other than unity can be obtained by simply multiplying the unit hydrograph ordinates by the indicated runoff depth. Any inaccuracies due to the linearity assumption for routing the runoff are generally less than the inaccuracies associated with deciding how much of the rainfall to route, i.e., the problem of estimating the effective rainfalls or runoff coefficient for an event (Beven 1987).

2- Applying superposition, the summation of the corresponding ordinates of these hydrographs gives the composite hydrograph.

The term ‘synthetic’ in synthetic unit hydrograph (SUH) denotes the unit hydrograph (UH) is derived from watershed characteristics rather than from rainfall-runoff data (Bhunya et al. 2003). SUH methods were developed by studying several catchments with similar climatic conditions and spatial properties as well as their associated unit hydrographs. Relationships were found between these observed unit hydrographs and parameters used to derive synthetic unit hydrographs based on the assumption that all unit hydrographs can be expressed by a single curve or a family of curves, or a single equation (Saf, 2003). Among the various SUH methods the Snyder Unit Hydrograph and the SCS Unit Hydrograph are commonly used .

Snyder Synthetic Unit Hydrograph

Snyder (1938) introduced the concept of synthetic unit hydrograph developed from analyzing 20 hydrographs from catchments in the Appalachian region (Ponce 1989; Wurbs and James 2002). Snyder selected three parameters to describe the unit hydrograph: the lag, peak flow and total time base. The lag time is defined as

$$t_l = C_t \left(LL_c\right)^{0.3}$$

where t_l is the catchment or basin lag in hours, L the length along the mainstream form outlet to divide, L_c the length along the mainstream from outlet to the point closest to catchment centroid, and C_t a coefficient accounting for catchment gradient and associated storage. Then the peak discharge of the unit hydrograph of unit duration D is given by

$Q_p = \frac{2.78 C_p A}{t_l}$, where Q_p is the peak flow in m^3/s, assuming $D = \frac{t_l}{5.5}$,

where A is the catchment area in km^2 and t_l is in hours. Here C_p is taken to be 0.6.

NRCS (formerly SCS) Unit Hydrograph

The NRCS developed a dimensionless unit hydrograph in the 1950's based on analyses of many unit hydrographs for gaged watersheds varying widely in size and location (Ponce 1989; Wurbs and James 2002). In this case,

$$Q_p = \frac{2.08A}{t_p}$$

where Q_p is the unit hydrograph peak flow for 1cm of effective rainfall in cubic meters per second; A the catchment area in square kilometers; and t_p the time to peak in hours. Time to peak is

$$t_p = \frac{D}{2} + t_L$$

where D is the unit rainfall duration associated with the hydrograph.

5.3 Rainfall-Runoff Model Using HEC-HMS

According to Scharffenberg et al. (2003), "The Hydrologic Modeling System (HEC-HMS) developed by the US Army Corps of Engineers is designed to perform deterministic hydrologic simulation in support of engineering studies. It is intended to assist in planning, designing, and operating projects by providing information about current and future runoff from watersheds, with and without water control structures". HEC-HMS is considered one of the standard models in the United States for the design of drainage systems, quantifying the effects of land-use change on runoff and flooding (Singh and Woolhiser 2002).

There are three components to an HEC-HMS model to run: the basin model, the meteorologic model, and the control specifications. These are discussed briefly.

Basin Model

The basin model (Figure 19) collects information about the physical characteristics of the basin or sub-basins, the loss method (infiltration method), and the transform method which describes how the rainfall should be transformed into runoff. Parameters such as initial abstraction of the basins, percentage of impervious area, lag time and, in the case of the Snyder method, the peaking coefficient are entered. The loss method used was the

Curve Number method which assumes an initial abstraction and decreasing infiltration rate over time based on the CN value. The transformation methods used were the NRCS and Snyder unit hydrographs.

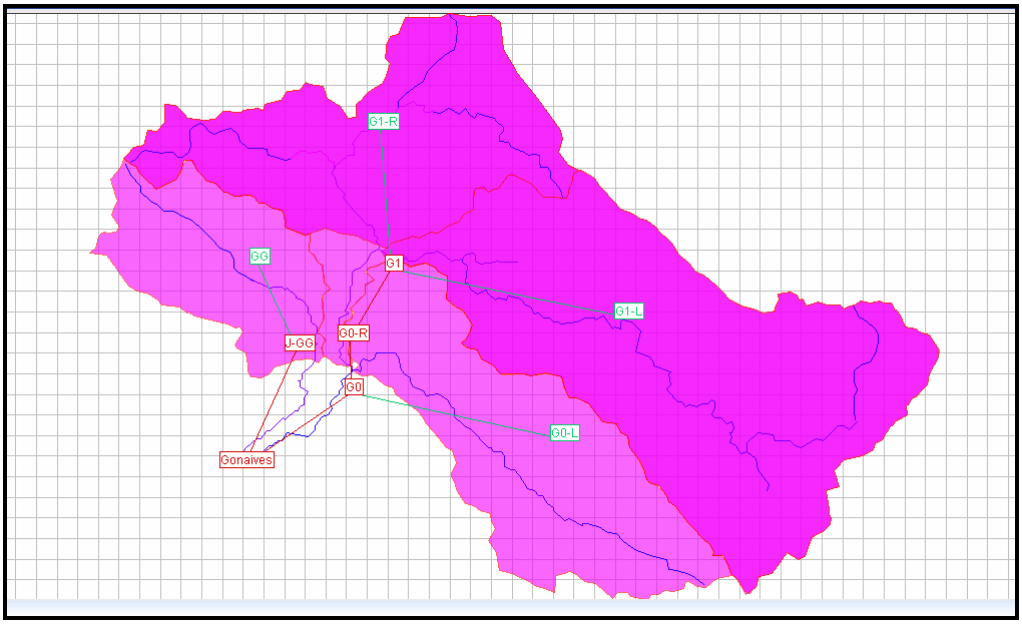

Figure 23: Basin Model in HEC-HMS

Meteorologic Model

The meteorologic model was specified assuming the SCS type II storm distribution with a total 24-hour precipitation depth corresponding to the return period of interest. For each return period, we will input the areal average precipitation estimate is input (areal reduction factor of 0.93).

Control Specifications

A 2-day simulation time has been chosen with a time increment of 1h. This duration was chosen in conformity with the smallest unit duration of the precipitation, which is 15min. HEC-HMS requires that the duration increment should at least be the same as the

smallest lag time. A similar idea exists for the total duration of the simulation process. This duration should at least be the total duration of the rainfall plus the unit hydrograph duration.

Summary of Results

A summary of results is presented for three outlets: GG, G0 and Gonaives. These three outlets are the ones that are going to be used to delineate the 10yr, 25yr, 50yr and 100yr floodplain. Results are shown in Table 16-Table 18 using both the NRCS method and the Snyder method, with the NRCS lag time for a range of CN values.

Table 16: Discharge (m^3/s) with CN=79, NRCS lag time

T		GG	G0	Gonaives
10	**snyder**	155	470	563
	scs	161	504	594
25	**snyder**	254	767	914
	scs	262	821	962
50	**snyder**	352	1064	1263
	scs	363	1139	1329
100	**snyder**	481	1460	1731
	scs	496	1562	1825
200	**snyder**	639	1948	2307
	scs	712	2190	2557
500	**snyder**	914	2808	3322
	scs	1017	3151	3675

Table 17: Discharge (m^3/s) with CN=69, NRCS lag time

T		GG	G0	Gonaives
10	**snyder**	94	291	349
	scs	108	330	387
25	**snyder**	162	495	592
	scs	184	560	656
50	**snyder**	232	707	844
	scs	264	800	936
100	**snyder**	327	999	1189
	scs	373	1130	1320
200	**snyder**	447	1368	1625
	scs	510	1545	1802
500	**snyder**	663	2030	2410
	scs	755	2291	2669

Table 18: Discharge (m^3/s) with CN=61, NRCS lag time

T		GG	G0	Gonaives
10	**snyder**	65	201	241
	scs	75	229	269
25	**snyder**	115	351	420
	scs	131	400	468
50	**snyder**	168	511	610
	scs	192	582	682
100	**snyder**	242	736	877
	scs	278	838	981
200	**snyder**	338	1026	1221
	scs	388	1169	1365
500	**snyder**	514	1560	1852
	scs	589	1774	2068

These results show how important agricultural practices and watershed management are. A shift from a poor CN (61) to a fair CN (69) increases the return period of the 25yr discharge to be in the range of a 100yr discharge, and the 100yr discharge becomes a 200yr discharge, which is a significant reduction in flood hazard. Fighting deforestation and improving agricultural practices could be important actions in decreasing the likelihood of major flood events.

Table 19 shows estimates for CN=69 and lag time computed using the Kirpich/Giandotti lag time formula. These values are unreasonably high, especially for the 10yr return period, indicating that the Kirpich/Giandotti formula is inappropriate for the basin under study. All subsequent calculations will use the NRCS lag time value. Additional sensitivity analyses (results obtained for the lower bound and upper bound of the rainfall for each return period) are presented in Appendix B.

Table 19: CN = 69 with Kirpich/Giandotti lag time

	10		25		50		100	
	snyder	**scs**	**snyder**	**scs**	**snyder**	**scs**	**snyder**	**scs**
GG	216	276	374	474	537	678	761	957
G0	837	1050	1445	1807	2076	2591	2941	3662
Gonaives	1000	1244	1715	2141	2456	3070	3470	4347

5.4 Discussion

The goal of a rainfall-runoff analysis is usually to estimate a design flood. This flood estimate is of great importance to many civil engineering works. However, very often it is difficult to evaluate the uncertainty associated with such estimates. Knowing the economic and safety impacts that arise from flood estimates, it would be desirable to have an idea of the associated uncertainty. In this particular study, uncertainties arise from the rainfall frequency analysis as discussed in the previous chapter, from the methods used such as Snyder and NRCS unit hydrograph methods, and also from the watershed parameters such as the Curve Number and the time of concentration. In the absence of flow data and of knowledge of the parameter values and their parent distributions, there is no way to rigorously quantify uncertainties. In this case, we resort to sensitivity analysis, which helps in quantifying the order of magnitude of the relative error through consideration of a range of possible values. The sensitivity analysis has been performed for both the time of concentration and the Curve Number, showing that those parameters should be estimated with care because they have a large impact on the peak discharge estimates. The Kirpich/Giandotti lag equation gives peak discharge results that are 2-3 and sometimes four times greater than when using NRCS lag time. The Curve Number has a similar impact on the flow estimates, with the specified range in CN values (61-79) leading to ranges of flow return periods of 10-50, 25-100, 50-200, and 100-500 years. Uncertainties in precipitation values are considered through calculations of the upper and lower bound of quantile estimates. As would be expected, the discharge is directly proportional to the rainfall amount. The effects of such uncertainties are evident when it comes to economical and safety issues.

CHAPTER 6- FLOODPLAIN DELINEATION

The flood plain is the low land that borders a river, usually dry but subject to flooding. The most common causes of flooding are the overflow of streams and rivers and abnormally high tides resulting from severe storms (Chow et al. 1988). The floodplain carries flow in excess of the channel capacity, and the greater the discharge, the further the extent of flow over the flood plain (Chow et al. 1988).

Floodplain delineation is the process of determining inundation extent and depth by comparing river water levels with ground surface elevations (Noman et al. 2001). In recent years, GIS and remote sensing have played key roles in delineating floodplain. While conventional methods for floodplain delineation put more emphasis on flood extent rather than depth, computer-based techniques consider the accuracy of flood extent, flood depth, and facilitate impact analysis (Noman et al. 2001).

A triangulated irregular network (TIN) or a gridded digital elevation model (DEM) is an essential input to any GIS-based watershed model. A DEM can be extracted from topographical maps or satellite images. The 90m DEM used in this study was produced from the Shuttle Radar Topography Mission Elevation Dataset. These data products result from a collaborative mission by the National Aeronautics and Space Administration (NASA), the National Imagery and Mapping Agency (NIMA), the German space agency (DLR), and Italian space agency (ASI) to generate a near-global digital elevation model (DEM) of the Earth using radar interferometry. The data was provided by W. Kuntzel of PROSISA (http://www.gdin.org/products/hatiDEMapr04.html).

The 30m DEM was derived from Aster level 1A images and was obtained from the Earth Observing System Data Gateway (EOS).

The 90m DEM accuracy requirements are ± 16m absolute and ± 6m relative vertical accuracy. The relative accuracy describes the error in a local 200-km scale, while the absolute accuracy indicates the error budget throughout the entire mission (Rabus et al., 2003).

The DEM does not represent hydrography (elevations below the water surface). However, in our case, the base discharge is very low, and due to lack of channel survey data, DEM elevations will be considered as channel elevations. The potential effects of this assumption will be addressed later.

6.1 Using Remote Sensing

An historical rainfall event occurred in the Gonaives watershed on September 19, 2004. During this event 261mm of precipitation were recorded in Ennery, and the whole city of Gonaives and surrounding areas were inundated. An Advanced Spaceborne Thermal Emission Radiometer (ASTER) satellite image taken on September 26, 2004 (one week after the flood) has the potential to reveal areas that were inundated. These areas were most likely wetter than before and/or had more sediment than before. A first look at the image (Figure 24) shows clearly some of the inundated areas. By contrasting this image taken in 2004 with another ASTER image taken in August 2001, it is obvious that a change detection algorithm could easily capture the flooded areas (light blue).

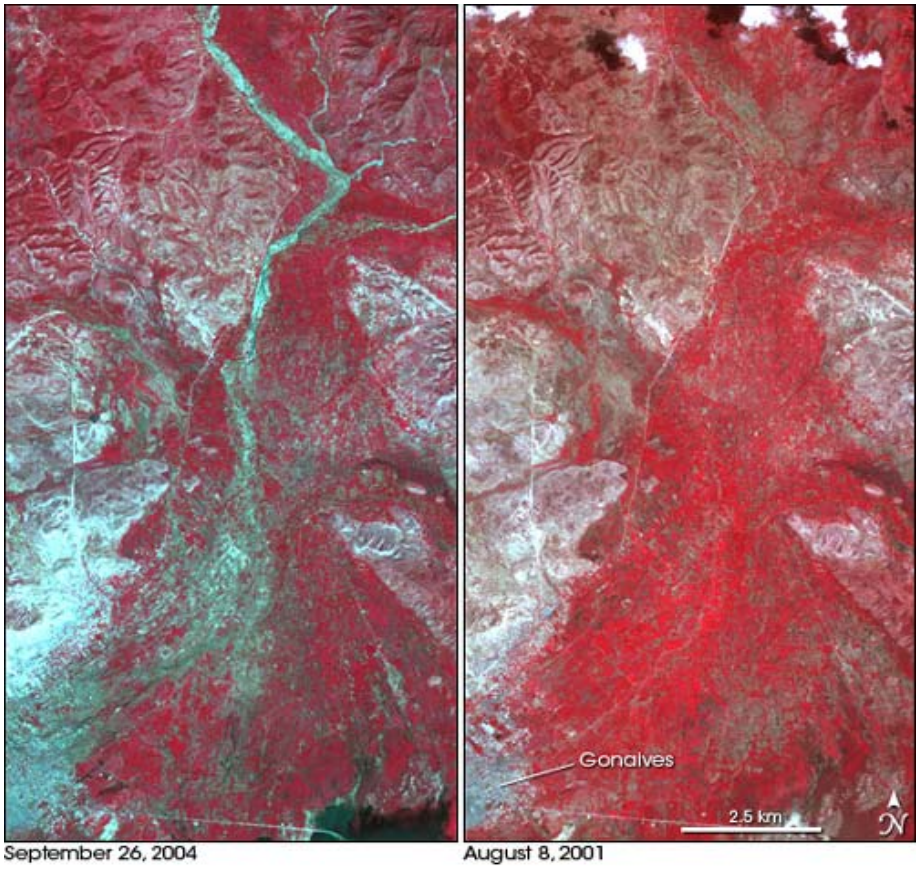

Figure 24: After and before the September 2004 flood : Aster images (source: NASA Earth Observatory: http://earthobservatory.nasa.gov/Newsroom/NewImages/images_topic.php3?topic=life&img_id=16682)

Quick looks at those images show how widespread the flood event was. The width of the channel has obviously increased, and when approaching the city, it splits into two paths: one inside the city and one outside the city. The path inside the city seems to be the main one since it was wider.

Use of these ASTER images offers three advantages: a) they are drawn from the same satellite, b) they have the same spatial and spectral resolution, and c) they have similar anniversary dates. ASTER has three bands in the visible near-infrared (VNIR), six bands in the short wave infrared (SWIR), and five bands in the thermal infrared (TIR), with

15m, 30m and 90m ground resolution, respectively, with along-track coverage in band 3 nadir (3N) and backward (3B) views (Yamaguchi et al. 1998).

The first three bands of the ASTER 2001 and the 2004 images were used in the change detection process since wetness will be easier to detect in those bands, particularly the near infrared (NIR) band. The two images were georeferenced and registered to a coordinate system (UTM, Zone 18, and WGS 84) and then stacked to produce a six-band image. This process was done with care as misregistration of images could have considerable impacts on change detection analysis (Dai and Khorram 1998). The referencing was made within ±7.5m. The spatial coordinates were gathered from 1:50,000 maps available for the area. As the extent of the original images was different, they were subsetted to obtain a common spatial extent for all bands in the image. The first three bands are the before image, and the three subsequent bands are the after image. The statistics of the composite image were calculated, and it was obvious that a significant change had taken place: the min, mean, median, mode each has decreased (see Table 20).

Table 20: Composite Image digital number statistics

Band	min	max	mean	median	mode	std deviation
1	55	255	88.673	83	72	23.221
2	32	255	64.048	57	42	25.634
3	22	186	68.557	72	33	29.311
4	39	255	71.231	65	46	24.903
5	18	255	48.836	42	22	27.265
6	11	190	59.729	61	22	34.366

There are numerous methods for change detection (Fung, 1990). The choice of a method is based on the goal of the change detection. Here we are only interested in wetted areas,

and therefore we believe that procedures such as Principal Component Analysis (PCA) and Univariate Image Differencing should be sufficient.

PRINCIPAL COMPONENT TRANSFORMATION

Principal component transformation (PCT) or analysis is a well known change detection method in remote sensing. It takes advantage of the decorrelation potential of the PCT to obtain a map where changes are easily detectable. The difficulty of this procedure is that it is hard to tell what caused the changes (Lillesand et al. 2004). However, for floodplain delineation, this is usually not a problem since the area of change is well known. This procedure was used by Gianinetto et al. (2006) with very good agreement with ground measurements of flood water volumes.

A principal component analysis is made on the composite image. The factor loadings indicate the provenance of the information (percent of band information) contained in the principal component. The factor loadings as well as the six PC components are presented in Table 21 and Figure 25-Figure 30 below. For more information about the factor loadings and how they are calculated, please refer to Jensen (2005).

Table 21: Factor Loading of composite image

Band\comp	1	2	3	4	5	6
1	0.8693	-0.4122	0.2486	-0.0539	-0.0636	0.0752
2	0.8937	-0.3746	0.2212	-0.0662	0.0616	-0.0627
3	0.9073	0.3246	0.1508	0.2207	-0.0062	-0.0042
4	0.9333	-0.2196	-0.2580	0.0204	-0.1088	-0.0428
5	0.9298	-0.2213	-0.2722	0.0646	0.0836	0.0352
6	0.8955	0.4163	-0.0250	-0.1554	0.0034	0.0062

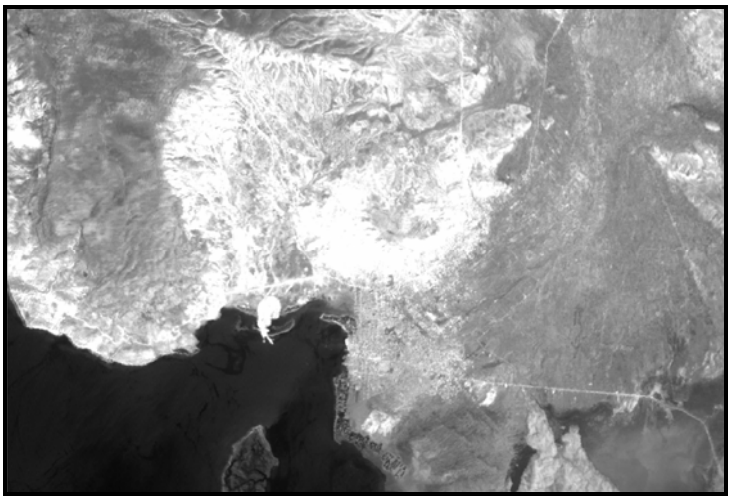

Figure 25: PC 1

Figure 26: PC 2

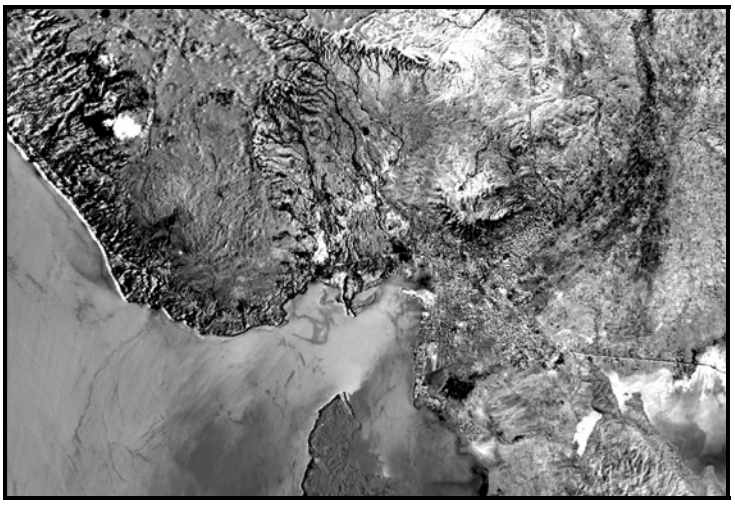

Figure 27: PC 3

Figure 28: PC 4

Figure 29: PC 5

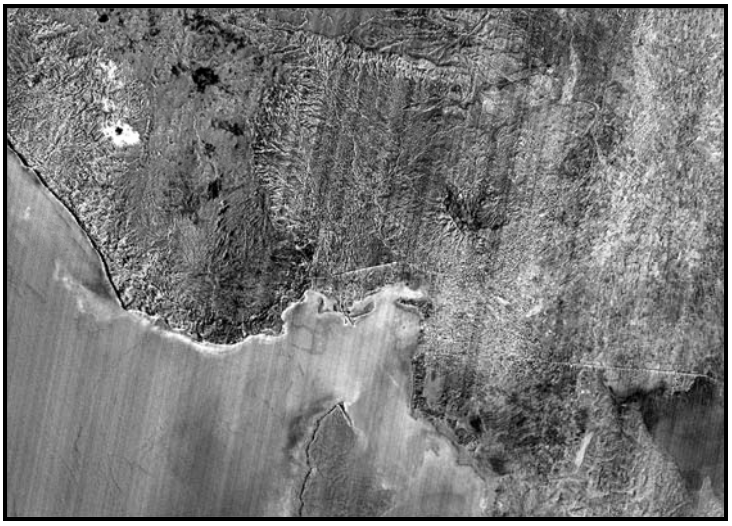

Figure 30: PC 6

PC4 seems to have the best potential for indicating change. The extents of the new lake are clear, as are the flows paths. It is worth noting that information from PC4 comes mostly from band3 of both images, but that those two bands are negatively correlated (see Table 21). Based on the histogram of PC4 (Figure 30), which suggested three major classes, an unsupervised classification with three classes was done with the 95% convergence threshold attained. The results (Figure 31) were close to the ones obtained from manual classification based on the histogram. The results from the unsupervised classification were chosen to work with.

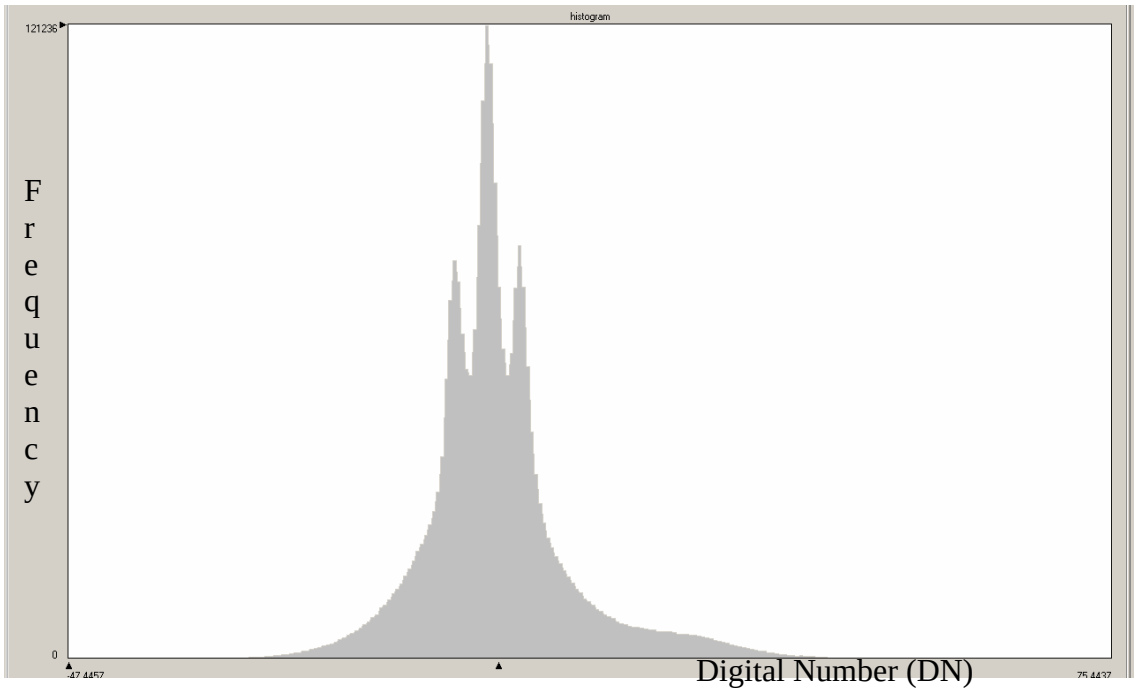

Figure 31: Histogram of PC4

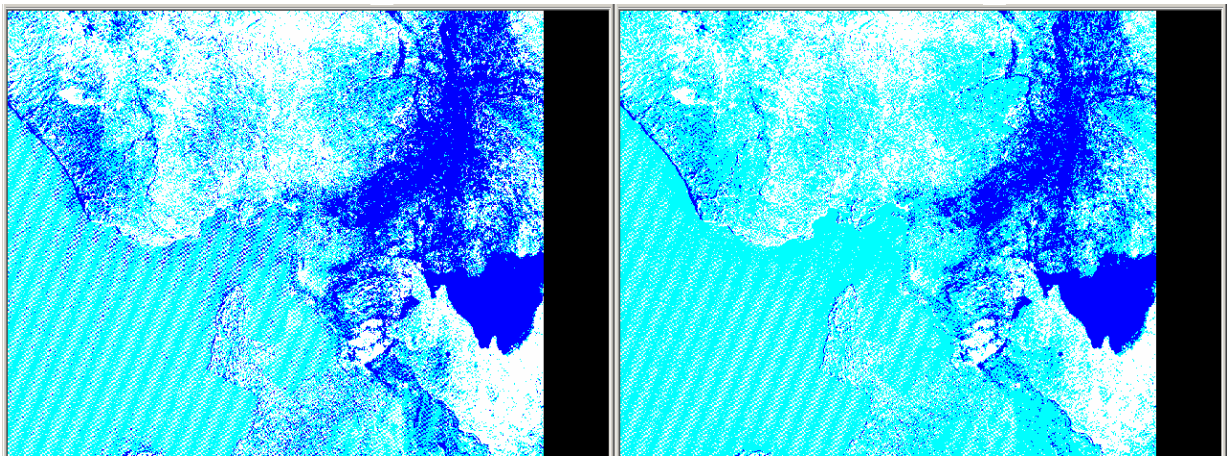

Figure 32: PC4 classes 1) histogram 2) unsupervised

BAND DIFFERENCING

Band differencing is used in order to assess change detection. Only the first three bands of the ASTER images were used. Atmospheric correction was considered unnecessary as this would only be shifting thresholds used for assessing change levels (Song et al. 2001). By use of ERDAS IMAGINE, a band differencing of before and after images was done. Pixels impacted by water will have positive values as their spectral response would have decreased due to the presence of water. All three bands were used. The following figures show the results.

Figure 33: Band 1- Band 4

Figure 34: Band 2 - Band 5

Figure 35: Band 3 - Band 6

The Band 3 – Band 6 differencing gave the best results. Using Bands 1-4 and 2-5 differences, the digital numbers (DN) in the flooded areas were positive instead of negative, which would mean that the spectral response of the pixels has increased for these areas. Band 1 and 2 also showed a smaller area compared to Band 3. The histogram of the difference image of band 3 is shown in Figure 36.

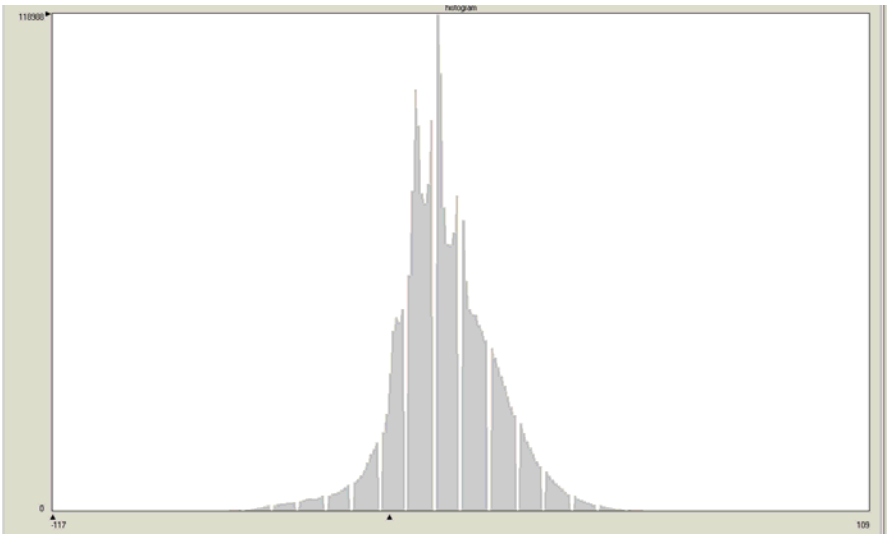

Figure 36: Histogram of Band 3-6 difference

Even though the histogram of the difference image of band 3 suggested 14 classes, just as for the PC, an unsupervised classification with three classes was done with a convergence threshold of 95%. The resulting image was used to classify areas as high risk, medium risk and low risk: high risk being the areas that were inundated the longest (areas having the same spectral response as the new lake); medium risk are areas that were flooded for a lesser duration; and low risk are areas that were not flooded.

ACCURACY

An accuracy assessment was done to quantify the agreement of the two images, i.e., the two procedures. The PC and the difference image were reduced to a smaller area, closest possible to the area of interest, in order to focus on the floodplain of the Quinte River. Fifty random points were generated, and an overall accuracy of 82% was obtained when comparing the difference image to the PC image.

Table 22: Classified area in square miles

Risk level	PC4	diffimage	Ratio: PC/diff
Low	14.34	13.31	1.08
Medium	25.44	26.20	0.97
High	15.95	15.21	1.05

The lack of agreement of the two procedures can be attributed to the use of an unsupervised classification on diff with three classes. Probably increasing the number of classes and then merging related classes would have helped. Another reason, related to

the first, is the lack of well-defined thresholds for the classes. Reducing the histogram of the difference image to three classes adds to the fuzziness of the threshold, which affects the unsupervised classification of the difference image. However, 82% accuracy in those conditions can be considered as acceptable and proves the ability of the principal component to model changes. The classification from PC4 image will be used for delineating the floodplain. The chosen image was aggregated and then converted into a polygon-coverage. The algorithm was not able to distinguish clearly the flooded areas in the city which were mostly classified as medium risk. However, some parts of northern Gonaives are classified as high risk zones. As the aggregation connected pixels of the same class to one another, it failed to capture the high risk zone in the city. The flooded area located outside the city is estimated as 32.43 km^2 (see Figure 37).

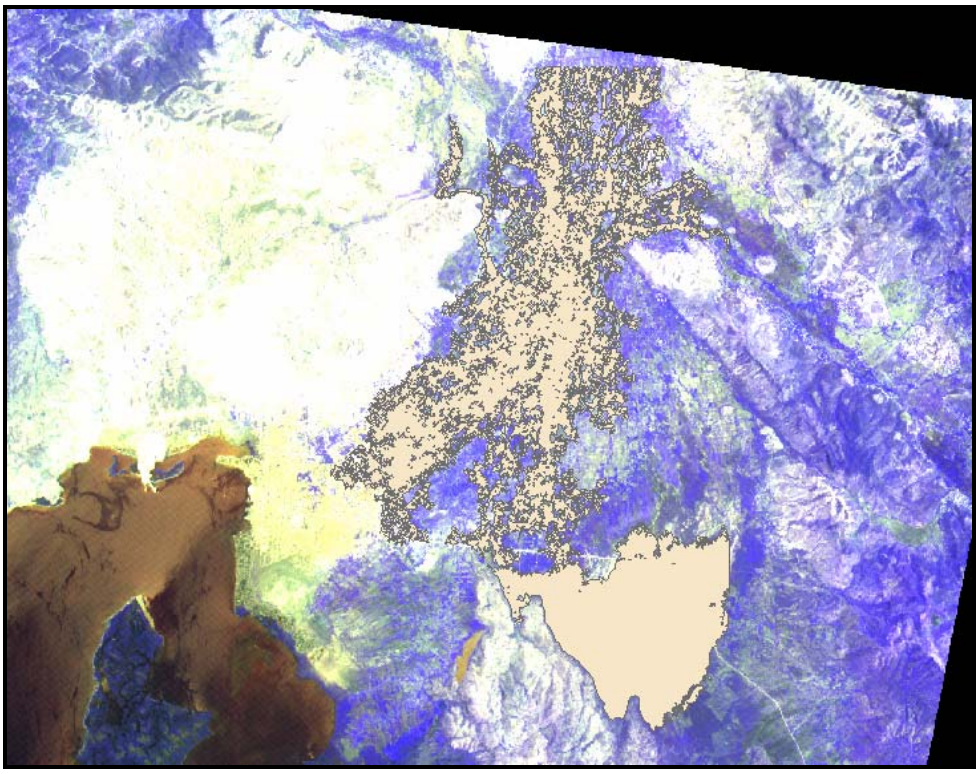

Figure 37: Inundated areas outside of the city

6.2 Using HEC-GeoRas

While the use of the 90m DEM is considered acceptable for delineation of the watersheds, it is advisable to use the lowest resolution available when it comes to floodplain delineation. The 30m DEM from ASTER was used to understand the hydraulic processes in the lower part of the watershed. Basically, it shows that the city of Gonaives is divided into two parts: one north of the road network and the other south of the road network, and the two have different contributing areas and therefore receive different volumes of water during flood events. As the contributing area of the southern side is smaller, it may be less impacted by flood waters compared to the northern part of the city. Analyses of the elevation data in ArcGIS also show that many parts of the city (both northern and southern) are under sea level. Additionally, contrary to observed data, flow paths go straight into the city, which indicates that the natural path of the river is inside the city of Gonaives rather than to the south. The procedure for watershed delineation, including flowpaths for the lower reaches of the basin, is presented in the appendix.

Hydraulic modeling is accomplished using HEC-RAS (Bunner et al. 2001), and HEC-GeoRAS (USACE, 2005). Using HEC-GeoRAS, the channel cross sections and geometry were extracted from ArcMap and exported to HEC-RAS. HEC-RAS then performed steady flow analyses using flow information entered by the user. The flow information was obtained from simulations in HEC-HMS. Results were then exported back to ArcMap to delineate the floodplain. HEC-GeoRAS is a set of ArcGIS tools

specifically designed to process geospatial data for use with HEC-RAS. It is used as an extension of ArcGIS and its role is to facilitate floodplain delineation by using the automated capabilities of ArcGIS and HEC-RAS. Both of those software programs produce outputs that are used as inputs in the other software.

The floodplain delineation starts by drawing the river channels, the flowpath lines, the banks and the cross sections. If necessary, there can be other features too such as levees, obstructions, storage areas, and bridges. The present model only contains levees as additional information. One limitation of HEC-RAS which negatively impacted the model is that it only allows one levee per bank. While this is in most cases sufficient, when modeling low lands care must be taken in choosing the most efficient location of the levee. Actually, the levee may not exist in reality but it may be used to keep the flow contained in the proper channel. After identifying the different rivers and reaches, as well as left and right overbank flowlines, all needed information involving elevation and distances can be extracted from the DEM and exported to HEC-RAS for hydraulic modeling. Some cross-sections of the floodplain are provided in the Appendix D.

6.3 Hydraulic Modeling

The model output from HEC-GeoRAS is exported to HEC-RAS. However, the roughness coefficient is not automatically defined and is entered manually for all the rivers and reaches. As this is an important parameter of hydraulic models, and it cannot be measured but only estimated, the roughness coefficient could be a source of uncertainty. A range of roughness coefficients is possible for floodplains, usually from 0.02 to 0.05. Floodplains will be delineated for a range of roughness coefficients, and the differences will be ascertained. The roughness coefficient that gives the most reasonable results (comparable to the remote sensing analyses) is the one that should be chosen.

After the geometric data was imported from HEC-GeoRAS, it is still necessary to enter the flow data in HEC-RAS. A simple steady flow analysis corresponding to the peak discharges is considered sufficient for floodplain mapping. The flood discharges corresponding to the different return periods are entered for the two upper reaches and for the junction. A normal depth boundary condition is used with the slope being 0.003. The simulation is run and the cross sections and water surface profiles are then available. The cross sections and water elevations can then be exported back to HEC-GeoRAS, which reads the imported water surface elevations and couples the data with the chosen DEM to compute water depths and floodplain extents. Here are some examples chosen from the results obtained for different return periods. A value of n = 0.05 was selected based on remote sensing analysis.

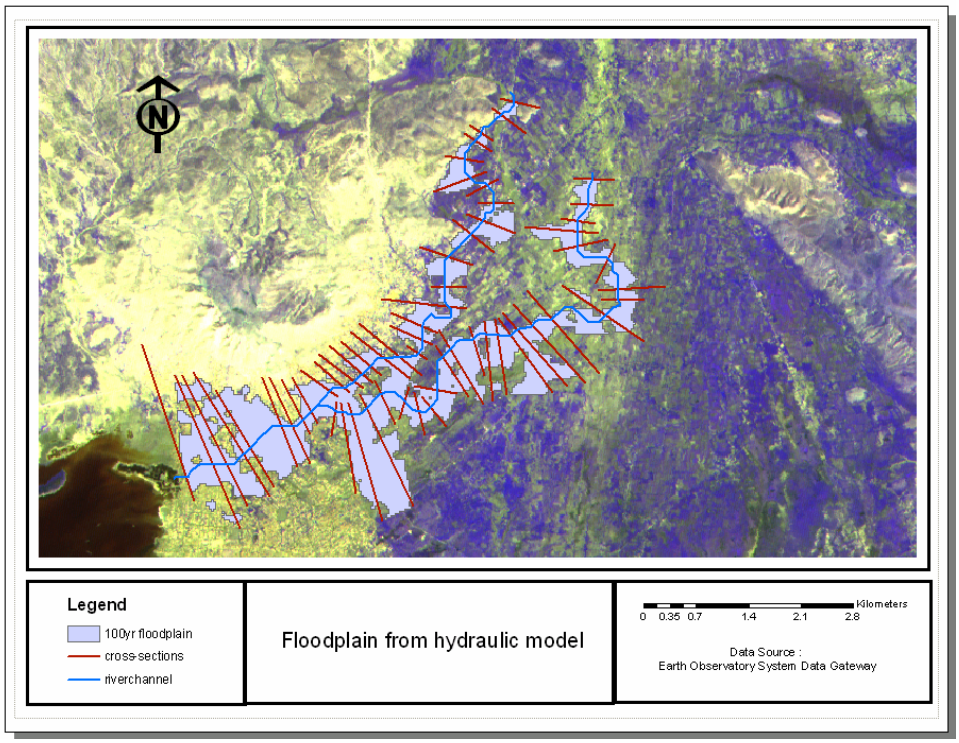

Figure 38: 100 yr floodplain with n=0.05

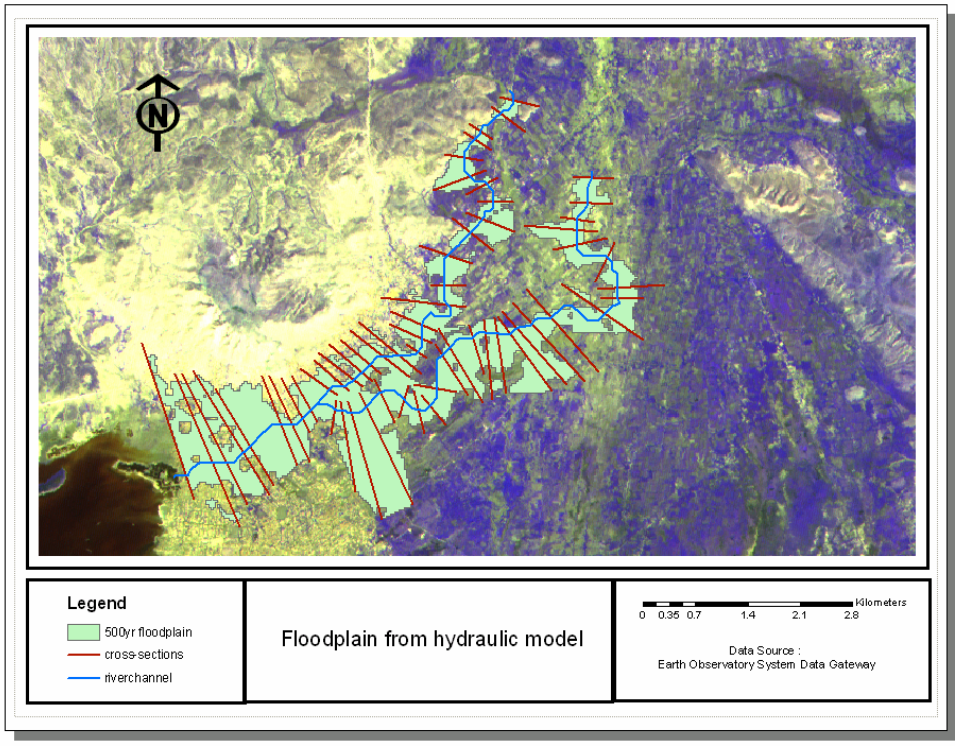

Figure 39: 500 yr floodplain with n=0.05

Figure 40 shows the variation of the inundated area with the roughness coefficient and the return period. A table corresponding to the figure is provided in Appendix D.

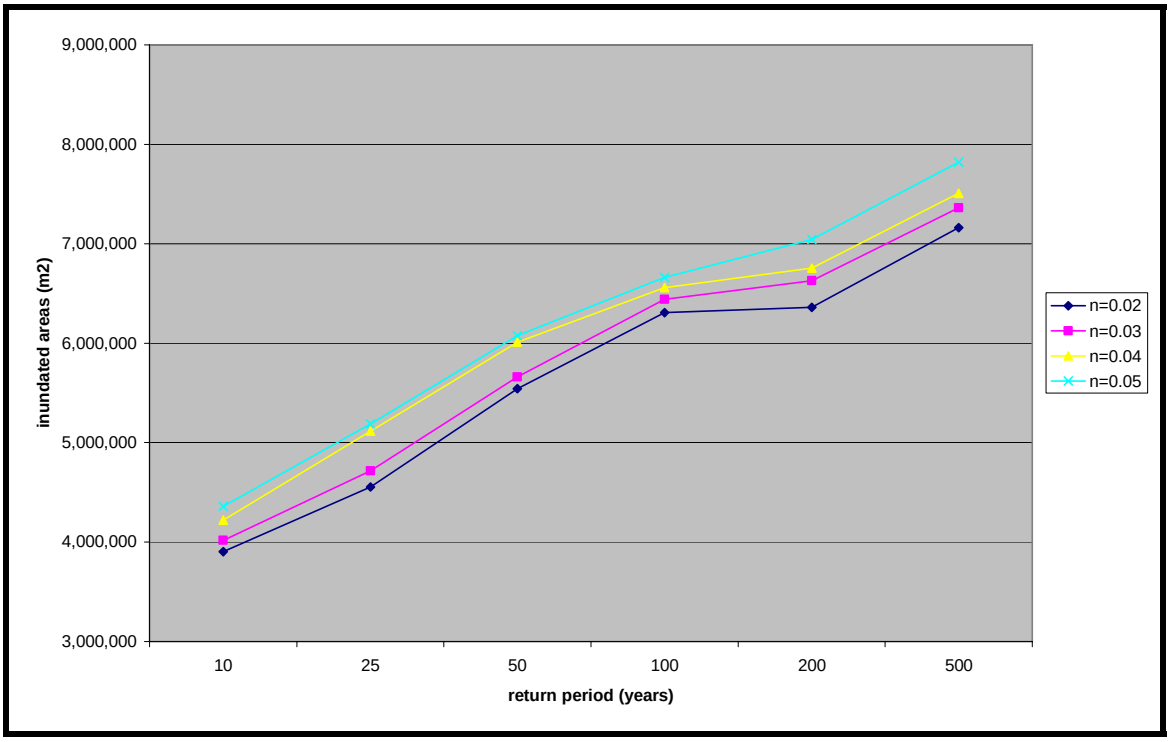

Figure 40: Effect of roughness coefficient

As expected, the return period has quite an impact on the extent of the floodplain. However, between the 100 and 200 yr flood, the growth rate decreases significantly, resulting in smaller differences between the inundated areas. This is not a result of the precipitation but rather a characteristic of the topography of the region under study.

It was found that the roughness coefficient does not significantly impact the inundated area. The variation in inundated areas due to the roughness coefficient for the range considered (0.02-0.05) for each return period was than 10% (see Table 38 in Appendix D). Differences due to roughness coefficient for the range considered are usually 10% or

less. This is an important finding since the roughness parameter cannot be measured but only estimated.

6.4 Hazard Map

Two sets of results are available for developing a hazard map—the floodplain maps developed from the GIS-based hydraulic modeling, and the change detection map developed using remote sensing. The two approaches are compared, and considering the uncertainties and limitations inherent in each approach, a hybrid method is recommended.

Figure 41 shows a hazard map developed using PC4 and Figure 41 shows a hazard map using the image difference. Even if the values are not the same, the classification is basically similar. However, results of PC4 will be used in subsequent analyses. The underlying assumption is that areas more at risk were those subjected to flooding for a longer duration. Depending on the level of change of the pixel during the flood, it is subjectively assigned a number from 1 to 9 (highest risk to lowest risk). No return period is assigned to the risk level; only the wetness duration is considered, as indicated by the change detection analysis.

A hazard map developed using the hydraulic modeling results is shown in Figure 43. In this case, a pixel is assigned a number from 1 to given its likelihood of being inundated, with areas inundated during a flood more common than the 10-yr flood assigned a risk value of 1, 20 yr flood assigned a value of 2 and so on.

Alternatively, simulated flood depths during a particularly severe flood, say, a 500-yr flood, could be used to quantify risk. This has been done using the water depth of the 500-yr flood. The results are shown in Figure 44.

A hybrid map (see Figure 45) resulting from the three procedures is found by weighting each of them equally.

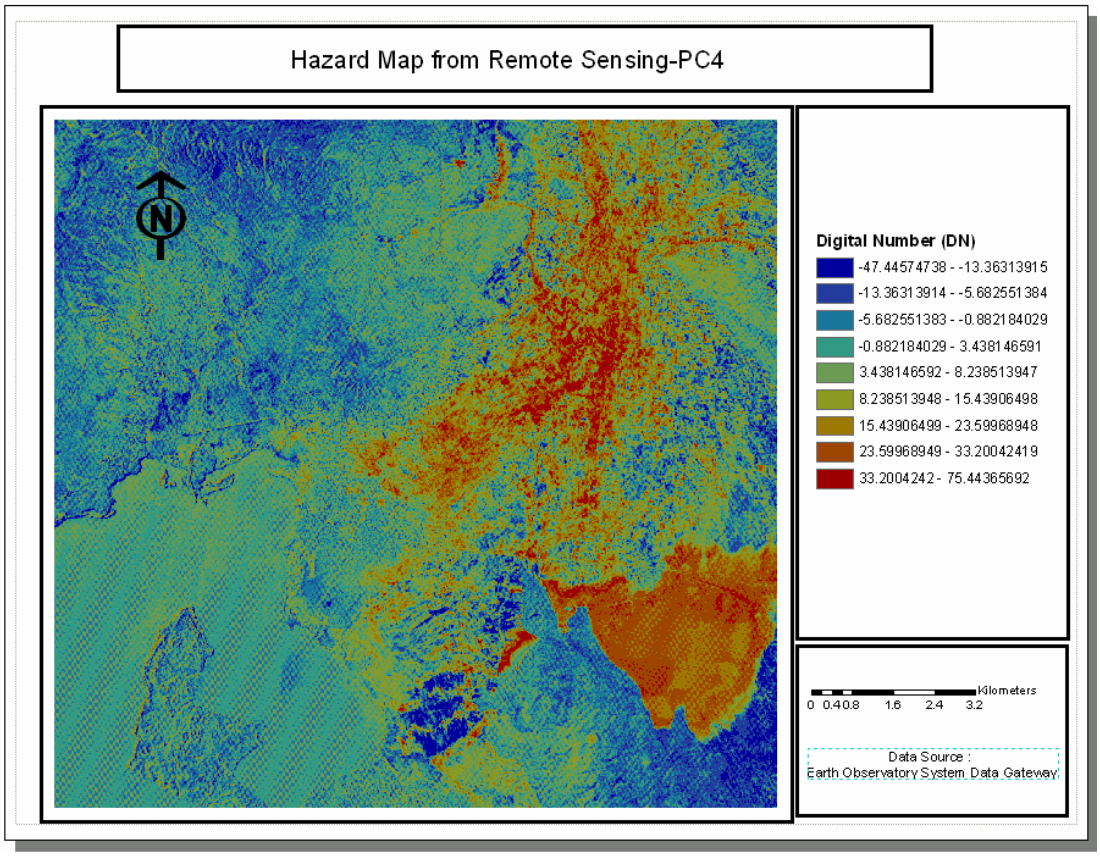

Figure 41: Hazard map from remote sensing change detection analysis using PC4.

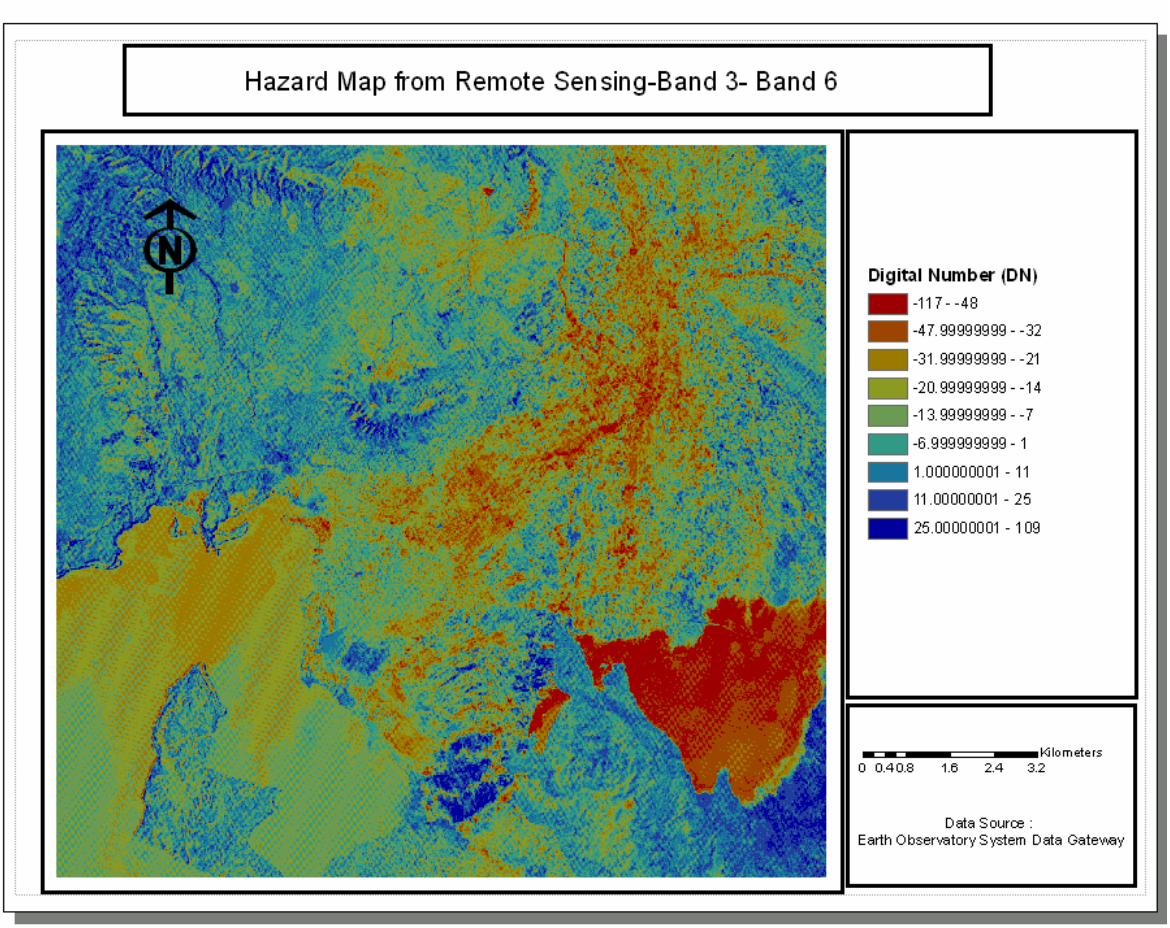

Figure 42: Hazard map from remote sensing change detection analysis using image difference.

From the remote sensing results, it can be seen that areas in the hills of Morne Bienac and Savane Desolee have relatively low hazard value (low DN) compared to other areas. The fact that they are located in high grounds at relatively small distance to the city make them interesting places to place shelters in case of evacuation. However, the site of Savane Desolee is easier to access because of relatively mild slopes.

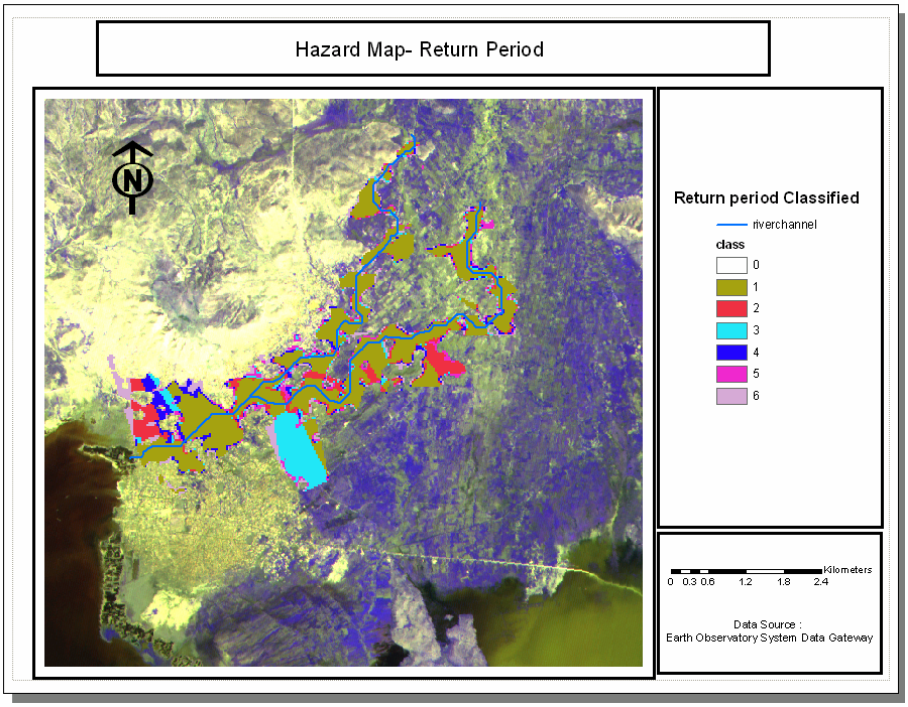

Figure 43: Return period hazard map

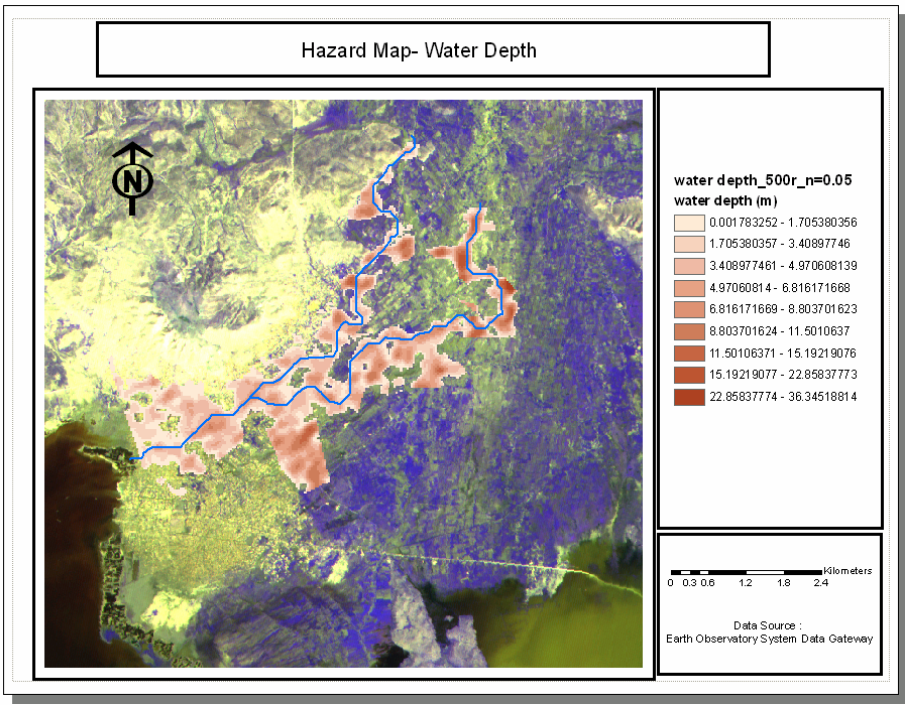

Figure 44: Water depth hazard map

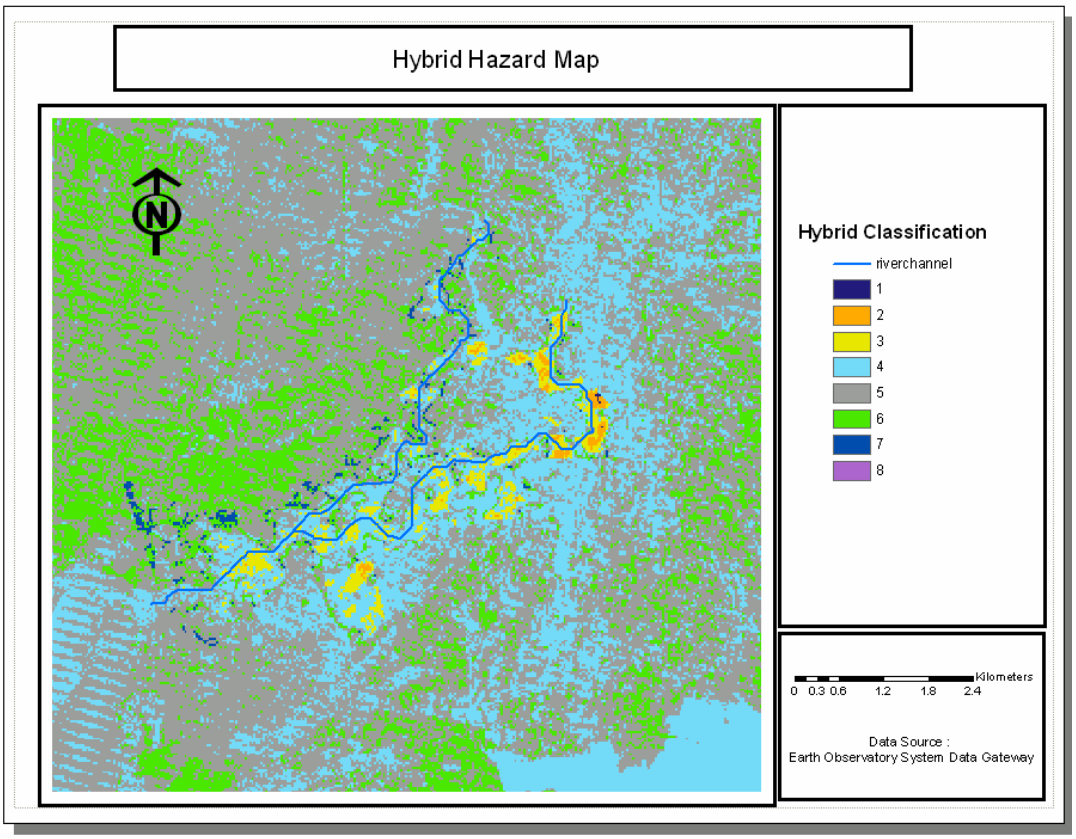

Figure 45: Hybrid hazard map

In the present study we have only considered the river flow path which goes inside the city of Gonaives in the HEC-RAS model. This choice introduces some bias in the hybrid risk map, where certainly the southern flow path which contributes to forms a new lake in Savane desolee would show higher hazard values. However, this oversight is likely to affect only a small portion of the hybrid hazard map.

CHAPTER 7- VULNERABILITY AND RISK ASSESSMENT

(Mora 1995) 's map of main hurricanes' path over the island of Haiti from 1886 to 1996 shows Gonaives and surrounding areas as being very much subject to hurricanes. With such likelihood of being in the path of a hurricane, as well as being located in an alluvial plain with some areas being under sea level and with a river's natural path going straight into the city, it is obvious that the city of Gonaives is at risk of flooding. Furthermore,

> "deforestation (in Haiti) combined with the heavy agricultural pressure on marginal farm lands, accelerates soil erosion, which increases the volume of sediment carried by the streams and degrades the water quality of the upland and downstream areas. Soil from eroded slopes clogs streams, drainage channels, impoundments, and water systems, resulting in higher operation and maintenance costs. Inland deforestation is causing increased sedimentation in the rivers discharging to the coast which is damaging the barrier reef and associated fragile ecosystems. Increased turbidity is adversely affecting mangroves, coral reefs, and seagrass beds. As erosion increases, the river regime will become steeper, which increases the amount of runoff and decreases the amount of infiltration with each passing year, the rivers and streams flow more like torrents and less like stable permanent rivers." (USACE 1999)

But rather than considering floods just as a physical event (hazard), vulnerability assessment gives us a tool to consider all those processes that can exacerbate the impact of floods as well as make recovery more difficult.

Everything being equal in terms of hazard, the more vulnerable a region is, the more it is going to experience disasters. "Vulnerability is the characteristics of a person or group and their situation that influence their capacity to anticipate, cope with, resist and recover from the impact of a natural hazard" (Wisner 2004). Although there is no agreed upon definition of vulnerability (Heijmans 2001), the previous definition has the advantage of emphasizing the human aspect of natural disasters.

The natural hazards literature is full of studies identifying vulnerability factors (Bankoff 2003; Cutter et al. 2003; Prowse and Chronic Poverty Research Centre 2003). Some themes like poverty, population density, education level, past flood experience, environmental and political injustice and unprotected infrastructures are common (D'Ercole 1996; Masozera et al. 2006; Morrow 1999; Rashid 2000; Satterfield et al. 2004). Cutter et al. (2003) identifies a set of 15 parameters that should be taken into account in social vulnerability assessment. These parameters are socio-economic status, gender, race or ethnicity, age, commercial or industrial development, employment loss, residential property, infrastructures and lifelines, renters, occupation, family structure, population growth, medical services, social dependence, and special needs population. Information about all those parameters is available in rare cases. In our case, only a few parameters will be considered.

7.1 Vulnerability Model

In the case of Gonaives, the goal is to map people's vulnerability to floods using readily available information at the scale of interest. The parameters that are taken into account are: land use/land cover, importance of transportation infrastructure, and distance to road network. Each of those parameters were classified and ranked from 1-9 (highest to lowest)

The Land Use/Land Cover map was obtained from analysis of the August 2001 image using the NDVI index. It can be used as an indicator of population density and the economic activities of the population. The land use/land cover map (Figure 46) was classified into five categories: 1- urban, 2-peri-urban/bare soil, 3-agriculture, 8-sparse vegetation, and 9-water. Urban areas were ranked as 1 because these areas have the highest population density and suffer the most economic damage; and peri-urban/bare soil is ranked 2. Rural areas generating revenues from agriculture and stock farming were ranked as 3, with other areas of less importance ranked as 8 and 10.

Transportation infrastructure is also very important in the consideration of vulnerability. Not only do roads account for a large percentage of the damages in terms of repair cost, they also play a vital role during the evacuation process. Therefore, their vulnerability is also a measure of the vulnerability of the affected population. The more important a road is in the network, the more vulnerable it is since it will take more financial resources to rebuild it. Two types of roads are considered in this analysis: the primary and the secondary roads. The primary road network connects cities and departments to one

another whereas secondary roads connect areas inside the county. Primary roads were assigned a vulnerability of 1 and secondary roads a vulnerability of 5 (see Figure 47).

Also, the distance to a road network was considered as a factor of vulnerability. As the further a person is located from a road, the more vulnerable this person is since it will take more time for this person to evacuate. Distance to road network was ranked from 1 to 9 in increments of approximately 750 meters (e.g., 1: 6,015 – 6767 m, 2: 5,264 – 6,015 m, etc.) Figure 48 shows the resulting map.

The composite vulnerability map (Figure 49) is obtained by giving equal weight (presuming that they have the same importance in the model) to all the layers and ranking them from 1 to 9 using the weighted overlay available in GIS, on a pixel-by-pixel basis. The vulnerability model is thus

Vulnerability = (1/3) Land use/Land cover + (1/3) Transportation network + (1/3) Distance to road network.

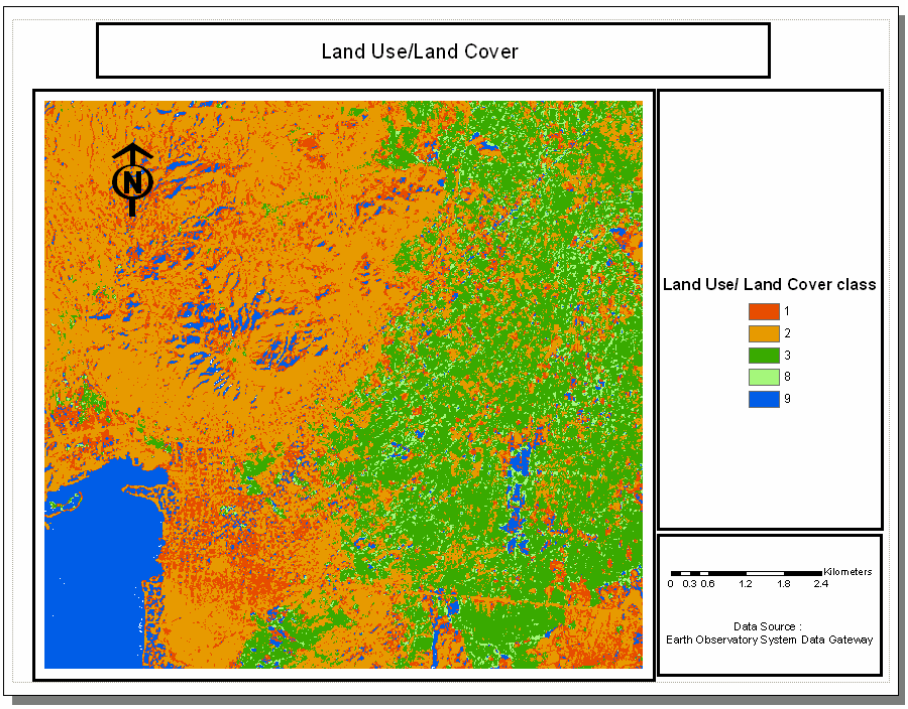

Figure 46: Land Use map

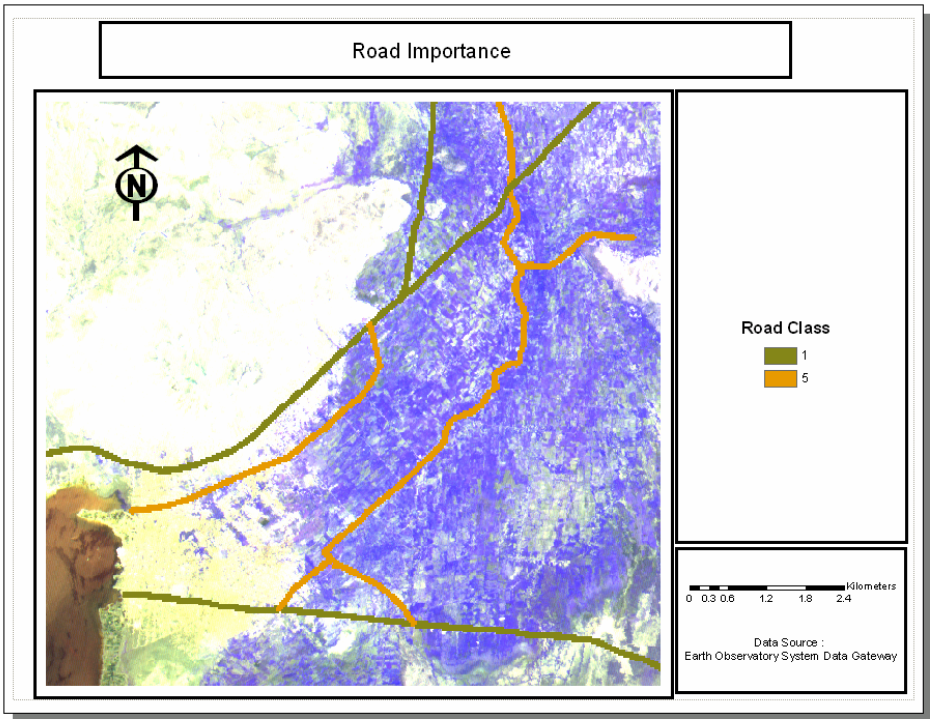

Figure 47: Importance of road

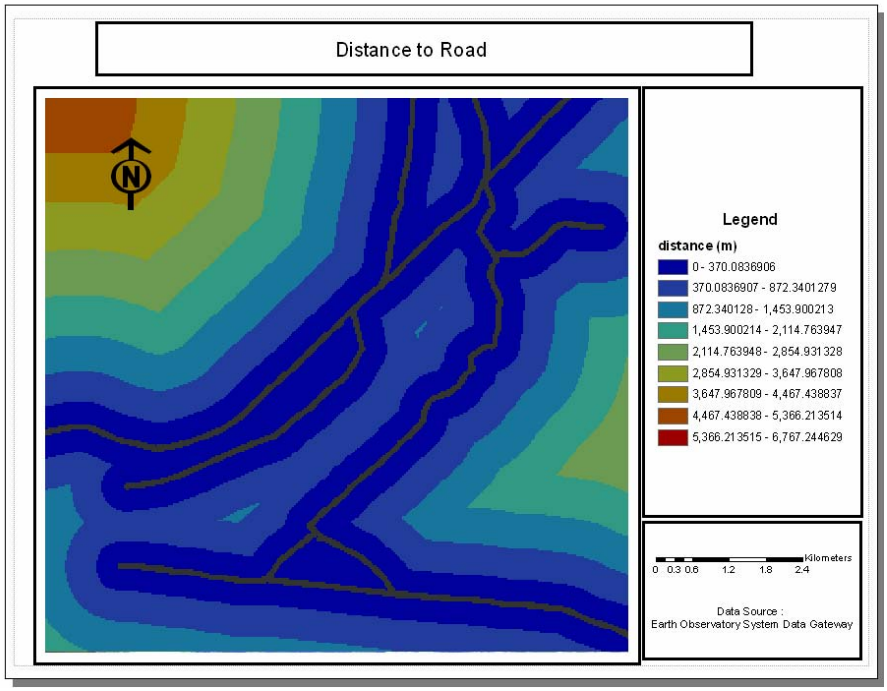

Figure 48: Distance to nearest major road

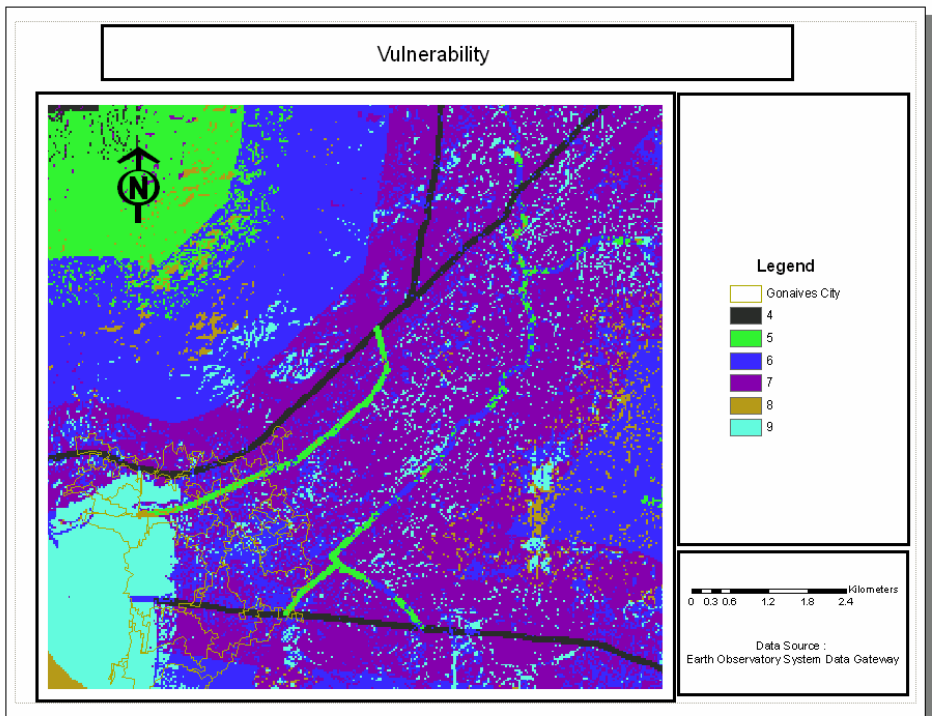

Figure 49: Vulnerability map

The vulnerability map presented above reflects the potential effects of floods mainly on economic activities. It does not consider the potential for loss of life that could be taken into account through population density, except through consideration of land use classification. This is because of the lack of adequate data at the scale of interest.

7.2 Risk Model

The flood risk map (Figure 51) is obtained by using the weighted overlay method of the hazard and the vulnerability map:

Risk = Hazard * Vulnerability

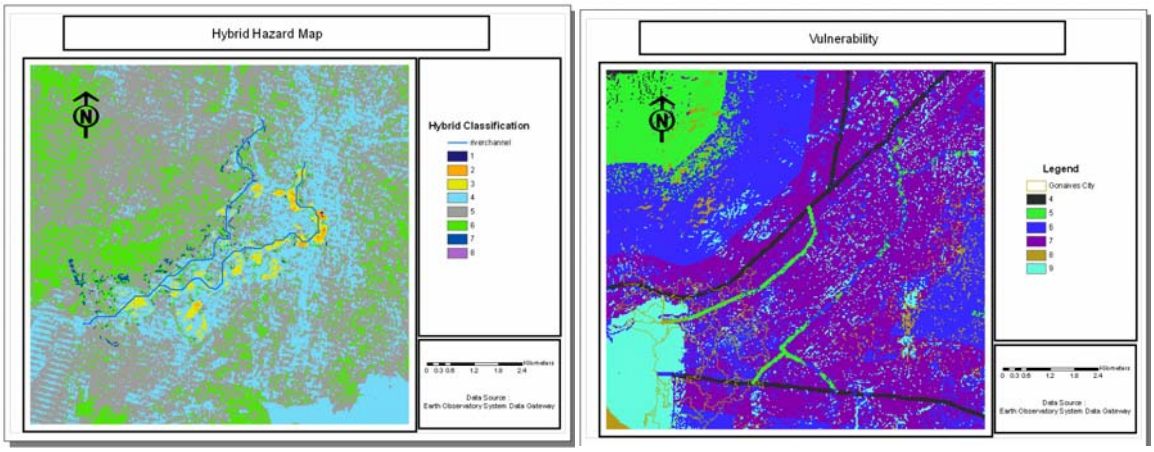

Figure 50: Hazard and Vulnerability maps

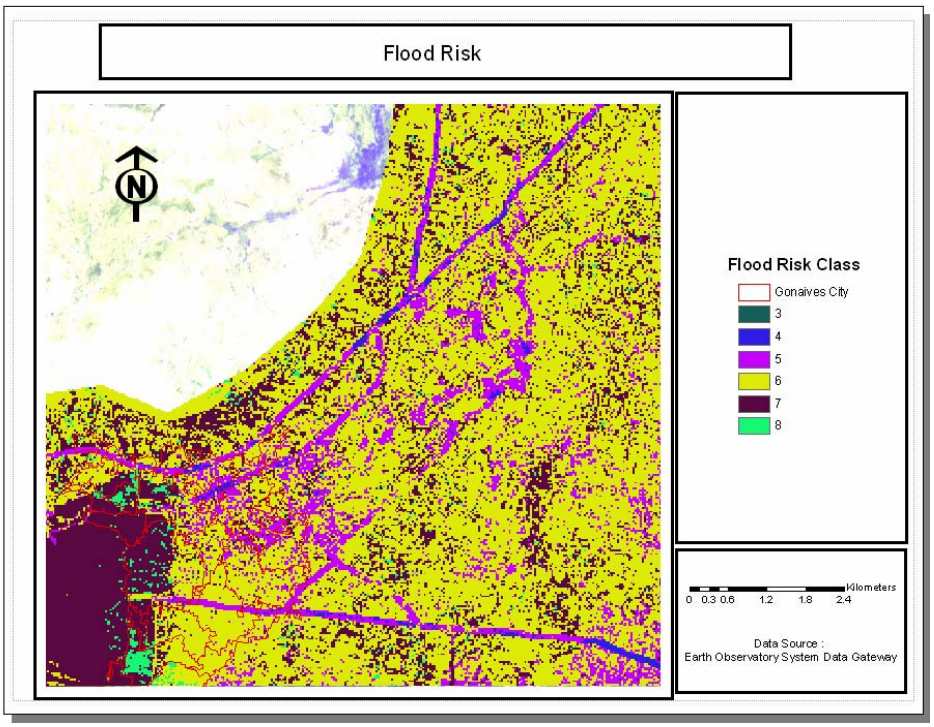

Figure 51: Risk map

7.3 Discussion

A common feature of vulnerability analyses is that they are somewhat subjective. Many of the choices depend on the analyst's judgment. This makes it difficult to ascertain the quality of vulnerability analysis.

Vulnerability analyses are also very goal-specific; some may be oriented toward the impact of loss of life and goods, others toward economic disruption, and others toward evacuation complexities.

This subjectivity and complexity of vulnerability analyses should always be considered in the interpretation of vulnerability results, and the results should only be considered within the context and the framework for which they were developed. As risk quantification is a product of hazard and vulnerability indices, it also inherits the assumptions and limitations of the vulnerability analyses.

Apart from the ranking subjectivity introduced by the analyst, the processes used also introduce some more subjectivity. A hierarchical map obtained through weighted overlays would probably not lead to the same conclusions as a boolean overlay, a pairwise comparison, or a decision rule method. This is illustrated by Yalcin and Akyurek (2004).

CHAPTER 8- CONCLUSIONS AND RECOMMENDATIONS

Results from the analyses show that coastal Gonaives is less at risk to flooding than surrounding areas. It also appears that the natural path of the Quinte River goes straight into the city as shown by the 30m and 90m DEMs. Evacuation, if necessary, should be carried out early to shelters that would be located on the hill next to Savane Desolee. However, if late, routing evacuees toward Morne Bienac is probably the best choice.

Foreign consultancies may advise according to standards and conditions with which they are familiar, rather than the ones that may be appropriate or those that prevail in the country in question (von Sperling and Fattal, 2001). It is also to be expected that industrialized countries, which have more resources, will have more stringent standards and regulations than developing countries. For many developing countries, where adequate data is lacking, such standards should be considered as targets rather than rigid norms. One way to address the lack of data is to use different methods and cross-validation. In this study, GIS was combined with hydrologic and hydraulic modeling, and Manning's roughness coefficient was chosen based on the remote sensing analysis. Combining methods in this way can help determine the likely order of magnitude of the parameter under investigation, providing a framework for sensitivity analysis to identify important parameters and their effect on the results. Later on, if field work is possible, the areas of investigation would have been already identified which will save time and money.

In floodplain delineation, there are a number of other methods that could be used. Application of the methods depends on the region, available data, and existing technical expertise. Geomorphic methods (Nardi et al., 2006) and alluvial fan methods (Pelletier et al., 2005) are promising and should be investigated. In the particular case of Gonaives, hydrologic and hydraulic modeling methods were limited because of insufficient data, as would be the alluvial fan and geomorphic methods, especially due to the unique characteristics of the river divergence during the 2004 flood. However, remote sensing has proven promising and is expected to play a more important role in the future for flood risk assessment, particularly in developing countries.

REFERENCES

Alexander, D. (1997). "The study of Natural Disasters, 1977-1997: Some reflections on a changing field of knowledge." *Disasters*, 21(4), 284-304.

Arnaud, P., Bouvier, C., Cisneros, L., and Dominguez, R. (2002). "Influence of rainfall spatial variability on flood prediction." *Journal of Hydrology*, 260(1-4), 216-230.

Bankoff, G. (2003). "Constructing vulnerability: The historical, natural and social generation of flooding in metropolitan manila." *Disasters*, 27(3), 224-238.

Bates, P. D., and De Roo, A. P. J. (2000). "A simple raster-based model for flood inundation simulation." *Journal of Hydrology*, 236(1-2), 54-77.

Beven, K. (1987). "Towards the Use of Catchment Geomorphology in Flood Frequency Predictions." *Earth Surface Processes and Landforms*, 12(1), 69-82.

Bhunya, P. K., Mishra, S. K., and Berndtsson, R. (2003). "Simplified two-parameter gamma distribution for derivation of synthetic unit hydrograph." *Journal of Hydrologic Engineering*, 8(4), 226-230.

Bondelid, T. R., Mccuen, R. H., and Jackson, T. J. (1982). "Sensitivity of Scs Models to Curve Number Variation." *Water Resources Bulletin*, 18(1), 111-116.

Bradbrook, K., Waller, S., and Morris, D. (2005). "National floodplain mapping: Datasets and methods - 160,000 km in 12 months." *Natural Hazards*, 36(1-2), 103-123.

Brunner, G. W., United States. Army. Corps of Engineers., Institute for Water Resources (U.S.), and Hydrologic Engineering Center (U.S.). (2001b). *HEC-RAS river analysis system : user's manual*, US Army Corps of Engineers Institute for Water Resources Hydrologic Engineering Center, Davis, CA.

Bruzzone, L., and Prieto, D. F. (2000). "Automatic analysis of the difference image for unsupervised change detection." *Ieee Transactions on Geoscience and Remote Sensing*, 38(3), 1171-1182.

CDERA. (2003). "Status of Hazard Maps: Vulnerabiltiy assessements and digital maps-Haiti : country report." (http://www.cdera.org/projects/cadm/docs/haiti_hmvadm.pdf; date accessed: june 28, 2007)

CEPALC (2005), "Le cyclone Jeanne en Haiti: Degats et Effets sur les departements du Nord'Ouest et de l'Artibonite: approfondissement de la vulnerabilite" (http://www.cepal.org/cgi-bin/getProd.asp?xml=/publicaciones/xml/1/20971/P20971.xml&xsl=/mexico/tpl-f/p9f.xsl&base=/mexico/tpl/top-bottom.xslt; date accessed: june)

Chang, C. L., Lo, S. L., and Chen, M. Y. (2007). "Uncertainty in watershed response predictions induced by spatial variability of precipitation." *Environmental Monitoring and Assessment*, 127(1-3), 147-153.

Chang, K.-T. (2006). "Introduction to geographic information systems." Recording for the Blind & Dyslexic, Princeton, N.J.

Chow, V. T., Maidment, D. R., and Mays, L. W. (1988). *Applied hydrology*, McGraw-Hill, New York.

Chowdhury, J. U., and Stedinger, J. R. (1991). "Confidence-Interval for Design Floods with Estimated Skew Coefficient." *Journal of Hydraulic Engineering-Asce*, 117(7), 811-831.

Chowdhury, J. U., Stedinger, J. R., and Lu, L. H. (1991). "Goodness-of-Fit Tests for Regional Generalized Extreme Value Flood Distributions." *Water Resources Research*, 27(7), 1765-1776.

CNSA. (2002). "Haiti-Insecurite Alimentaire 2001-2002." (http://www.cnsahaiti.org/docs_cnsa/Bilan2002.pdf; date accessed: June 28, 2007)

Coles, S., Pericchi, L. R., and Sisson, S. (2003). "A fully probabilistic approach to extreme rainfall modeling." *Journal of Hydrology*, 273(1-4), 35-50.

Cunnane, C. (1978). "Unbiased Plotting Positions - Review." *Journal of Hydrology*, 37(3-4), 205-222.

Curtis, D. C., and Burnash, R. J. C. "Inadvertent rain gauge inconsistencies and their effects on hydrologic analysis." *California-Nevada ALERT users group conference*, Ventura, CA.

Cutter, S. L., Boruff, B. J., and Shirley, W. L. (2003). "Social vulnerability to environmental hazards." *Social Science Quarterly*, 84(2), 242-261.

D'Ercole, R. (1996). "Representations cartographiques des facteurs de vulnerabilite des populations exposees a une menace volcanique;." *Bulletin de l'Institut francais d'etudes andines*, 25(3), 479-507.

D'Ercole, R. (2003). "Catastrophes et Disparites de Developpement dans le bassin caraibe." *MappeMonde*, 72, 37-42. (http://www.mgm.fr/PUB/Mappemonde/M403/Catastrophes.pdf; date accessed: June 18, 2007)

Dai, X. L., and Khorram, S. (1998). "The effects of image misregistration on the accuracy of remotely sensed change detection." *Ieee Transactions on Geoscience and Remote Sensing*, 36(5), 1566-1577.

Dalrymple, T. (1960). *Flood frequency analyses*, Washington, D.C. : U.S. G.P.O.

Daniil, E. I., and Michas, S. N. (2006). "Discussion of "Factors Affecting Estimates of Average Watershed Slope" by A Jason Hill and Vincent S Neary." *Journal of hydrologic engineering*, 11(4), 2.

De Michele, C., and Rosso, R. (2001). "Uncertainty assessment of regionalized flood frequency estimates." *Journal of Hydrologic Engineering*, 6(6), 453-459.

Dilley, M. (2006). "Setting priorities: global patterns of disaster risk." *Philosophical Transactions of the Royal Society*, 364, 2217-2229.

El-Jabi, N., and Sarraf, S. (1991). "Effect of Maximum Rainfall Position on Rainfall-Runoff Relationship." *Journal of hydraulic engineering*, 117(5), 681.

FewsNet. (2005). "Profils des modes de vie en Haiti." (http://www.fews.net/livelihoods/files/ht/profiling.pdf; date accessed: June 18, 2007)

Filliben, J. J. (1975). "Probability Plot Correlation Coefficient Test for Normality." *Technometrics*, 17(1), 111-117.

Fung, T. (1990b). "An Assessment of TM Imagery For Land-Cover Change Detection." *IEEE transactions on geoscience and remote sensing : a publication of the IEEE Geoscience and Remote Sensing Society*, 28(4), 681.

Gall, M., Boruff, B. J., and Cutter, S. L. (2007). "Assessing Flood Hazard Zones in the Absence of Digital

Floodplain Maps: Comparison of Alternative Approaches." *Natural Hazards Review*, 8(1).

Gianinetto, M., Villa, P., and Lechi, G. (2006). "Postflood damage evaluation using landsat TM and ETM plus data integrated with DEM." *Ieee Transactions on Geoscience and Remote Sensing*, 44(1), 236-243.

Griffis, V. W., and Stedinger, J. R. (2007a). "Evolution of flood frequency analysis with Bulletin 17." *Journal of Hydrologic Engineering*, 12(3), 283-297.

Griffis, V. W., and Stedinger, J. R. (2007b). "The log-Pearson tye 3 distribution and its application in flood frequency analysis, 2. Parameter estimation methods." *Journal of Hydrologic Engineering*, in press.

Harter, H. L. (1984). "Another Look at Plotting Positions." *Communications in Statistics-Theory and Methods*, 13(13), 1613-1633.

Heijmans, A. (2001). *Vulnerability : a matter of perception*, Benfield Greig Hazard Research Centre, London, England.

Herschfield, D. M. (1961). "Rainfall frequency atlas of the United States for durations from 30 minutes to 24 hours and return periods from 1 to 100 years, TP 40." Washington, DC.

Hill, A. J., and Neary, V. S. (2005). "Factors affecting estimates of average watershed slope." *Journal of Hydrologic Engineering*, 10(2), 133-140.

Horton R.E (1923), Accuracy of Areal rainfall estimates. *Monthly Wheater Review*, National Oceanic and Atmospheric Administration (NOAA)

Hosking, J. R. M. (1990). "L-Moment - Analysis and Estimation of Distributions Using Linear-Combinations of Order-Statistics." *Journal of the Royal Statistical Society Series B-Methodological*, 52(1), 105-124.

Hosking, J. R. M. (1992). "Moments or L-Moments - an Example Comparing 2 Measures of Distributional Shape." *American Statistician*, 46(3), 186-189.

Hosking, J. R. M., and Wallis, J. R. (1997). *Regional frequency analysis : an approach based on L-moments*, Cambridge University Press, Cambridge ; New York.

Hoyt, W. G., and Langbein, W. B. (1955). *Floods*, Princeton University Press, Princeton, N.J.,.

Hudson, P. F., and Colditz, R. R. (2003). "Flood delineation in a large and complex alluvial valley, lower Panuco basin, Mexico." *Journal of Hydrology*, 280(1-4), 229-245.

Hudson, P. F., Colditz, R. R., and Aguilar-Robledo, M. (2006). "Spatial relations between floodplain environments and land use - Land cover of a large lowland tropical river valley: Panuco basin, Mexico." *Environmental Management*, 38(3), 487-503.

IACWD. (1982). "Guidelines for determining flood flow frequency, Bulletin 17B." Reston, VA.

Institut haïtien de statistique et d'informatique. Bureau du 4ème recensement. (2003). *4ème recensement général de la population et de l'habitat : résultats préliminaires*, Ministère de l'économie et des finances Institut haïtien de

statistique et d'informatique (IHSI) Bureau du 4ème recensement, République d'Haïti.

Islam, M. M., and Sado, K. (2002). "Development priority map remote sensing data with for flood countermeasures by geographic information system." *Journal of Hydrologic Engineering*, 7(5), 346-355.

Jensen, J. R. (2005). *Introductory digital image processing : a remote sensing perspective*, Prentice Hall, Upper Saddle River, N.J.

Kokkonen, T. S., and Jakeman, A. J. (2001). "A comparison of metric and conceptual approaches in rainfall-runoff modeling and its implications." *Water Resources Research*, 37(9), 2345-2352.

Kresch, D. L., Mastin, M. C., Olsen, T. D., Geological Survey (U.S.), and United States. Agency for International Development. (2002). "Fifty-year flood-inundation maps for Catacamas, Honduras." U.S. Geological Survey, Reston, Va.

Kundzewicz, Z. W., and Kaczmarek, Z. (2000). "Coping with hydrological extremes." *Water International*, 25(1), 66-75.

Landwehr, J. M., Matalas, N. C., and Wallis, J. R. (1979). "Probability Weighted Moments Compared with Some Traditional Techniques in Estimating Gumbel Parameters and Quantiles." *Water Resources Research*, 15(5), 1055-1064.

Lettenmaier, D. P., Wallis, J. R., and Wood, E. F. (1987). "Effect of Regional Heterogeneity on Flood Frequency Estimation." *Water Resources Research*, 23(2), 313-323.

Levy, B., and McCuen, R. (1999). "Assessment of storm duration for hydrologic design." *ASCE Journal of Hydrologic Engineering*, 4(3), 209-213.

Lillesand, T. M., Kiefer, R. W., and Chipman, J. W. (2004). *Remote sensing and image interpretation*, Wiley, New York.

Linnerooth-Bayer, J., Mechler, R., and Pflug, G. (2005). "Refocusing Disaster Aid." *Science*, 309(5737), 3.

Linsley, R. K., Crow, J. T., and Warren, C. A. (1992). *Water resources engineering*, McGraw-Hill, New York.

Loukas, A., and Quick, M. C. (1995). "24-H Design Storm for Coastal British-Columbia." *Journal of Hydraulic Engineering-Asce*, 121(12), 889-899.

Lu, L. H., and Stedinger, J. R. (1992a). "Sampling Variance of Normalized Gev Pwm Quantile Estimators and a Regional Homogeneity Test." *Journal of Hydrology*, 138(1-2), 223-245.

Lu, L. H., and Stedinger, J. R. (1992b). "Variance of 2-Parameter and 3-Parameter Gev Pwm Quantile Estimators - Formulas, Confidence-Intervals, and a Comparison." *Journal of Hydrology*, 138(1-2), 247-267.

Maidment, D. R. (1993). *Handbook of hydrology*, McGraw-Hill, New York.

Maidment, D. R., and Hoogerwerf, T. N. (2002). "Parameter Sensitivity in Hydrologic Modeling." The University of Texas at Austin, Austin, TX.

Martins, E. S., and Stedinger, J. R. (2000). "Generalized maximum-likelihood generalized extreme-value quantile estimators for hydrologic data." *Water Resources Research*, 36(3), 737-744.

Masozera, M. K., Alavalapati, J. R. R., Jacobson, S. K., and Shrestha, R. K. (2006). "Assessing the suitability of community-based management for the Nyungwe Forest Reserve, Rwanda." *Forest Policy and Economics*, 8(2), 206-216.

Mastin, M. C., Geological Survey (U.S.), and United States. Agency for International Development. (2002). *Flood-hazard mapping in Honduras in response to Hurricane Mitch*, U.S. Dept. of the Interior U.S. Geological Survey, Tacoma, Wash.

Mather, J. R. (1975). *Estimation of areal average precipitation using different network densities and averaging techniques*, C.W. Thornthwaite Associates, Elmer, N.J.

Melesse, A. M., and Graham, W. D. (2004). "Storm runoff prediction based on a spatially distributed travel time method utilizing remote sensing and GIS." *Journal of the American Water Resources Association*, 40(4), 863-879.

Moglen, G. E., and Hartman, G. L. (2001). "Resolution effects on hydrologic modeling parameters and peak discharge." *Journal of Hydrologic Engineering*, 6(6), 490-497.

Mora, S. C. (1995). "Extent and Socio-economic significance of slope-instability on the island of Hispaniola (Haiti and Dominican Republic)." *Earth Science Series*, 16.

Morrow, B. H. (1999). "Identifying and mapping community vulnerability." *Disasters*, 23(1), 1-18.

Mosquera-Machado, S., and Ahmad, S. (2007). "Flood hazard assessment of Atrato River in Colombia." *Water Resources Management*, 21(3), 591-609.

Nardi, F., Vivoni, E. R., and Grimaldi, S. (2006). "Investigating a floodplain scaling relation using a hydrogeomorphic delineation method." *Water Resources Research*, 42(9), -.

Noman, N. S., Nelson, E. J., and Zundel, A. K. (2001). "Review of automated floodplain delineation from digital terrain models." *Journal of Water Resources Planning and Management-Asce*, 127(6), 394-402.

Noman, N. S., Nelson, E. J., and Zundel, A. K. (2003). "Improved process for floodplain delineation from digital terrain models." *Journal of Water Resources Planning and Management-Asce*, 129(5), 427-436.

Nozdryn-Plotnicki, M., and Watt, W. (1979). "Assessment of Fitting Techniques for the Log Pearson Type 3 Distribution using Monte Carlo Simulation " *Water Resources Research* 15(3), 714-718.

O'Connor, J. E., Costa, J. E., and Geological Survey (U.S.). (2003). *Large floods in the United States : where they happen and why*, U.S. Dept. of the Interior U.S. Geological Survey ; U.S. Geological Survey Map Distribution distributor, Denver CO.

Overton, I. C. (2005). "Modelling floodplain inundation on a regulated river: Integrating GIS, remote sensing and hydrological models." *River Research and Applications*, 21(9), 991-1001.

Peel, M. C., Wang, Q. J., Vogel, R. M., and McMahon, T. A. (2001). "The utility of L-moment ratio diagrams for selecting a regional probability distribution." *Hydrological Sciences Journal-Journal Des Sciences Hydrologiques*, 46(1), 147-155.

Pelletier J. D, Pearthree P.A, House P.K, Densey K.A, Klawon J.E, Vincent K.R. (2005). " An integrated approach to flood hazard assessment on alluvial fans using numerical modelling, field mapping and remote sensing" *GSA Bulletin*, no 9/10, p. 1167-1180

Ponce, V. M. (1989). *Engineering hydrology : principles and practices*, Prentice Hall, Englewood Cliffs, N.J.

Prophete, J. (2006). "Definition d'un plan d'amenagement axe usr l'agroforesterie pour le bassin versant de la riviere la Quinte, Gonaives, Haiti," Universite de Laval.

Prowse, M., and Chronic Poverty Research Centre. (2003). *Towards a clearer understanding of 'vulnerability' in relation to chronic poverty*, Chronic Poverty Research Centre, Manchester.

Quinones, M., Gould, W., and Rodriguez-Pedraza, C. D. (2006). "Geospatial Data Availability for Haiti: An Aid in the Development of GIS-Based Natural Resource Assessments for Conservation Planning."

Rabus, B., Eineder, M., Roth, A., and Bamler, R. (2003). "The shuttle radar topography mission - a new class of digital elevation models acquired by spaceborne radar." *Isprs Journal of Photogrammetry and Remote Sensing*, 57(4), 241-262.

Rao, P. B. S., Murty, K. S. R., and E, A. (2005). "Estimation of Flood Vulnerability Index for Delta Areas through RS&GIS." *Ieee Transactions on Geoscience and Remote Sensing*.

Rashid, S. F. (2000). "The urban poor in Dhaka City: Their struggles and coping strategies during the floods of 1998." *Disasters*, 24(3), 240-253.

Reis, D. S., and Stedinger, J. R. (2005). "Bayesian MCMC flood frequency analysis with historical information." *Journal of Hydrology*, 313(1-2), 97-116.

Roman, S. J., and United States. Air Weather Service. (1966). *An annotated bibliography on the climate of Haiti*, U.S. Dept. of Commerce Environmental Science Services Administration Environmental Data Service, Washington, D.C.

Rosbjerg, D., and Madsen, H. (1995). "Uncertainty Measures of Regional Flood Frequency Estimators." *Journal of Hydrology*, 167(1-4), 209-224.

Saf, B. (2003). "Role of Rainfall Pattern and Basin Physiography on the Probability Distribution of floods," Dokuz Eylul University.

Satterfield, T. A., Mertz, C. K., and Slovic, P. (2004). "Discrimination, vulnerability, and justice in the face of risk." *Risk Analysis*, 24(1), 115-129.

Scharffenberg, W. A., Fleming, M. J., and Hydrologic Engineering Center (U.S.). (2006). *Hydrologic modeling system HEC-HMS : user's manual*, US Army Corps of Engineers Hydrologic Engineering Center, Davis, CA.

Schuurmans, J. M., and Bierkens, M. F. P. (2006). "Effect of spatial distribution of daily rainfall on interior catchment response of a distributed hydrological model." *Hydrology and Earth System Sciences Discussions*, 3, 2175–2208.

Shah, S. M. S., OConnell, P. E., and Hosking, J. R. M. (1996). "Modelling the effects of spatial variability in rainfall on catchment response .2. Experiments with distributed and lumped models." *Journal of Hydrology*, 175(1-4), 89-111.

Singh, S. K. (2004). "Analysis of Uncertainties in Digital Elevation Models in Flood (Hydrualic) Modelling," International Institute for Geo-Information Science and Earth Observation, ENSCHEDE.

Singh, V. P., and Woolhiser, D. A. (2002). "Mathematical modeling of watershed hydrology." *Journal of Hydrologic Engineering*, 7(4), 270-292.

Smith, K., and Ward, R. C. (1998). *Floods : physical processes and human impacts*, Wiley, Chichester ; New York.

Snyder, F. F. (1938). "Synthetic unit-graphs." *Trans. Am. Geophys. Union*.

Song, C., Woodcock, C. E., Seto, K. C., Lenney, M. P., and Macomber, S. A. (2001). "Classification and change detection using Landsat TM data: When and how to correct atmospheric effects?" *Remote Sensing of Environment*, 75(2), 230-244.

Stedinger, J. R. (1980). "Fitting Log Normal-Distributions to Hydrologic Data." *Water Resources Research*, 16(3), 481-490.

Stedinger, J. R. (1983). "Confidence-Intervals for Design-Events." *Journal of Hydraulic Engineering-Asce*, 109(1), 13-27.

Stedinger, J. R., and Lu, L. H. (1995). "Appraisal of Regional and Index Flood Quantile Estimators." *Stochastic Hydrology and Hydraulics*, 9(1), 49-75.

Stephen, L., and Downing, T. E. (2001). "Getting the scale right: A comparison of analytical methods for vulnerability assessment and household-level targeting." *Disasters*, 25(2), 113-135.

Stephenson, D. (1984). "Kinematic Study of Effects of Storm Dynamics on Runoff Hydrographs." *Water Sa*, 10(4), 189-196.

Taylor, G. C., and Lemoine, R. C. (1949). *Ground-water geology of the Gonaives Plain, Haiti*, U.S. Geological Survey, Washington, D.C.

TSO. (2006). "Planning Policy Statement 25: Development and Flood Risk." (http://www.communities.gov.uk/pub/955/PlanningPolicyStatement25DevelopmentandFloodRisk_id1504955.pdf; date accessed: June 18, 2007)

USACE. (1999). "Water Resources Assessment of Haiti." (http://www.sam.usace.army.mil/en/wra/Haiti/Haiti%20Water%20Resources%20Assessment%20English.pdf; date accessed: June 18, 2007)

USACE. (2005). "HEC-GeoRas, GIS tools for support of HEC-RAS using ArcGIS." (http://www.hec.usace.army.mil/software/hec-ras/hec-georas_downloads.html; date accessed: June 18, 2007)

USAID. (2007). "Environmental Vulnerability in Haiti." (http://www.wilsoncenter.org/events/docs/Haiti_Final.pdf; date accessed: June 18, 2007)

UTSIG. (2004). "Carte de Pauvrete d'Haiti." (http://www.mefhaiti.gouv.ht/actualite/CARTE%20DE%20PAUVRET%C9%20VERSION%202004.pdf; date accessed: June 18, 2007)

Vogel, R. M. (1986). "The Probability Plot Correlation-Coefficient Test for the Normal, Lognormal, and Gumbel Distributional Hypotheses." *Water Resources Research*, 22(4), 587-590.

Vogel, R. M., and C.N, K. (1989). "Low-Flow Frequency Analysis Using Probability-Plot Correlation Coefficients " *Water Resources Planning and Management*, 115(3), 338-357.

Vogel, R. W., and McMartin, D. E. (1991). "Probability Plot Goodness-of-Fit and Skewness Estimation Procedures for the Pearson Type 3 Distribution (Paper 91WR02116)." *Water resources research*, 27(12), 3149-3158.

von Sperling, M., and Fattal, B. (2001). "Implementation of guidelines: some practical aspects." *Water Quality: Guidelines, Standards and Health*.

Wang, Q., Watanabe, M., Hayashi, S., and Murakami, S. (2003). "Using NOAA AVHRR Data to Assess Flood Damage in China." *Environmental Monitoring and Assessment*, 82(2), 30.

Wang, Q. J. (1998). "Approximate goodness-of-fit tests of fitted generalized extreme value distributions using LH moments." *Water Resources Research*, 34(12), 3497-3502.

Wang, Y. (2002). "Mapping the extent of floods, what we have learned and how we can do better." *Natural Hazard Review*, 3(2).

Whiteaker, T. L., Robayo, O., Maidment, D. R., and Obenour, D. (2006). "From a NEXRAD rainfall amp to a flood inundation map." *ASCE Journal of Hydrologic Engineering*, 11(1), 37-45.

Willems, P., Vaes G., Popa D., Timbe L., and J., B. (2002). "Quasi 2D river flood modelling." River Flow.

Wisner, B. (2004). *At risk : natural hazards, people's vulnerability and disasters*, Routledge, Routledge ; New York.

Wonkovich, M. A. (2007). "Evaluation of High Resolution Digital Elevation Models for Creating Inundation Maps," Bowling Green State University.

WorldBank. (2002). "Natural Hazard Risk Management in the Caribbean: Revisiting the Challenge."

WorldBank. (2006). "Social Resilience and State Fragility in Haiti."

(http://siteresources.worldbank.org/SOCIALANALYSIS/1104894-1115795935771/20938696/Haiti_CSA.pdf; date accessed: June 18, 2007)

Wurbs, R. A., and James, W. P. (2002). *Water resources engineering*, Prentice Hall, Upper Saddle River, NJ.

Yalçın, G., Z. Akyürek, Analysis Flood Vulnerable Areas with Multicriteria Evaluation. *"XXth International Society for Photogrammetry and Remote Sensing Congress "*, on CD, (2004), p..

Yamaguchi, Y., Kahle, A. B., Tsu, H., Kawakami, T., and Pniel, M. (1998). "Overview of Advanced Spaceborne Thermal Emission and Reflection Radiometer (ASTER)." *Ieee Transactions on Geoscience and Remote Sensing*, 36(4), 1062-1071.

APPENDIX A : Precipitation Data and Frequency Analysis

- **Rainfall Data**

a) annual precipitation

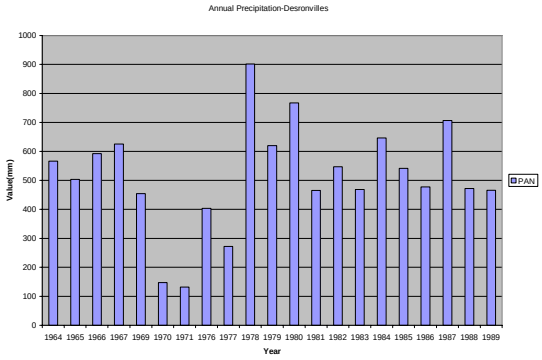

b) annual maximum daily precipitation

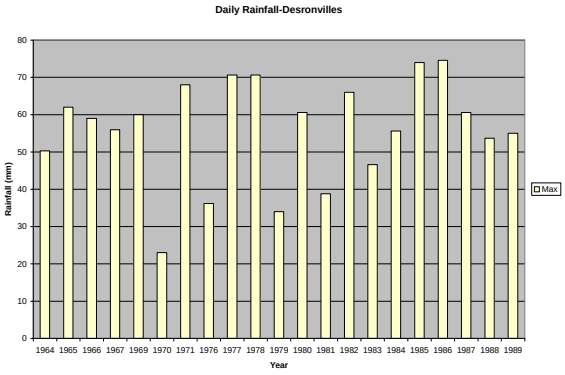

Desronville

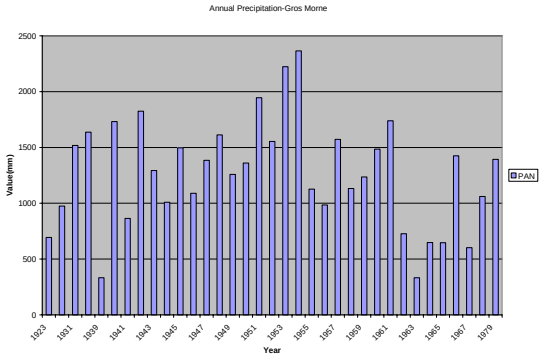

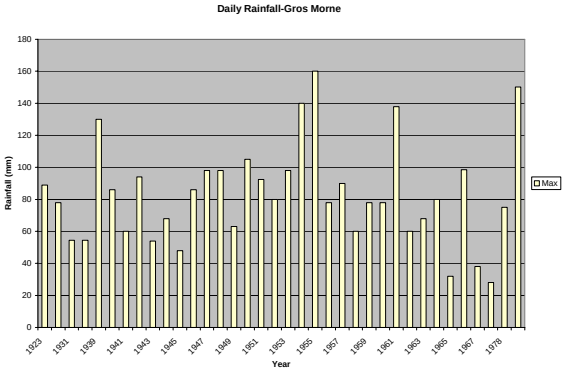

Gros Morne

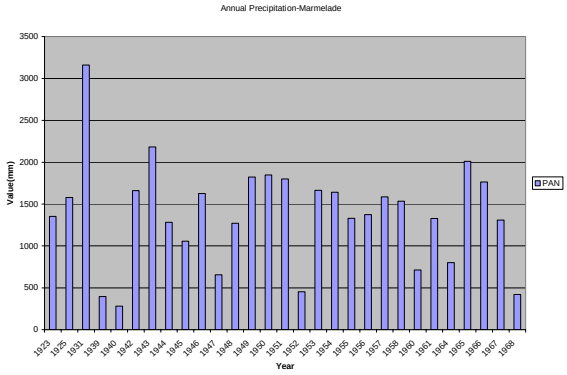

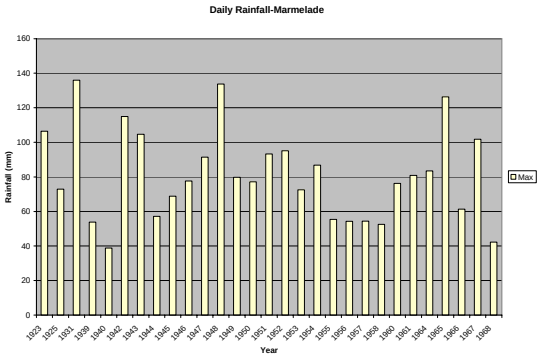

Marmelade

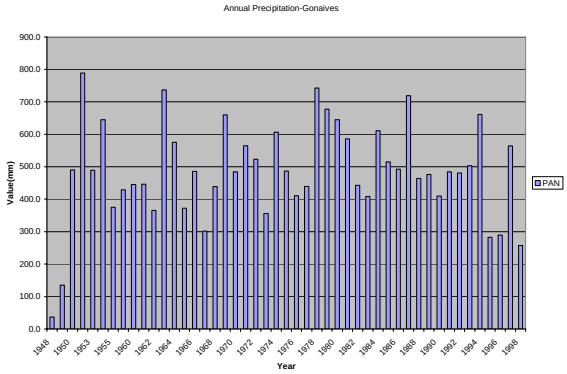

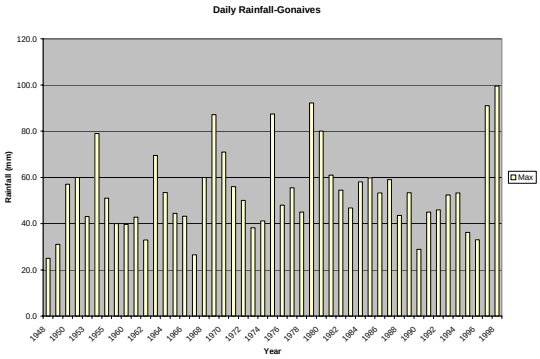

Gonaives

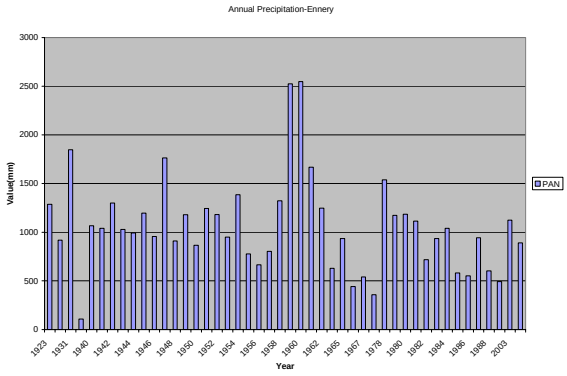

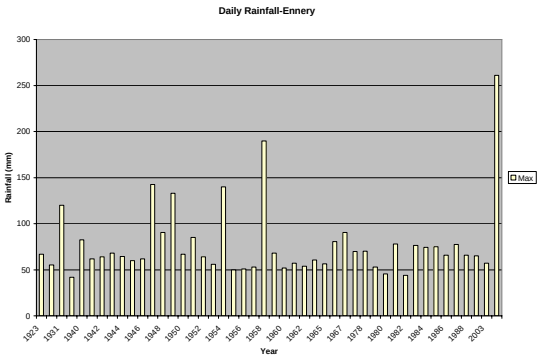

Ennery

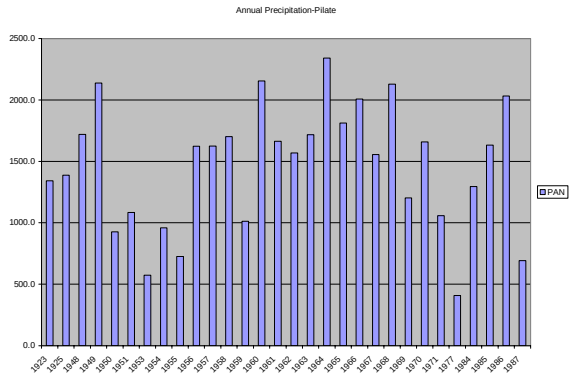

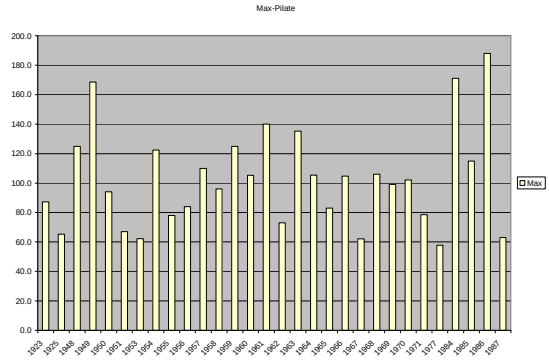

Pilate

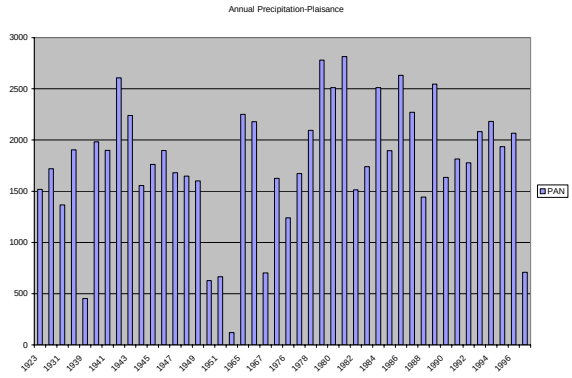

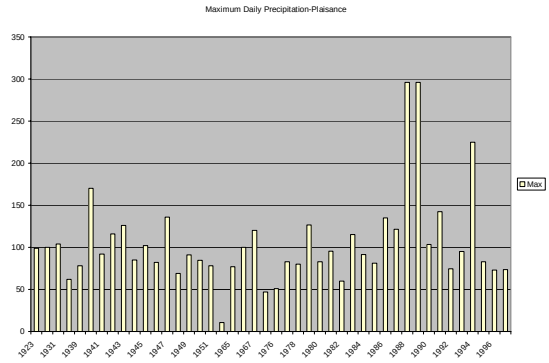

Plaisance

Figure 52: Annual rainfall and number of rainy days for the seven stations

Table 23: Rainfall quantile estimates of daily precipitation (mm) at Desronville (n=21, k=0.6)

T	p	Xgev	Xgevr	XLr	XUr	η
10	0.1	72	87	75	98	0.81
25	0.04	75	118	98	138	0.40
50	0.02	76	148	116	181	0.25
100	0.01	77	187	134	239	0.18
200	0.005	77	234	146	322	0.14
500	0.002	77	316	140	492	0.11

Table 24: Rainfall quantile estimates of daily precipitation (mm) at Ennery (n=46, k=-0.43)

T	p	Xgev	Xgevr	XLr	XUr	η
10	0.1	111	120	101	139	0.91
25	0.04	154	164	133	195	0.50
50	0.02	198	206	158	253	0.36
100	0.01	259	259	183	334	0.28
200	0.005	340	325	201	448	0.24
500	0.002	492	438	195	682	0.21

Table 25: Rainfall quantile estimates of daily precipitation (mm) at Gonaives (n=46, k=-0.03)

T	p	Xgev	Xgevr	XLr	XUr	η
10	0.1	78	84	74	94	0.91
25	0.04	92	115	96	133	0.50
50	0.02	102	144	114	174	0.36
100	0.01	113	181	131	231	0.28
200	0.005	124	227	144	311	0.24
500	0.002	139	307	139	475	0.21

Table 26: Rainfall quantile estimates of daily precipitation (mm) Gros Morne (n=36, k=0.07)

T	p	Xgev	Xgevr	XLr	XUr	η
10	0.1	125	129	113	146	0.87
25	0.04	146	175	156	197	0.46
50	0.02	161	220	197	246	0.32
100	0.01	174	277	249	308	0.24
200	0.005	187	347	314	385	0.20
500	0.002	204	469	424	519	0.17

Table 27: Rainfall quantile estimates of daily precipitation (mm) at Marmelade (n=29, k=0.08)

T	p	Xgev	Xgevr	XLr	XUr	η
10	0.1	117	125	106	145	0.84
25	0.04	135	171	139	203	0.43
50	0.02	147	215	166	264	0.29
100	0.01	159	270	192	348	0.21
200	0.005	169	339	211	467	0.17
500	0.002	183	458	205	710	0.14

Table 28: Rainfall quantile estimates of daily precipitation (mm) at Pilate (n=26, k=0.01)

T	p	Xgev	Xgevr	XLr	XUr	η
10	0.1	152	168	145	191	0.83
25	0.04	177	229	192	265	0.42
50	0.02	195	288	230	346	0.27
100	0.01	213	362	264	459	0.20
200	0.005	230	454	289	618	0.16
500	0.002	253	613	280	946	0.13

Table 29: Rainfall quantile estimates of daily precipitation (mm) at Plaisance (n=40, k=-0.27)

T	P	Xgev	Xgevr	XLr	XUr	η
10	0.1	151	159	136	183	0.89
25	0.04	195	217	178	257	0.48
50	0.02	235	273	212	335	0.33
100	0.01	284	343	244	442	0.26
200	0.005	342	431	268	594	0.21
500	0.002	438	582	259	905	0.19

where

T: recurrence interval

p: probability of annual exceedance

Xgev: quantile estimate using the GEV at site distribution

Xgevr: quantile estimate using the regional GEV distribution

XLr: lower bound of the confidence interval using the regional GEV distribution

XUr: upper bound of the confidence interval using the regional GEV distribution.

Table 30: Rainfall Station Location and Characteristics

NAME	LONGITUDE	LATITUDE	ELEVATION (m)	Mean annual precipitation (mm)
Gonaives	-72.683333	19.450000	5	483.3
Desronville	-72.666667	19.466667	19	626.8
Ennery	-72.483333	19.483333	320	1187.4
Gros Morne	-72.683333	19.666667	220	1344.7
Marmelade	-72.366667	19.516667	710	1781.8
Plaisance	-72.466667	19.600000	420	1921.5
Pilate	-72.550000	19.666667	320	1782.4

Table 31: Degree of Correlation with distance to the regional k

Station	Correlation	Abs(difference)	Record length
Desronvilles	0.5953	0.96	21
Ennery	0.9964	0.1	46
Gonaives	0.9706	0.3	46
Gros morne	0.944	0.4	36
Marmelade	0.9405	0.41	29
Pilate	0.9573	0.34	26
Plaisance	0.9989	0.06	40

Table 32: Lower bound of regional rainfall frequency estimates

Stations	T-10	T=25	T=50 yr	T=100 yr	T=200yr	T=500yr
Desronville	75	98	116	134	146	140
Ennery	101	133	158	183	201	195
Gonaives	74	96	114	131	144	139
Gros Morne	113	156	197	249	314	424
Marmelade	106	139	166	192	211	205
Pilate	145	192	230	264	289	280
Plaisance	136	178	212	244	268	259
average	107	142	170	200	225	235
areal	100	132	158	186	209	218

Table 33: Upper bound of regional rainfall frequency estimates

Stations	T=10	T=25	T=50 yr	T=100 yr	T=200 yr	T=500 yr
Desronville	98	138	181	239	322	492
Ennery	139	195	253	334	448	682
Gonaives	94	133	174	231	311	475
Gros Morne	146	197	246	308	385	519
Marmelade	145	203	264	348	467	710
Pilate	191	265	346	459	618	946
Plaisance	183	257	335	442	594	905
average	142	198	257	337	449	676
areal	132	184	239	314	418	628

Appendix B: Watershed model and Sensitivity analysis

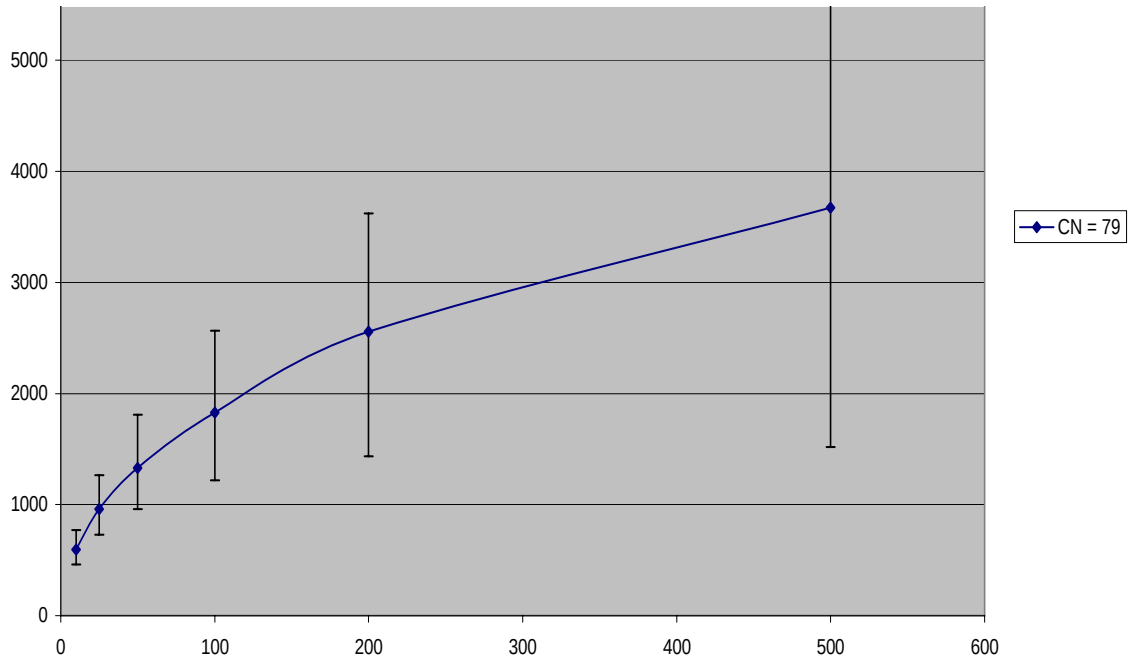

Figure 53: Variation of discharge with the precipitation (SCS model)

Table 34: Discharge estimates using CN =79 with SCS method

	10		25		50		100		200		500	
	LB	**UB**	**LB**	**UB**	**LB**	**UB**	**LB**	**UB**	**LB**	**UB**	**LB**	**UB**
GG	124	215	199	354	262	506	333	714	391	1004	414	1584
G0	390	656	623	1082	822	1550	1043	2199	1228	3107	1301	4946
Gonaives	461	769	731	1266	962	1811	1217	2567	1433	3624	1519	5763

Table 35: Discharge estimates with CN=69 using SCS method

	10		25		50		100		200		500	
	LB	**UB**	**LB**	**UB**	**LB**	**UB**	**LB**	**UB**	**LB**	**UB**	**LB**	**UB**
GG	82	136	136	236	184	350	240	512	318	744	306	1218
G0	250	414	415	714	560	1059	727	1552	869	2257	925	3711
Gonaives	294	486	486	836	657	1237	851	1810	1016	2629	1082	4317

Table 36: Discharge estimates with CN = 61 using SCS method

	10		25		50		100		200		500	
	LB	**UB**	**LB**	**UB**	**LB**	**UB**	**LB**	**UB**	**LB**	**UB**	**LB**	**UB**
GG	56	95	95	170	131	259	173	390	210	580	224	979
G0	171	291	291	516	400	783	526	1174	634	1746	678	2950
Gonaives	202	341	341	605	468	916	616	1371	743	2036	794	3435

APPENDIX C: Remote Sensing accuracy assessment

Table 37: Accuracy assessment of PC and image difference

ERROR MATRIX

Classified Data	Reference Data	unclassified	high risk	medium risk	low risk
	Unclassified	0	0	0	0
	high risk	0	13	0	0
	medium risk	0	3	22	2
	low risk	0	0	4	6
Column	Total	0	16	26	8

ACCURACY TOTALS

	Class Name	Reference Totals	Classified Totals	Number Correct	Producers Accuracy	Users Accuracy
	Unclassified	0	0	0	---	---
	high risk	16	13	13	81.25%	100.00%
	medium risk	26	27	22	84.62%	81.48%
	low risk	8	10	6	75.00%	60.00%
	Totals	50	50	41		

Overall Classification Accuracy = 82.00%

KAPPA (K^) STATISTICS

Overall Kappa Statistics = 0.702

Conditional Kappa for each Category.

Class Name	Kappa
Unclassified	0
high risk	1
medium risk	0.6142
low risk	0.5238

APPENDIX D: Floodplain Hydraulics modeling

Table 38: Inundated areas in m^2 obtained from the hydraulic model for CN=79

T \ n	0.02	0.03	0.04	0.05
10	3,901,500	4,018,500	4,220,100	4,360,500
25	4,552,200	4,717,800	5,115,600	5,190,300
50	5,542,200	5,661,000	6,011,100	6,076,800
100	6,308,100	6,441,300	6,558,300	6,659,100
200	6,360,300	6,626,700	6,755,400	7,044,300
500	7,161,300	7,359,300	7,506,900	7,821,000

- **Sample Cross Sections**

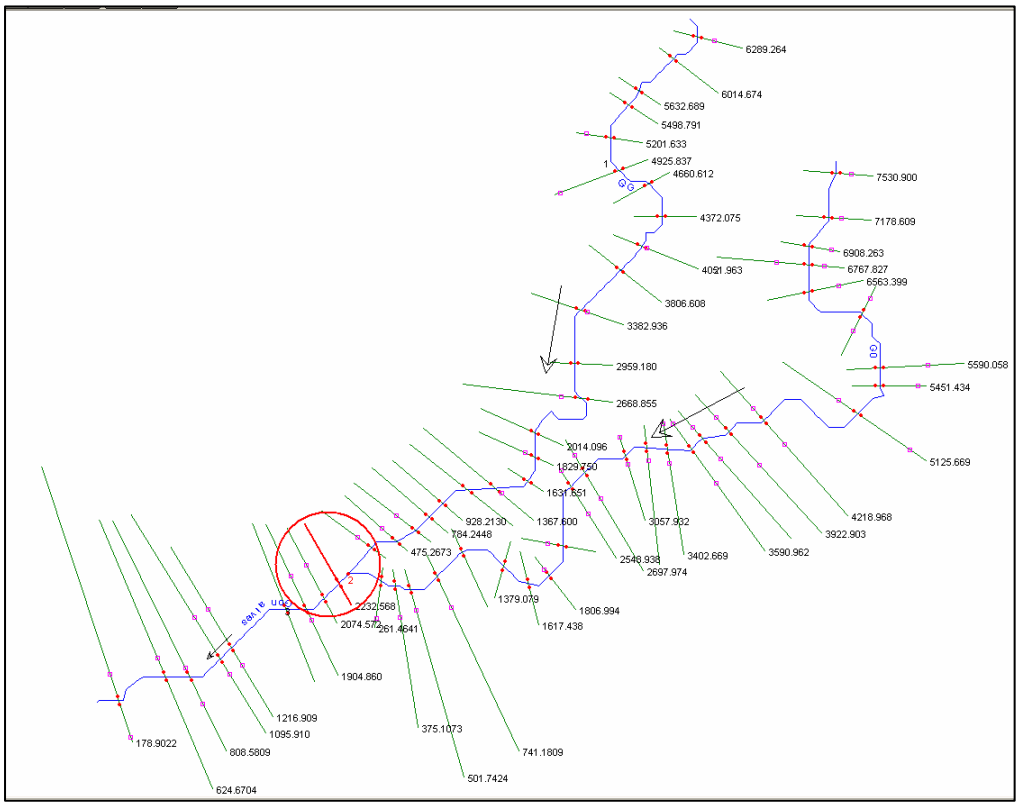

Figure 54: Location of cross section 1

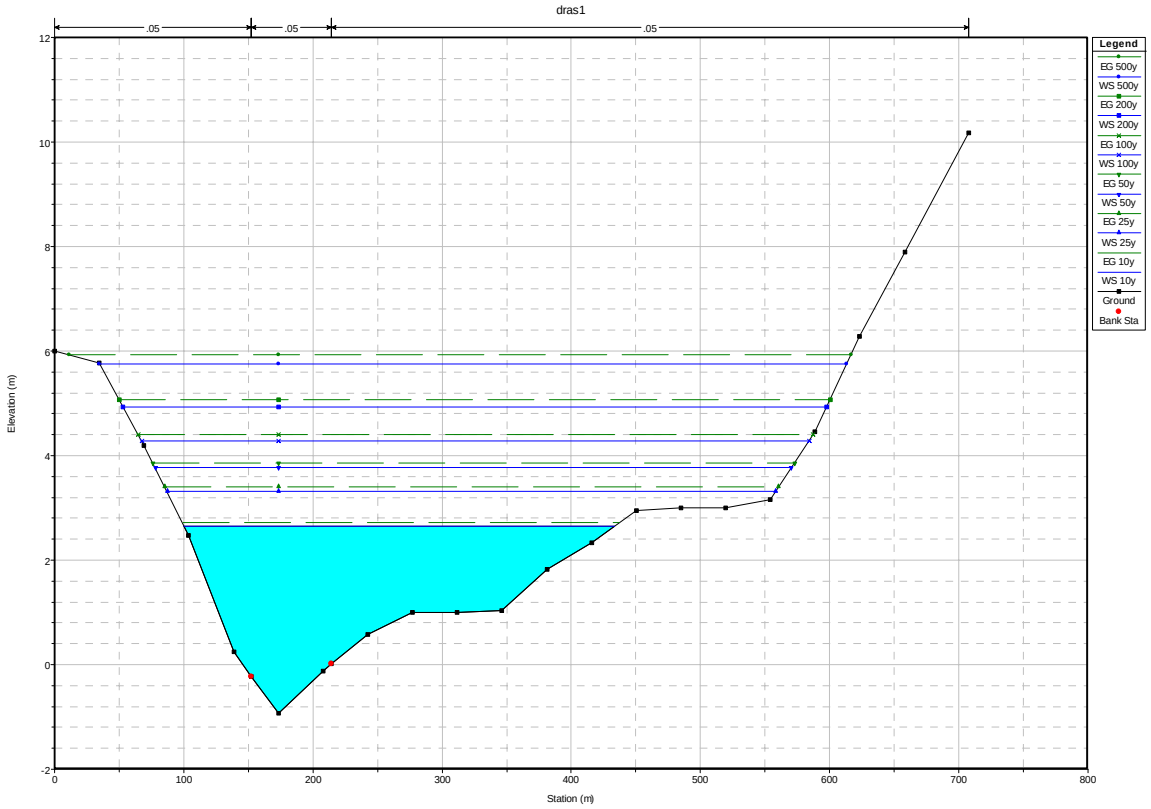

Figure 55: Cross section 1

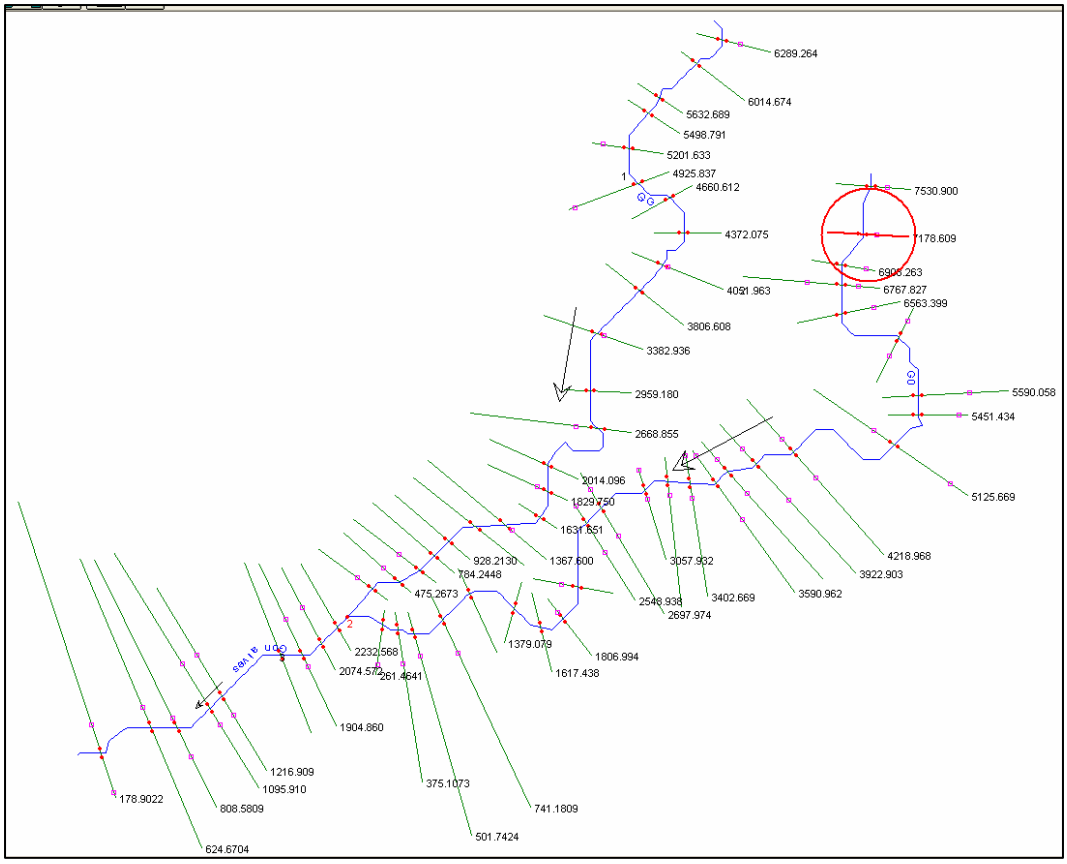

Figure 56: Location of cross section 2

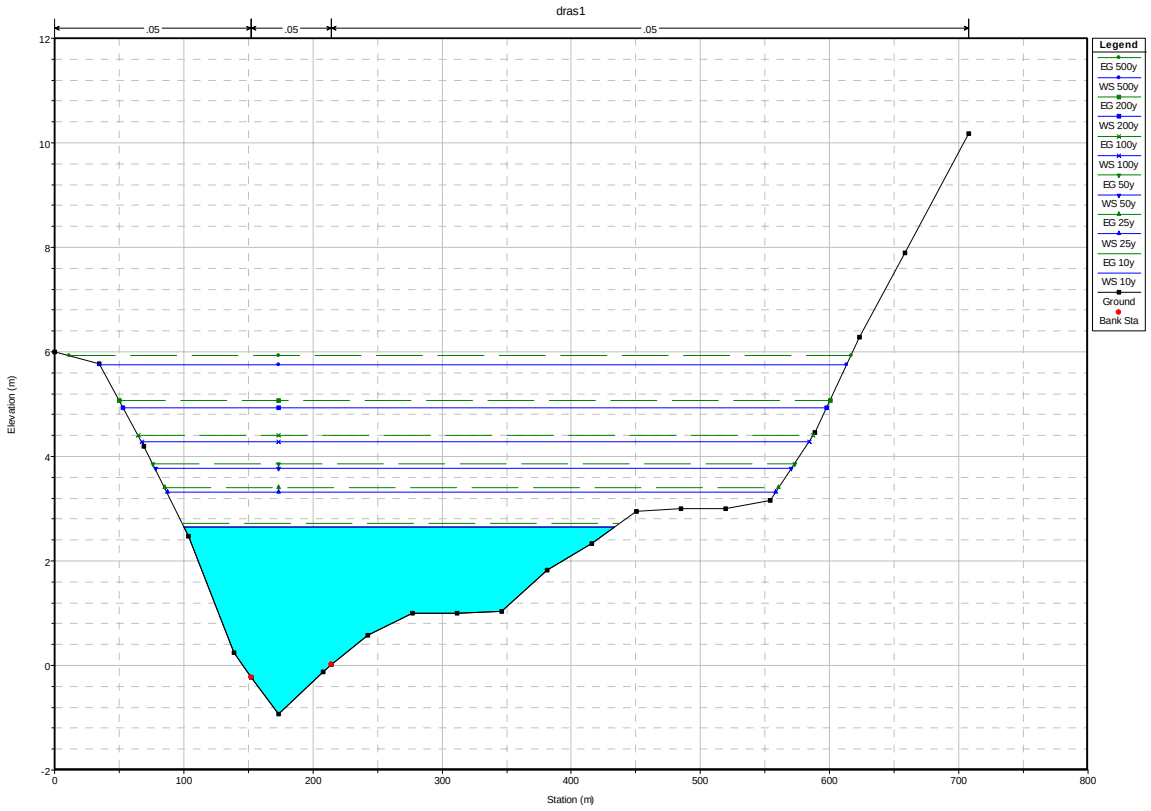

Figure 57: Cross Section 2

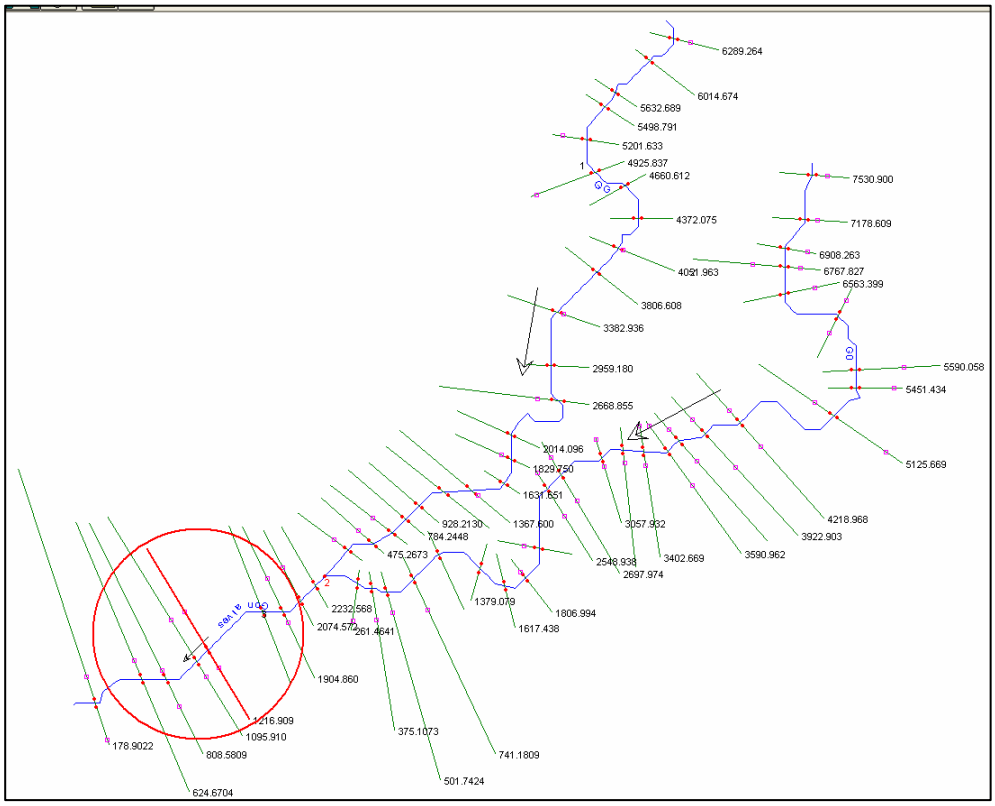

Figure 58: Location of cross section 3

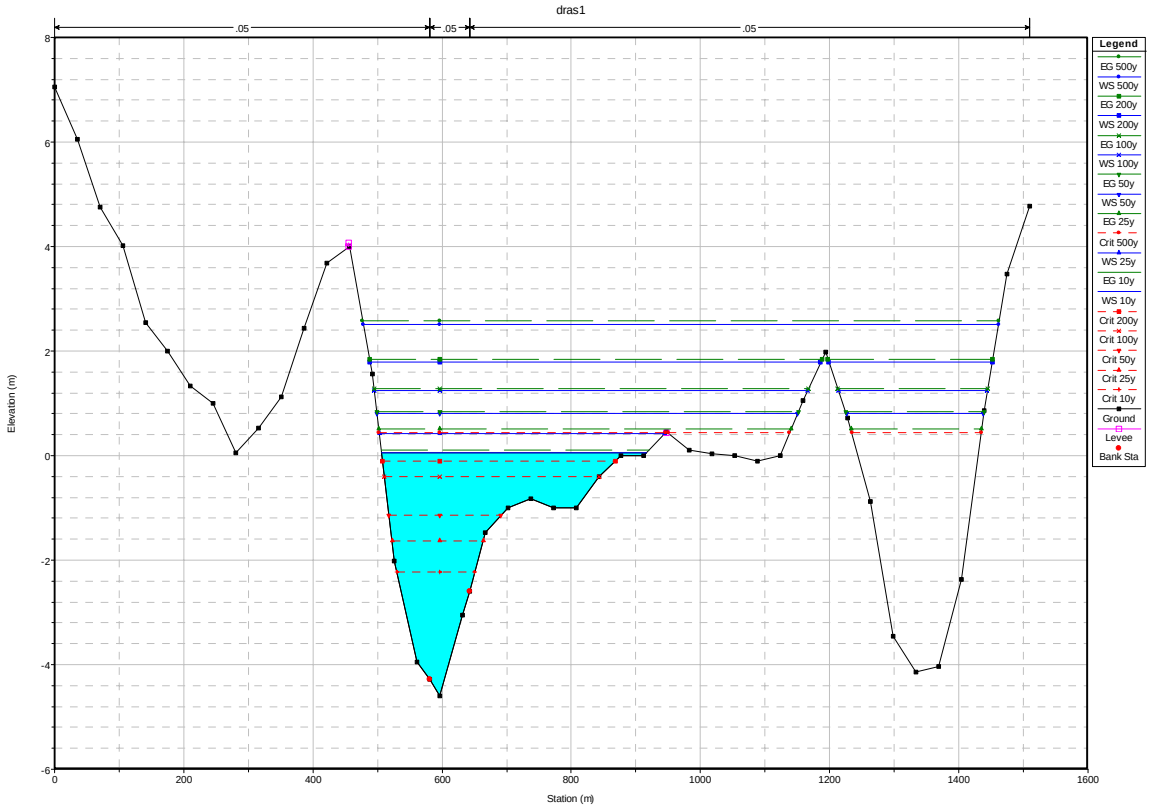

Figure 59: Cross section 3